AUTONOMOUS SURFACE VEHICLE FOR MECHANIZED BATHYMETRIC SURVEYS

BY

THOMAS SEBASTIAN COLLINS
0540656

GRADUATE THESIS
SUPERVISOR: ULF RUNESSON

FACULTY OF NATURAL RESOURCES MANAGEMENT
LAKEHEAD UNIVERSITY

21 SEPTEMBER 2022

ABSTRACT

Collins, Thomas Sebastian. 2022. Autonomous Surface Vehicle For Mechanized Bathymetric Surveys. Lakehead University: Thunder Bay.

Keywords: Autonomous Surface Vehicle, ASV, Survey, Bathymetry, Transects, SONAR, Tailings, Gold Mine, Geographic information systems, GIS, Boat, Kayak, Mokai.

This study evaluates the efficacy of an Autonomous Surface Vehicle (ASV) constructed from inexpensive consumer off the shelf components for suitability in surface-based bathymetry of large-scale tailing impounds found in North Western Ontario. The ASV model will be compared with the current human operated, surfaced based model of conducting bathymetric surveys. The craft was field tested in West Oliver Lake, a shallow, warm water lake with a soft bottom. Depth data were collected at speeds of 2.5ms^{-1}, 3.0ms^{-1}, 4.0ms^{-1}, and 5.0ms^{-1} along the same transects with comparisons made to historical data. Tailings impound surveys when conducted by surface crews pose significant risk to human operators through exposure to hazardous chemicals with both short and long-term effects. Utilizing an autonomous survey vehicle would allow human crews to maintain a safe distance from the tailings impound, potentially reducing interactions with harmful substances present in and around the tailings environment. A Mokai jet kayak was selected as the instrument platform after consideration of its size, propulsion power, and robustness. A Lowrance HDS-7 Live fish finder using a '3-in-1' transducer was used for SONAR mapping, and a Pixhawk 4 Cube autopilot module was used to facilitate remote and autonomous control. Custom interfacing hardware was developed to allow the autopilot

module to interact with the existing kayak propulsion system and otherwise enable autonomous operation. It was determined that using properly tuned autopilot configuration in conjunction with appropriate interfacing hardware, the ASV was able to repeatedly perform accurate transects within a width of 2.6296m at speeds ranging from 2.5ms^{-1} to 5.0ms^{-1}. There was no significant difference in bathymetric data between survey speeds (P>0.05), using 2.5ms^{-1} data as a reference. The highest root mean square error was 0.2168m at 5.0ms^{-1} with respect to the 2.5ms^{-1} data. There was significant difference (P=0.0018) between historic (2003) data and that collected during this study when compared the 2.5ms^{-1} data. Historic data had a root mean square error of 0.8705m when compared to 2.5ms^{-1} data. The details of the historic survey make its accuracy hard to discern as there is little information about how it was collected, though the discrepancy is likely due to a comparatively small number of sample locations combined with inappropriate transect spacing for the shallow waters which constitute the study area. Ultimately, more field data must be collected in an area with temporally relevant depth information to draw concrete conclusions. The compelling consistency between survey speeds conducted during this study illuminates the prospect of field crews working in safety while completing systematic bathymetric surveys at speeds of up to 5.0ms^{-1}.

CONTENTS

TABLES

FIGURES

ACKNOWLEDGEMENTS

I must begin by thanking Kimberly Teager. She facilitated the crucial introductions that indirectly led to my admission to this masters program. Her ongoing support has altered my life in positive and unexpected ways, and for that I'm extremely grateful. Kimberly arranged a meeting with Alex Bilyk, who arranged a subsequent meeting with my now supervisor, Ulf Runesson. Alex and I mused about possible incarnations of this project and eventually settled on the current vehicle platform. Throughout this project he has been a source of great support and guidance in all matters relating to remote operated vehicles. I will always appreciate Ulf's confidence in my ability to succeed in the faculty of Natural Resource Management despite coming a background in engineering. He has been a constant source of realistic life and project advice, and always has the best interest of his students in mind. He was instrumental in the acquisition of the vehicle and provided logistical support at all levels whenever it was needed. Alex and Ulf gave me so much confidence in the success of this project, and ultimately helped open my future to more opportunities than I thought possible.

Ian Gillies of KBM Resource Group accepted me as a research intern after a much needed and appreciated field season with the company. The work provided unique opportunities and experiences, giving me fantastic insight into industrial surveillance which shaped my approach to this study. Without Ian's direct actions and support this project would likely have never come to pass. Colin Pazdzior from KBM with whom I've worked on a variety of projects ranging from IT to rapid prototyping has been an excellent supervisor. Colin has been a great source of advice for a variety of technical matters, having introduced me to new and interesting technologies.

The CARIS Lab has been an accommodating host for myself and this project.

They've provided an exceptional work environment and facilities, both for executing the construction of this project and storage of project components. The lab directly funded some initial purchases to capitalize on product availability, greatly improving the initial project timeline.

Tomislav Sapic provided early guidance in how to approach the analysis of my data, spending many hours in zoom calls patiently answering my questions in topics ranging from ArcGIS to what statistical methods to investigate. Scott Hamilton has given many hours of his time reviewing this document and providing excellent guidance. He was indispensable when collecting field data by volunteering his energy and personal watercraft for use as a safety vessel. I feel incredibly fortunate to have both Tomislav and Scott as committee members.

Ryan Wilkie, Robert Glover, and Chris McEvoy have all loaned their time to various aspects of this project in and out of the field. They provided excellent insight into overlooked practical matters and continue to be an active sounding board with great suggestions. Without their time and input the field season would had been lost entirely.

Jennifer Bain-Manion and Eva Scollie have been instrumental in ensuring all the required bureaucratic tasks have been performed at the faculty level. They've both provided me endless support through processing project paperwork and supplying the required administrative assistance that has helped move this project from application to defence, and I can't thank them enough.

I want to thank Leonard and Patty Roy who were serendipitously located in Thunder Bay, selling the only Mokai kayak in the country. With input from Ulf and Kim the kayak was able to be purchased and transported, accelerating the project development by months. Leonard and Patty have been accommodating in all aspects of the kayak, motorcycle maintenance, and general advice.

A final thanks to my friends and family whose constant support is always

appreciated and has allowed me to succeed where I may have failed.

Time is the only currency any of us possess that has any true value, so I am deeply appreciative of the time and effort contributed by these individuals to the ultimate success of this project. It would have remained just an idea if not for them.

INTRODUCTION

BACKGROUND

Many hazardous tasks are conducted directly by human beings. With the rapid development of increasingly sophisticated technology, this necessity is declining as remotely controlled or automated equipment is developed to undertake these operations. This study addresses the efficacy of bathymetric mapping using remotely controlled consumer-grade equipment by first developing and then testing it under field conditions. The intent is to undertake 'proof of concept' evaluation to assess the utility of such approaches for mapping surveys of large tailings ponds.

North Western Ontario (NWO) contains a large number of operating gold mines; the gold amalgamation process includes significant amounts of Arsenic and Cyanide which become bioavailable in the resulting tailings, and are present with other compounds which can be inhaled, absorbed, or ingested. These tailings ponds require regular sub-surface monitoring capacity. Conventional bathymetric surveys are conduced by a crewed watercraft utilizing a SONAR device to facilitate depth measurements, these craft require a minimum operating depth to avoid propeller strikes, and the crew is potentially exposed to the tailings medium. Alternative methods of surveying are available such as airborne platforms, however the cost of aerial surveillance is significantly greater than that of watercraft and they require a calm water surface and good flying weather. Purely remote or autonomous commercial solutions attempt to address the issue of safety, however the cost is often exorbitant and the product does not have the required field longevity to perform the extensive surveys required by some of NWO's largest mines.

The focus of this study is the development and evaluation of a low-cost

Autonomous Surface Vehicle (ASV) constructed from Consumer Off The Shelf (COTS) components for use in large scale tailings bathymetry. If the ASV is found to maintain consistent depth measurements and navigation between missions at increasing speeds, the survey vehicle may have the potential to produce superior results to those offered by conventional crewed surveys. Success may imply such an ASV would be also have applications in more general purpose roles, but further study would be required to draw such conclusions.

The purpose of this study is not to advocate for the automation of human work and the reduction employment prospects, but to examine the efficacy of autonomous machines in certain high risk roles that pose a threat to the short and long-term health of people.

STUDY OBJECTIVES

The aim of this study is to evaluate the efficacy of a low-cost ASV built from COTS components for the purpose of tailings impound bathymetry when compared to conventional, surface-based, crewed impound surveys. The objectives of the study are:

- Characterize the instrument platform to determine its control requirements, characterize the autopilot system to determine interfacing requirements, and examine the COTS SONAR system to determine its electrical requirements and capabilities.
- Develop software and hardware to interface the existing vehicle control, autopilot, and SONAR systems.
- Amalgamate the vehicle, autopilot, SONAR system, interfacing systems, and any peripheral hardware to create a functioning ASV.
- Determine the repeatability of survey transects performed by the ASV.

- Statistically compare ASV bathymetric data captured at 2.5ms^{-1}, 3.0ms^{-1}, 4.0ms^{-1}, 5.0ms^{-1} to historic data to determine if an ASV comprised of primarily COTS components is able to perform bathymetry comparable to crewed surface surveys, and to evaluate the consistency of its data collection.

The short-term goal of this study is to determine if an ASV built from COTS components is capable of performing autonomous bathymetry with consistent results. Comparisons will be made between multiple surveys, and against historic data of the study location. Positive results in this regard may provide the ability to remove people from the tailings surface, giving survey proponents a more cost-effective, safe, and temporally accurate method of performing tailings impound surveys for use in volume reporting. This study does not include volume calculations or attempt to include them as part of the autonomous process, but to instead provide an attractive tool for large scale bathymetry.

As a long-term item, it may be possible to automate regular waterbody surveillance to such a level that the craft begins and ends the survey on a schedule, automatically uploads the resulting data to a local or remote server where the volume report is calculated and distributed to relevant parties. If this is not possible, the functional ASV would still allow for a wide range of applications that extend to other industries civil, academic, and commercial such as search and rescue, subsurface archaeology, or construction.

Initial vehicle testing took place in Lake Tamblyn (16UCU3258665487), a small, shallow, man-made lake on the Lakehead University campus. The water is highly turbid and the bottom is soft and muddy. Early in the course of this study, the COVID-19 pandemic had begun which prohibited access to a real-world tailings impound for field data collection, as such, a similarly featured freshwater lake was used. The location is West Oliver lake (16UCU0662449302), the waterbody has a soft muddy bottom, natural and artificial sunken features, and both shallow and deep portions as part of the survey area. The waterbody was deemed sufficient to adequately capture field data and had available historic data for comparison.

LITERATURE REVIEW

RELEVANCE

Canadian environmental policy demands that mine operators comply with regulations including the management and monitoring of effluent impounds and reporting their available volume. In order to accurately determine that volume, a bathymetric survey of the impound must be completed (Minister of the Environment and Climate Change, 2019).

Monitoring of the mine and tailings must be maintained throughout the life of the operation and into decommission (Government of Canada, 2020c; Government of Canada, 2020b; Government of Canada, 2020a). These regulations are required to mitigate the significant hazard to human health, watersheds, and ecology posed by stored effluent (Dubé et al., 2005; LeBlond and Duffy, 2001; Muscatello et al., 2006; Bakatula et al., 2012; Clark, 1991). The hazard posed by the mine tailings is so significant that a release would devastate local and downstream ecology, rendering the land hazardous for human and animal life (Glotov et al., 2018; Moore and Luoma, 1990; Datta, 2003; Mara et al., 2007). Gold effluent contains an amalgamation of toxic elements and compounds that include Arsenic, Cadmium, Lead, Cyanide (Cashion and Brown, 1998) and others depending on the mining process, or process-supporting chemical composition of the tailings medium (Glotov et al., 2018; Fawcett et al., 2015). Many compounds present in mining effluent may pose a long-term cancer risk to humans (Ngole-Jeme and Fantke, 2017).

Cyanide plays such a significant role in modern mining since it is used in the extraction of gold from gold ore (Glotov et al., 2018). Since most gold is confined to ore as microscopic particles (Fawcett et al., 2015) a chemical extraction process is required for recovery. The ore is pulverized and mixed with a lixiviant[a] of sodium, potassium, or calcium cyanides to facilitate the leaching process. The result is a water soluble

[a]A liquid medium used to selectively extract desired metal from ore or mineral (contributors, 2022a).

gold-cyanide complex such as $4NaAu(CN_2)$+ 4NaOH (Medina and Anderson, 2020), where gold is eventually removed from the mixture via absorption by activated charcoal. The charcoal bound gold is then chemically removed to solution, and finally removed by electrolysis (Abdalla et al., 2010; Medina and Anderson, 2020). If the ore and subsequent solution contain a high content of other minerals, such as copper, higher levels of free cyanide must be maintained in the lixiviant (Xie, Dreisinger, and Doyle, 2013; Markovic, Vusovic, and Milanovic, 2010). Cyanide is recovered as part of the amalgamation process though there is a portion ever present in the resultant tailings.

This is of particular concern for Ontario; as of 2011, Ontario has been home to 33 mines. 40% of which were gold mines (Burkhardt, Rosenbluth, and Boan, 2012). As of 2021, the number of active mines in Ontario has increased to 41 (Ontario Mining Association, 2021) which includes five of Canada's 10 largest gold mines.(Basov, 2021). The number of mining operations in the province is only likely to increase given a predicted 30bn in revenue from the upcoming 'Ring of Fire' projects (Government of Ontario, 2022). As the number of mine operations increases so will the burden of responsibility on mining proponents, emphasizing the environmental, societal, and economic potential of this project to facilitate safe mining operations.

CURRENT EFFORT

Modern methods of acquiring bathymetric information are most commonly done by watercraft equipped with SONAR, and airborne vehicles utilizing LiDAR, microwave, altimeter measurements, or a combination thereof. Space-borne systems exist with similar functionality(Mason, Gurney, and Kennett, 2000; Wölfl et al., 2019), however, water penetration depth is approximately 1m compared to approximately 50m with aircraft based LiDAR in favourable conditions (Danson, 2006), and up to 13km with SONAR (Rusby and Revie, 1975).

Effluent emission into the tailings impound comprises both a liquid and pulverized solids which segregate during deposition (M D MacKinnon, 1989; Allen, 2008). The

coarse, sand-like elements tend to settle quickly forming beaches and subsurface topology (Oil Sands Magazine, 2021), while most of the finely ground solids, such as silts and clays tend to form a stable, low-laying suspension above the pond bed. This low-laying layer requires more time to fully consolidate, and ultimately settle to form mature fine solids (Mikula, Kasperski, and Burns, 1996; Allen, 2008). The resulting stratified medium tends to be clear with low concentrations of solids from the surface to approximately 10m, solids then increase with depth, eventually forming a well defined mud layer which comprises the pond bottom (M. D. MacKinnon and Boerger, 1986). These particles occupy volume in the impound facility, and are the subject of the 'available volume' calculations determined through bathymetry.

Airborne Bathymetry

Airborne surveys conventionally rely on small aircraft equipped with a suite of measurement tools. Traditionally Light Detection and Ranging (LiDAR) systems are employed, these may be used in conjunction with systems to provide elevation information. LiDAR uses visible and infrared light (McManamon, 2019b), facilitated by an active sensor which emits and receives reflected electromagnetic (EM) waves. The properties of the reflected wave carry information about the target itself, such as albedo, texture, distance, velocity, shape, etc. (McManamon, 2019b).

When utilizing LiDAR for bathymetry, blue-green wavelengths are used as these best penetrate the water (McManamon, 2019b; Charles Kerfoot et al., 2012) to return information about the water clarity and bottom features. Near Infrared (NIR) light penetrates water very poorly and is mostly reflected by the surface, this beam then carries with it information about surface features such as wave action, but more importantly it provides the distance between the aircraft and the water. The result of this combination of information is the ability to determine the water level and the sub-surface features or sediment, providing sufficient measurements to determine the water depth (Charles Kerfoot et al., 2012; Banks et al., 2007).

With ideal water conditions, such as high clarity and a reflective bottom, airborne

LiDAR may penetrate depths up to 50m (Danson, 2006), however in water that has recently been agitated, turbidity may limit the effectiveness of the laser to penetrate the surface (Bowen and Waltermire, 2002; McManamon, 2019a; Bhargava and Mariam, 1991) between one and two metres (Danson, 2006). Considering the lowest strata of the tailings medium tend to be saturated with suspended silts and clays, results may be ambiguous depending on the density and thickness of this layer (Davies-Colly and Smith, 2001). In good conditions, airborne LiDAR is successful in measuring water surface elevation in narrow water bodies providing a low root mean square error (Schumann et al., 2008), however since flying must be done under favourable conditions, the data's temporal resolution may be reduced.

Airborne surveys are performed by flying transects above the water, spacing depends on the height of the aircraft and desired overlap (Dashora, Lohani, and Deb, 2014). Since the aircraft's exact position is required to geolocate the resulting data, Global Positioning System (GPS) or other Global Navigation Satellite Systems (GNSS) are required to determine the aircraft's position in flight. Because the aircraft will experience changes in yaw, roll, and pitch while flying survey transects, it must also take corrective measurements from an Inertial Measurement Unit (IMU) which is used to compensate the LiDAR data (Hayley, 2021).

There are several advantages to performing bathymetric measurements from aircraft, notably the flight crew is completely removed from the tailings medium, and large areas can be covered while collecting multiple types of data. The disadvantages specifically relate to the penetration depth of LiDAR under non ideal circumstances and dependence on good flight conditions. These factors exclude the cost of aircraft operation, contracting, and specialized training required for pilots and operators.

Surface Bathymetry

Conventionally, bathymetric data is collected using some form of echo-sounder, a type of active SONAR device. SONAR is provided in two types, active and passive (Waite, 2002c; Hodges, 2010a). Passive SONAR is a method that utilizes full spectrum

noise emitted by potential targets. Active systems differ significantly such that they emit acoustic energy as pulses, pulse-trains, frequency sweeps, or other more complex patterns (Waite, 2002c; Hodges, 2010a). Echo sounding is used to determine distance between an acoustic source and a given target. An acoustic pulse is released by the source which travels for a period of time until it contacts the target, a portion of the emission reflects from the target and returns to the source where it is received. The reflection provides information about the target, such as motion, texture, distance, shape, etc. (Waite, 2002a).

When planning the survey of a given waterbody, the desired area is divided into parallel transects which the serve as navigation guides for the craft (Furnans and Austin, 2008). Special consideration must be given for spacing between transects as water depth, desired data granularity, and view angle of the SONAR beam affect the size of the sample area beneath the craft. Should the transects be too far apart, the ensuing scan would under-sample the survey area resulting in data gaps that fail to document, or misreport features such as dips or reefs. This is because the sample area, or 'footprint' of the beam will cover less area in shallow water, necessitating a heavy reliance on interpolation (Bouwmeester and Heemink, 1993), conversely, the footprint will cover more area in deeper water, permitting a greater distance between the transects (Che Awang, 2011).

Conventional surface-based surveys rely on a watercraft and crew of one or more people. These individuals tend to be in open air and may contact spray from the engine, mist stirred by wind, and off-gassing of compounds from the tailings medium. One such compound of interest that may be present in the air above, and in the vicinity of the effluent impound is Hydrogen Cyanide gas (HCN). HCN may disassociate from the medium after excitement by solar radiation in combination with low enclosure pH (Türkman, 1998; Zagury, Oudjehani, and Deschênes, 2004). Exposure to HCN poses an acute health risk to humans (Barcroft, 1931; Souren, 2000), generally through inhalation, however contact with dissolved Cyanide may occur via ingestion of particles and absorption through mucous membranes (Henny, Hallock, and E. F. Hill, 1994; Reece,

1997; Ryan and Shanks, 1996). While the lethal dose of cyanide is 1 to 3mg·kg^{-1} for human adults, frequent or prolonged exposure to sub-lethal doses may cause eye irritation, headache, dizziness, and damage to the central nervous system and thyroid gland (Taylor, 2006; Müezzinogˇlu, 2003). HCN is handled slowly by the body and is therefore an accumulative poison (Barcroft, 1931). The possible presence of HCN or harmful elements such as Arsenic implies there is a significant risk to human operators performing surface-based measurements.

Surface-based SONAR has the advantage of being able to penetrate turbid water and is less effected by waves and weather (Birkebak et al., 2018). The SONAR module tends to be either hull mounted or towed behind the craft below the water line, called a 'tow fish'. Water is highly permissive to acoustic disturbance, making SONAR surveys highly effective, especially in deep water (Waite, 2002b; Hodges, 2010c). SONAR is able to propagate through various layers of deep water allowing data to be collected at long range from the source (Waite, 2002b; Hodges, 2010c), analogous to radio waves in the atmosphere (Hulburt, 1935). Using side-scan SONAR, an operator is able to return near photo quality images (Pailhas, Petillot, and Capus, 2010), whereas bottom sounding SONAR returns depth between the transducer and the sub-surface topology.

A key danger of surface-based surveys is the risk of watercraft collisions with sub-surface features or sunken objects (Furnans and Austin, 2008). In tailings bathymetry this poses a threat to the survey crew if they traverse a section of water too shallow for their boat and SONAR instruments to function. SONAR and other radiative devices have a frequency dependant minimum range called the 'near field' which is roughly one wavelength of the SONAR frequency (Hodges, 2010b; Noreland, 2003; Siemens, 2020). When in the near field, the medium only appears to vibrate and there is not enough distance for a wave to propagate and reflect, making depth measurements erroneous without specific design considerations (Siemens, 2020). A craft in this range would be unable to determine the water depth, therefore, planning to avoid suspected shallow areas is essential but may result in a reduction of the survey area.

Modern Solutions

Survey methods which reduce costs and improve safety in hazardous environments are an attractive option for consideration by industry. The literature suggests the use of multi-rotor drones as replacements for comparatively cumbersome aircraft surveys since they are well suited to many of the same roles. Unfortunately, at this time drones tend to have flight times of less than one hour (Shahmoradi et al., 2020) which may be insufficient for the large tailings impounds found in NWO. Aerial drones require licensing through Transport Canada (Transport Canada, 2020) and the operator is legally bound to follow regulations such as maintaining constant and unassisted line of sight. The goal of these limitations are to protect people and property, but limit the extent the technology can operate with low human interaction. Interestingly, surface vehicles aren't subject to regulations other than those required by standard watercraft.

Similar surveillance and mapping projects to this study have been proposed which utilize electric ASVs, yet these are limited by battery capacity (Lee, Phang, and Wong, 2020; Madeo et al., 2020; Ferreira et al., 2007; Ocean Alpha, 2018), or rely on solar energy and therefore are bound to fair weather conditions (K. Pyrchla, J. Pyrchla, and Kantak, 2018; Dunbabin, Grinham, and Udy, 2009). While these projects solve targeted problems and may make use of renewable energy sources, they are ill suited to the vast areas associated with NWO mines.

There is a clear niche well suited to a robust, long range vehicle capable of performing a variety of remote sensing tasks. The Woods Hole Oceanographic Institution (WHOI) in Falmouth Massachusetts created two projects that align with this profile and have potential to address these issues. They present a good model, but they have not been designed for, or evaluated for use in tailings impounds.

The first of these two projects is the 'Jetyak' (Kimball et al., 2015) which used a Mokai jet propelled kayak as the instrument platform. The Mokai used by WHOI is an earlier model (2015) of the vehicle which required extensive modification to function as desired, such as the addition of an aftermarket clutch, and replacement of manual control

interface with servo-driven electronic controls. WHOI used an Ardupilot Mega 2.5 to facilitate autonomous navigation. The Ardupilot is a single board computer requiring external sensors and GPS connectivity originally intended for Do It Yourself (DIY) aerial drones. This project was used to track bathymetric changes of tidal sand waves and Acoustic Doppler Current Profile (ADCP) surveys of flow over the same area. The WHOI ASV performed well, being able to operate in water too shallow for conventional watercraft, and adhere well to the desired route despite energetic flows involving occasional breaking waves. Notably, the ASV collected data over a period of five days in close proximity to the Sarqardleq Glacier in Greenland, an area that poses a massive risk from falling ice if a human operator were to perform the same task (Kimball et al., 2015).

The second project is a later incarnation of the WHOI Jetyak (2015) named the 'Chemyak' which utilized similar modifications to facilitate autonomous operation (Nicholson et al., 2018), but was equipped with a new sensor suite to measure the concentration of various gasses in water, such as methane, carbon dioxide, oxygen, and nitrogen. This was performed via on-board laser spectrometer and gas extraction unit. The vehicle operates for 10 hours at $2.78 ms^{-1}$ with the ability to spatially characterize sampled gas distributions (Nicholson et al., 2018).

Based on these two projects, the benefits of the Mokai jet kayak as an instrument platform appear to be its ability to travel in waters too shallow for conventional watercraft, its longevity in the field, and its ease of modification to carry a variety of sensors. The Mokai appears to fit the niche of large tailing impound surveys, and therefore merits closer examination.

MOKAI JET KAYAK

Having superficially identified attractive features provided by the Mokai, we now investigate the technical details. The modern (2019) Mokai kayak model was evaluated for this project. As discussed, the kayak relies on an impeller drive hydrojet for propulsion, which is less likely to be entangled, obstructed, or strike sub-surface features

and provides an operating depth of approximately 15cm (Mokai Manufacturing, 2020). The Mokai is large and stable with X Y Z dimensions of 3.4036m x 0.9144m x 0.508m, weighing 90.7185 kg fully assembled before fuel and uses a fully electronic, two-axis joystick interface for control (Mokai Manufacturing, 2020). Full electronic control implies this system could be co-opted by external electronics to replicate human input. The field longevity is approximately eight hours using the maximum tank capacity of 15.1L automotive unleaded gasoline, though operating range would depend on throttle usage. The hull is made from rotomolded, high-impact polyethylene that is hardened against ultraviolet light degradation (Mokai Manufacturing, 2020). Polyethylene is known for its strong chemical resistance(Braskem, 2005; CDF Corporation, 2004; A.Schulman, 1981), allowing for little to no chemical breakdown at environmental temperatures while afloat in acidic tailings or other mediums.

The gasoline engine provides 9.5 horsepower (Mokai Manufacturing, 2020), equivalent to 6987.24 watts, Canadian law does not require licensing if the watercraft propulsion system is less than 7500W (Government of Canada, 2021) which reduces the regulatory complexity required to operate the craft. This amount of power also gives the Mokai an advantage over similarly sized electric vehicles in terms of torque, operating time, and range. The engine's stator provides 10 Amperes (A) of charging current which through careful current management would be sufficient to run all on-board systems while still providing charging current to the 12 Volt (V) battery.

Maintenance on the Kholer engine is simple as it is a generic single cylinder, carbureted, two valve engine (Mokai Manufacturing, 2020). The engine, and all parts of the vessel are removable, meaning there is short downtime if repairs or maintenance are required.

Given this close inspection of the kayak's technical details and favourable performance evaluation from the previous Jetyak and Chemyak studies, the author deems the Mokai to be an excellent instrument platform for use in this study.

LOWRANCE HDS-7 LIVE FISH FINDER

The decision to use a fish finder as a substitute for a scientific SONAR system is in line with the goal of the study to create an economic ASV comprised of COTS hardware while still delivering high quality data. The Lowrance HDS-7 Live system was selected specifically due to its favourable results in similar mapping studies (Klemens, 2017) (Halmai et al., 2020). For this study, a Lowrance HDS-7 Gen 3 (*HW version 20.1, DG4016 TC58NVG2S0F 4G 3.3V 8-BIT 2GiB PCB0 - 2 G31_ 00_T3, SW version 64.2.52*) SONAR module was paired with a '3-in-1' transducer for evaluation.

Strikingly little technical information is available from manufacturer sources. This is likely due to the target market being anglers rather than those seeking to use the device for academic studies. SONAR frequency ranges are provided, however positional accuracy of the GPS is not, nor is the accuracy of the backscatter data or its sample rate, however the available information tells us the transducer provides 200 kHz/High Chirp, 83 kHz/Medium Chirp, where 'Chirp' denotes a frequency sweep that begins low in the spectrum and reaches a maximum value of 200 or 83 kHz respectively, and side scan imaging with 455 kHz to 800 kHz (Navico Holding AS, 2018a). View angles were provided by Lowrance technical support and stated to be 20° for 200kHz and 180° for side scan imaging (Navico Technical Support, 2021). The data capture rate is not listed in the manual but the recommended top speed when mapping was 4.4704ms^{-1} when using both downscan (depth sounding) and side-scan (Navico Holding AS, 2018a). The SONAR module utilizes an internal GPS unit which updates at 10Hz and is capable of using a variety GNSS sources, such as GPS and GLONASS (Navico Holding AS, 2018b). While the positional accuracy of the GPS fix could not be ascertained, the module takes advantage of WAAS (North America), MSAS (Japan), and EGNOS (Europe) for positional corrections, which tend to result in target fixes better than 3m 95% of the time (Garmin Ltd., 2017; Central, 2021).

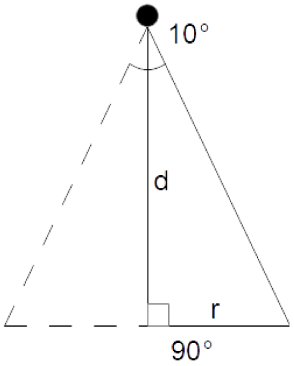

Figure 1: SONAR downscan cone cross section with angles.

Since SONAR field of view for 200KHz is a 20° cone, the area covered is directly related to depth. The triangle in Figure 1 is used to illustrate the cross section of the SONAR beam at the widest point. The black circle at the pinnacle of the triangle represents the acoustic source, d represents the distance between the acoustic source and the lakebed, and r, the radius of the SONAR footprint. Equations 1 and 2 show how this information is used to determine the footprint area. To illustrate, in water 1m in depth, the sample area would be 0.098m^2, 0.88m^2 in 3m water, 2.4m^2 in 5m, and 9.7m^2 in 10m water, Figures 2 and 3 show how these values are affected by depth, and therefore emphasises the need to adjust transect spacing as depth increases.

$$r = \frac{d \cdot sin10°}{sin80°} \tag{1}$$

where:

$r =$ Footprint radius

$d =$ Distance between SONAR transducer and bottom

$$A = \pi r^2 \tag{2}$$

where:

$r =$ Footprint radius

$A =$ Footprint area

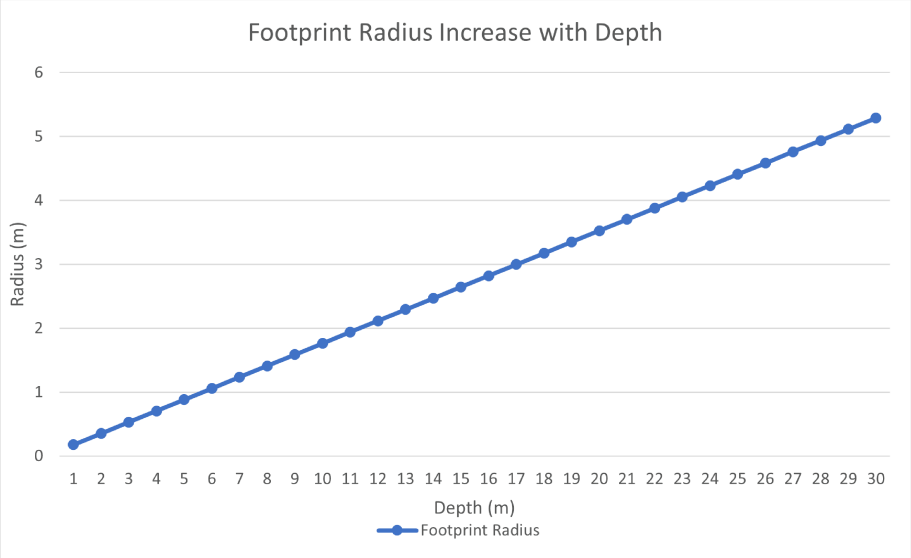

Figure 2: Lowrance fish finder footprint radius and depth.

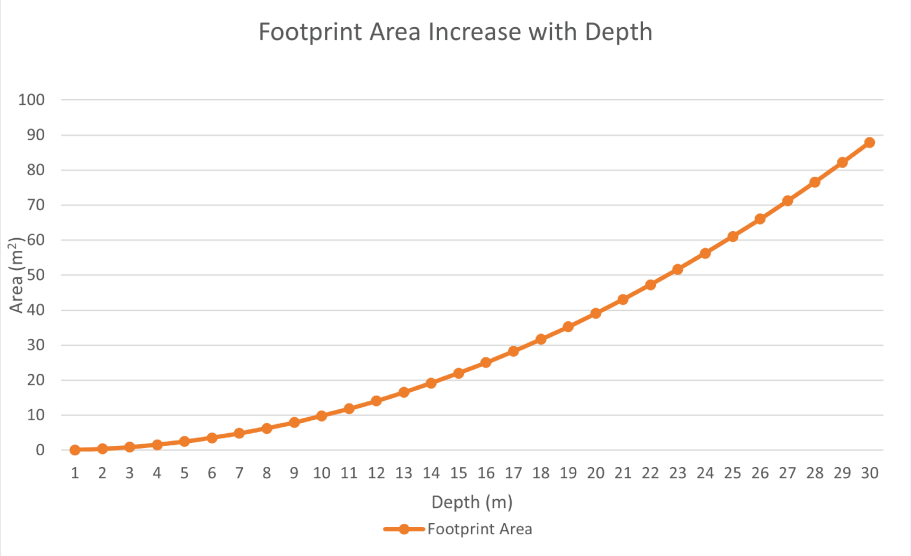

Figure 3: Lowrance fish finder footprint area and depth.

The SONAR module provides a large suite of features which are largely irrelevant for this study, though core features such as mapping (the saving of SONAR logs) are easily accessible via the touch screen user interface. Saved SONAR logs can be provided in multiple formats depending on the desired content. For this study the **.sl3* format was selected as it contains information from all available features of the SONAR module and transducer. The **.sl3* log file is a proprietary and closed source format normally only able

for viewing through Lowrance software or on the HDS-7 itself, though neither of these options allow for exporting positional depth information. For this reason third party resources were explored, multiple software packages were found that were able to read the log files however Reefmaster provided the most export options, such as the ability to export positional depth information as a Comma Separated Value (CSV) file for use in more sophisticated software such as ArcGIS, QGIS, or a programming language such as Python. ReefMaster can also display side-scan with some manipulation. Export options are limited, but sufficient for visualizing sunken features or developing a rough mosaic of the bottom topology.

PIXHAWK 4 CUBE AUTOPILOT

Both industrial and consumer grade drone electronics have become widespread, being found in multi-rotor aircraft for cinematography and toys alike. The result is a dramatic reduction of cost and increase in hardware availability to the market. A by-product of this availability is the emergence of hobbyist, Do It Yourself (DIY), and academic drone networks, supported by inexpensive, professionally designed and fabricated hardware (ArduPilot Dev Team, 2021).

For this project, the Pixhawk 4 Cube (Pixhawk) was selected as the autopilot module. As of this writing it is the current latest version of the Pixhawk autopilot, and finds itself in a variety of commercial, industrial, and academic applications (PX4, 2021). This product was selected for its well established community support, market share, and prevalence in autonomous and remote operated vehicles.

The Pixhawk 4 provides extensive internal sensors and a variety of input/output (IO) functions, notably redundant fail-safe processors, IMUs, and barometers (altitude). The device provides user programmable General Purpose IO (GPIO) functionality for arbitrary hardware, various communication methods for external devices, and 14 Pulse Width Modulation (PWM) outputs to communicate with motors and servos (ArduPilot Dev Team, 2021).

The unit requires certain external hardware to function, most obviously a GPS unit, some form of power management unit, and telemetry radio (ArduPilot Dev Team, 2021). For safety, the unit also requires an arm/disarm mechanism, however the GPS unit selected for this project had an integrated safety switch to fulfil this role. The GPS used by the SONAR module is separate from that used for navigation; both are discussed in greater detail in the methods section, and both are capable of positional accuracy better than 3m.

METHODS

The goals of this study focus on the conversion of the Mokai to an ASV, and then the evaluation of that ASV's suitability for bathymetric data collection. This section will begin by explaining the methods that were used to facilitate the conversion of the instrument platform, followed by those that pertain more strongly to the survey itself.

ASV CONSTRUCTION

The author of this work holds a diploma in electronics engineering technology from SAIT Polytechnic in Calgary, Alberta, a degree in electrical engineering from Lakehead University, Thunder Bay, Ontario, and over 10 years of professional, academic, and personal experience with electronics and software development. This provides sufficient training and experience to analyse the Mokai electronic systems and the subsequent integration with the various components required to convert the kayak to an ASV.

As there are multiple novel components required in the conversion process, the author made extensive use of 3D printed parts for unique housings, moving parts, and similar items. While this is primarily a decision made from necessity, the flexibility of generic rapid manufacturing is somewhat showcased by this project, giving some immunity to the material shortages caused by The COVID-19 pandemic and current kinetic conflict in Ukraine.

While the intention is to fully convert the Mokai to humanless operation, the seat was left in the craft to more easily facilitate testing. This was done to allow the author to be seated in the vehicle and take control should an autonomous tests need to be aborted without requiring other individuals or a recovery craft. As such, the modifications would be built around this concept.

Electronics characterisation

It is not inaccurate to state that the characterisation of a component is akin to learning the dialect it speaks. This analogy underlines the need to understand the language of each component if the intention is to translate the dialect of one device to another and facilitate a dialogue. This section describes this process for the key components that will comprise the ASV as a system. While there is less characterisation work required for the Pixhawk and Lowrance fish finder, their examination still provides essential information to their integration in the system as a whole.

Measurement devices used in the characterisation of all components were a Tektronix TBS1104 100MHz, 4 channel oscilloscope to capture and measure signals via a X10 calibrated probe. A Fluke 113 True RMS Multimeter for impedance, continuity, DC voltage, and miscellaneous measurements. Current readings were taken with a Valley DT-8300 Multimeter (max 10A).

Mokai Characterisation

The 2019 Mokai differs somewhat from those used in the WHOI 'Chemyak' and 'Jetyak' investigations, most notably by being equipped with a full electronic control system. Navigation is facilitated by a two-axis joystick, the X-axis will change the orientation of the thruster to allow the craft to steer left or right accordingly. Tilting the joystick forward from its neutral position will increase the throttle, tilting it to the rear has no function. The controller connects to the on-board control system through a 12-pin Deutsch connector located behind the operator seat.

(a) Mokai operator joystick.

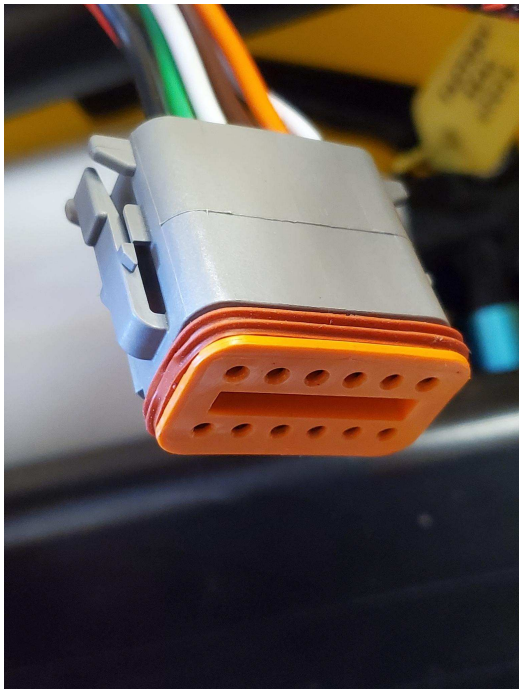

(b) Mokai 12 pin Deutsch connector.

Figure 4: Mokai joystick and terminating Deutsch connector.

The output of the Joystick control shown in Figure 4a was probed by inserting 30 AWG wire into each pin of the Deutsch connector shown in Figure 4b to use as a point of contact for oscilloscope probes. Measurements were taken with the controller in-situ and on-bench when required. Readings were taken with the key in the ’off’ and ’on’ position, and while the kayak engine was running. The complete pinout is presented in Appendix I, Table 18.

In order to power the desired suite of onboard components, voltage levels and available current must be known. Pins carrying 12 volts, can be considered ’automotive voltage’ meaning they will match the battery voltage while the engine is off, and match

the stator voltage while the engine is running. At idle the voltage level was 13.6 volts DC with insignificant fluctuations with changes in RPM. The manual states (Mokai Manufacturing, 2020) the first accessory line has a maximum current draw of 10A, and the second line a maximum of 3A. These are marked ’Aux 1’ and ’Aux 2’ on the joystick control box. Current use is enforced by fuses of the corresponding values in the engine compartment. The manual further states the maximum current to be drawn from the stator while the engine is running is 10A (Mokai Manufacturing, 2020). We now know the maximum current and operating voltage supplied by the kayak for use as a power source. The next step was to analyse the signals sent by the joystick controller and how they correspond to the thruster and throttle actions. The oscilloscope was used to probe pins 8 and 9, the thruster direction and throttle control pins, while the joystick was slowly moved from left to right, and front to back. This revealed the following information.

Position	Voltage(DC)	Pin	Action
Full Left	4.562V	9	Thruster 45° Left, Throttle Neutral
Full Right	0.511V	9	Thruster 45° Right, Throttle Neutral
Neutral	2.513V	9	Thruster Center, Minimum Throttle
Full Froward	0.515V	8	Thruster Center, Maximum Throttle
Full Rear	4.562V	8	Thruster Center, Minimum Throttle
Neutral	2.513V	8	Thruster Center, Minimum Throttle

Table 1: Mokai Joystick outputs.

Voltage levels were observed smoothly transitioning between the stated minimum and maximum values, indicating analog voltages controlled the kayak’s propulsion and navigation systems. The change in analog voltage was very smooth even with the engine running, this combined with the highly responsive nature of the both thruster and throttle leads us to the assumption that there is robust noise management on the control lines, as spikes or abrupt changes would be reflected in the physical system with potentially dangerous results. We assume these are also high-impedance inputs since this is a

common feature of electronics inputs, the relevance of this assumption is that the voltage dependent inputs of the kayak propulsion system will require low current from interfacing hardware to achieve the desired results, reducing the demand on interfacing circuity. It further tells us that autonomous control voltages must be equally smooth to those supplied by the joystick if the same degree of control granularity is desired.

Both throttle amount and thruster position are controlled by servo motors. The throttle servo is a standard 50Hz PWM controlled device. The thruster uses a 6-pin linear actuator whose movement angles the thruster either left of right, $\pm 45°$ from center axis. The type of actuator was unable to be ascertained from a physical inspection and control signals. To simplify the implementation, it was decided that instead of directly interacting with the servos, a replacement for the joystick controller would be implemented. This would introduce fewer changes to the kayak itself and increase the ease of modification should the task need to be performed on future crafts.

Pixhawk 4 Characterisation

The characterisation of the Pixhawk requires significantly less effort as the full range of specifications and functionality are available in its online documentation. The Pixhawk requires a 5V source and approximately 500mA of current to operate. Power for the device is often the output of a dedicated regulator which enables the user to view the current battery voltage in the base station software (PX4, 2021). The literature implies the Pixhawk will be connected directly to devices that expect a standard 50Hz PWM control signal and offers support in producing these signals. The signals vary only in percent duty cycle[b] to serve as positional information for servo motors (PX4, 2021). Without connecting a 5V source to boost the voltage on the servo control pins, they produce a 0 to 3.3V signal with limited current output. This is relevant as 3.3 Volts is a standard microprocessor voltage, allowing a microprocessor to act as interpreter between the autopilot and the kayak. Finally both dialects are known.

[b]Duty cycle refers to the ratio of pulse duration over the total period of the signal expressed as a percentage (Horowitz, W. Hill, and Robinson, 1989a).

Lowrance HDS-7 Live Characterisation

Because the Lowrance is a modern, 'easy to use' device with many features, we must focus on the extent of its technical capabilities as they relate to collecting bathymetric data and interfacing options rather than the superfluous functions emphasised by advertisers. We begin by ensuring the Lowrance will be compatible with the pre-existing kayak power system. The manual states the system requires 10 to 16 Volts Direct Current (VDC), and a maximum of 2.4A meaning the SONAR device will have no issues functioning with the Mokai. Since the Lowrance is a stand-alone device, the bulk of the interfacing effort is ensuring it has adequate power to collect data, however, since it is so heavily computerised, the extent of the networking capability must be investigated as this may provide additional interfacing options.

The Lowrance is able to host a local Wi-Fi network which gives the user access to cell phone integration and other features (Navico Holding AS, 2018b). Lowrance provides a mobile 'App' to remote control the SONAR module, though this would not likely be feasible for this project as the craft is expected to travel well outside the range of a reasonable Wi-Fi connection. To characterise the HDS-7, a laptop running Wireshark, a popular network protocol analyser, was connected the local Wi-Fi network and performed a port scan[c]. Some unadvertised functionality was immediately presented, the most useful being a File Transfer Protocol (FTP) service running on TCP port 21, a local web server running on TCP port 80 accessible through a web browser, a GStreamer rtspd on TCP port 554 accessible through video playback programs, a NMEA 0183 output on TCP port 10110, and several other unknown protocols on low UDP ports. Table 2 summarizes the use of these protocols in the SONAR module.

The FTP port allows an anonymous login with read access to the internal storage, and read-write access to the external SD card. This provides a means to download or delete SONAR logs without having to physically interact with the SONAR device or ASV. The web server provides the same ftp functionality but through a browser by navigating

[c]A port scan is used to search a host for open ports to determine what services are running (contributors, 2022b).

Protocol	TCP Port	Function
FTP	21	Enables the download of SONAR logs via FTP client over a local network.
Web Server	80	Allows a user to connect to connect to the SONAR head using a web browser to download SONAR logs over a local network.
GStreamer rtspd	554	Provides a live-steam of the SONAR display as it appears on the device, >1s latency.
NMEA	10110	Connect via PC using telnet, displays current depth, position, water temperature and other diagnostic information at 1Hz.

Table 2: Lowrance protocol summary.

to the SONAR head's IP. The GStreamer port allows for remote viewing of the user interface through 3rd party video playback software. VLC media player by VideoLAN (*version 3.0.16*) was used, and the following address entered in the 'Open Network Stream' dialogue *rtsp://DEVICE_ IP:554/screenmirror*, where '*DEVICE_ IP*' is the current IP address of the SONAR head. Remote viewing of the user interface was possible, though a latency of greater than one second was observed.

The mobile 'app' recommended by Lowrance was installed on a cell phone. While the 'app' is the only current method of remotely operating the SONAR module it failed to function reliably, it would fail to connect to the SONAR device, and then fail many of the automated processes intended to simplify the device connection process. Unfortunately the 'app' did not offer a method of performing the simple tasks manually. Wireshark analysis showed the 'app' attempted to connect to Facebook, Amazon, and other remote servers. Due to both the lack of functionality and concerns over data privacy, the 'app' was not used in this project.

There may be some method of remotely managing SONAR logging on the HDS-7 through Websocket or remote hardware means, but such an effort is outside the scope of the project. Instead, to ease the data capture process, a user programmable context button on the faceplate was configured to quickly start and stop SONAR logging.

Because the sample rate of the SONAR is not provided in documentation or through

conversations with sales people or technical support staff, the sample rate will be determined by analysing recorded depth data. Each entry in the **.sl3* log file is accompanied by a date-time stamp, visible after exporting the log file as **.csv* via Reef Master. Using Microsoft Excel, these values will be converted to seconds, and the minimum, maximum, and average sample rate will be determined for each survey speed. Sample rate informs the granularity of captured data which, depending on the capture rate may inform maximum survey speed. Too high a speed may reduce data resolution to undesirable levels, where the craft would 'overrun' the data capture rate, analogous to overrunning one's headlights when driving at night. Date-time entries will be parsed using Excel's *mid* command which returns a specified number of characters from a specified point in the a string. These hours and minutes will then be converted to seconds, and summed with the existing seconds data to give a total time in seconds which represents when the data was captured. The difference in time between samples can then be determined by subtracting a given sample time from the previous sample to acquire the time between samples. The time between samples informs how quickly data is being recorded. Basic statistical values will be extracted from the time differences using Excel commands *min*, *max*, *stdev.p*, and *average*. To acquire the average sample frequency, the average time between samples will be inverted as shown in Equation 3 to determine the sample frequency in Hertz (Hz).

$$f_{sample} = \frac{1}{T} \tag{3}$$

where:

f_{sample} = sample frequency
T = sample time in seconds

Pixhawk and Mokai Interface Circuit

The characterisation process has revealed, aside from power availability from the Mokai stator, the input signal requirements for kayak navigation, and the output signals sent by the autopilot to control throttle and steering of external hardware. Interfacing

hardware is required between the Pixhawk and the Mokai to translate the output signals from one to the expected input signals of the other. We know the Pixhawk will output a 0 to 3.3V square wave, PWM signal with a varied duty cycle between 5.5% and 9.5%, and that the Mokai requires varied DC on both the steering and throttle control lines that scales between approximately 0.5V and 4.5V as shown in Table 1.

The goal of the interfacing hardware is to equate the 5.5% and 9.5% duty cycle output signals to the 0.5V and 4.5V input signals expected by the kayak. A Texas Instruments MSP430G2553 Mixed Signal Reduced Instruction Set Computer (RISC) Microprocessor Unit (MCU) in a 16pin Dual Integrated Package (DIP) integrated circuit (IC) was selected for versatility. This device will perform linear calculations to equate the input values to the desired output values. Because the kayak expects varied DC and not the digital values that would otherwise be produced by the MCU, a MAX 518 Digital to analog Converter (DAC) (8 pin-DIP) was used to convert the result of the MCU's calculations to an analog voltage. The DAC receives digital words from the MCU which correspond to discrete analog output voltages, therefore the commands sent to the kayak will change at computer speeds rather than human speeds which may cause abrupt movement of the kayak hardware. Abrupt movements may increase wear on components and lead to a more inaccurate navigation process. To ensure smooth transitions between voltage levels and absorb any transient noise on the steering and throttle control lines, a Low Pass Filter (LPF) will be used at the output of the DAC. Figure 5 illustrates the signal flow from the Pixhawk to the kayak through the interfacing hardware. This process will be applied to both steering and thruster control signals.

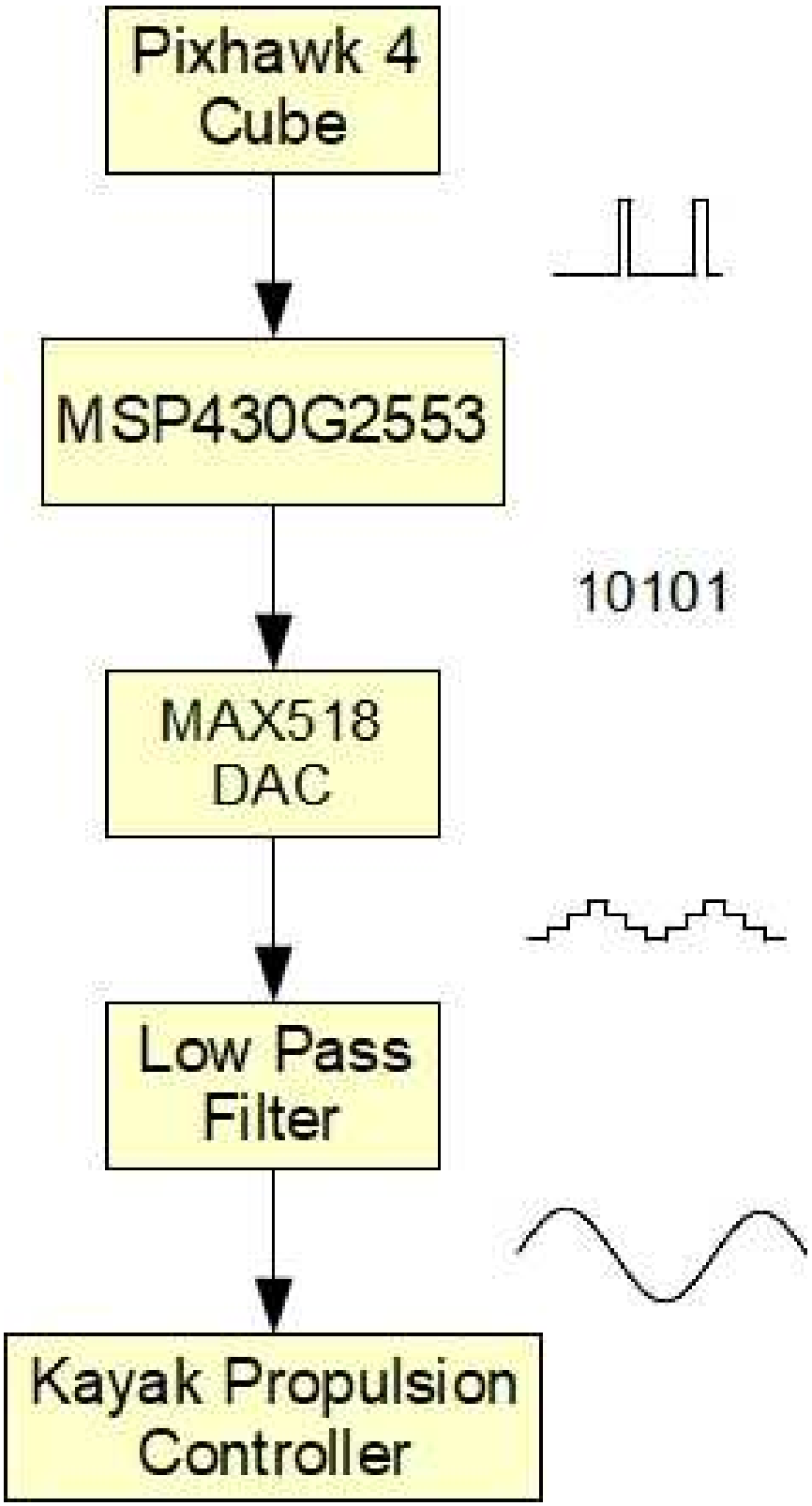

Figure 5: Signal flow from Pixhawk to Kayak.

Microprocessor

A TI-Launchpad MSP-EXP430G2ET development kit was used to program and debug the MCU. The kit allows for a single MCU to be programmed and then removed from the programming socket for use as a standalone device in an external circuit (Texas Instruments Incorporated, 2021). Texas Instruments provides development software for interacting with the MSP-EXP430G2ET, the package in use was Code Composer Studio, version 10.3.1, all code was written in C.

The conversion process begins when MCU samples the incoming waveform from the Pixhawk, but because both steering and throttle commands come at arbitrary intervals, the sampling thereof is a time sensitive process. If the MCU were to spend too long processing a steering waveform it may miss capturing a throttle waveform, or vice versa. While these waveform commands are being sent continuously from the Pixhawk, a lag in sampling may manifest as a delayed response. In order to achieve the fastest possible reaction time, the fastest possible MCU clock frequency was selected, for the MSP430G2553 this is 16MHz. At this rate, the MCU performs one cycle every $\frac{1}{16\times10^6 Hz} = 62.5 \times 10^{-9} Seconds$. Since all the Pixhawk control signals output with a frequency of 50Hz, or one cycle every $\frac{1}{50Hz} = 20 \times 10^{-3} Seconds$, when using a 16Mhz MCU clock rate, there are $\frac{50^{-1} Hz^{-1}}{62.5 \cdot 10^{-9} S} = 320 \times 10^3$ MCU cycles for every period of autopilot signal, ensuring the MCU can both sample and create the required output before the autopilot sends another command.

To sample the duty cycle, the MCU is configured with alternating edge sensitive interrupts on each of its two IO ports. Upon detection of a rising edge, the value of a time keeping variable is recorded for that input. The interrupt sensitivity is then changed to negative edges, as the signal leaves the high state (sends a negative edge), the value of the time keeping variable is again sampled and the edge sensitivity returned to positive edges. The difference between the two stored values is the 'time high' or the amount of time between the first rising edge and first negative edge. The 'time low' is calculated as the time between the last falling edge and the new rising edge, the period, or total time, is

the sum of the two. This process then repeats, continuously measuring the incoming waveforms. Equation 4 shows the calculation performed in software to determine the duty cycle. Usually duty cycle is represented as a percentage, which implies a floating point (decimal) number unless multiplied by 100. For our purposes, the numerator is scaled by 1×10^6 to ensure the 2 digit percentage and 4 decimal positions are expressed as a single integer. This is done to increase efficiency and avoid rounding errors that would otherwise occur from floating point math in MSP430 family MCUs (Report, 2006).

$$\frac{T_{High} \cdot 1 \times 10^6}{T_{High} + T_{Low}} = DC \tag{4}$$

where:

T_{High} = Time High
T_{Low} = Time Low
DC = Duty Cycle

The calculation of the desired output voltage results from a linear equation in slope intercept form, as represented in Equation 5. The scaled duty cycle represents the *x* value, however the slope, *m* and y-intercept, *b* values are not yet known.

$$y = m \cdot x + b \tag{5}$$

where:

y = Digital word to be sent to the DAC, representing the desired analog voltage.
m = Slope of the duty cycle vs analog voltage graph.
x = Scaled duty cycle from Equation 4.
b = Y intercept.

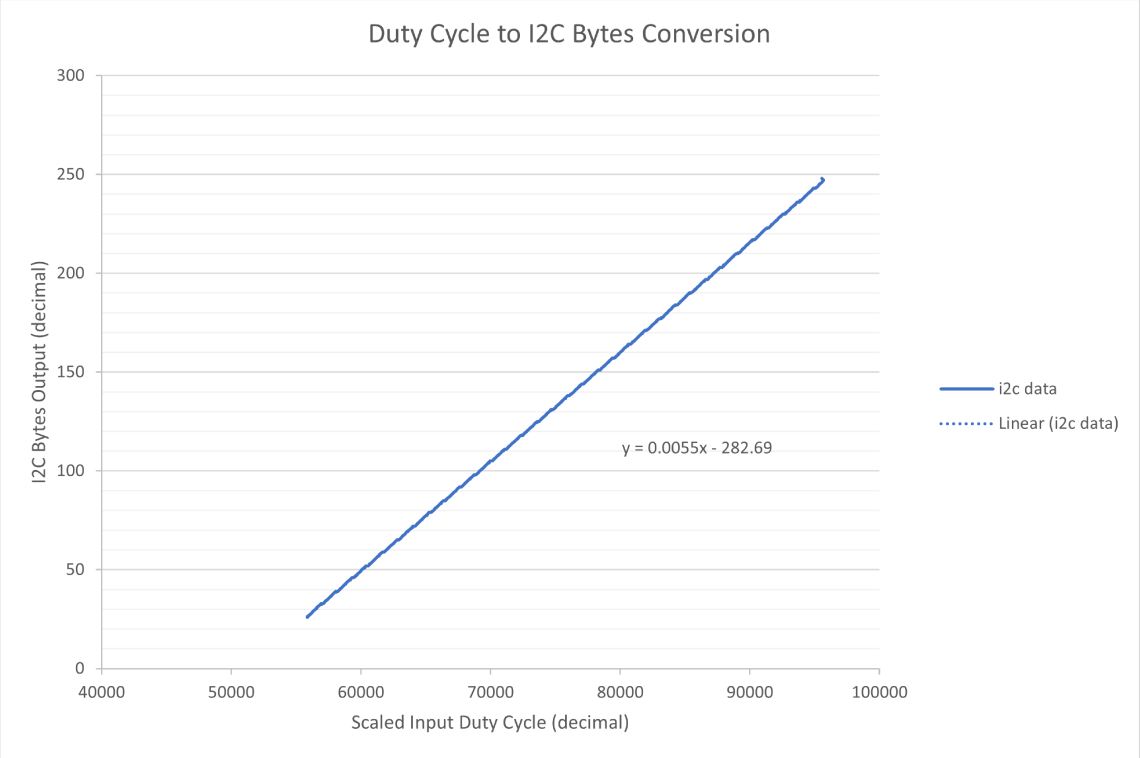

Figure 6: Input duty cycle to output 8-bit I2C word.

To quickly determine the *m* and *b* values, Microsoft Excel was used. Figure 6 shows the graph and linear equation produced by Excel. Values on the y-axis are the 8-bit words that represent a given voltage output from the DAC, this would equate to voltages from approximately 0.5V to 4.5V. The x-axis is the scaled duty cycle values that would occur as result of Equation 4. The axis values range from 55×10^3 to 95×10^3 as these would be the appropriately scaled duty cycle from 5.5% and 9.5%. In practice there would be some fine tuning of the required duty cycle values, but because the equation and behaviour are linear this formula should accurately represent values along the continuum of the line. Substituting the constants into Equation 6 gives:

$$Vout = 0.0055DC_{scaled} - 282.69 \tag{6}$$

where:

$Vout$ = Predicted output voltage
DC_{scaled} = scaled duty cycle

Similarly to the output of Equation 4, the *m* and *b* must be scaled to obtain integer

values to maintain software efficiency. To appropriately scale the equation's constants, they are shifted to the left by 14 bits, equivalent to multiplying them by 16384, and rounded to the nearest integer which results in Equation 7. The values were scaled via bit-shifts rather than decimal multiplication as the de-scaling will occur in software. Shifting bits left or right is equivalent to multiplication and division by powers of 2, however bit shifts are not as costly to processor resources in most cases. Equation 7 occurs in software, the constants *m* and *b* are pulled from memory, and the duty cycle is calculated as in Equation 4. The output of this equation is then bit-shifted to the right by 14 bits, equivalent to a division by 16384. The result is the appropriate 8-bit digital word to give the desired analog voltage for a given input duty cycle. The word is then sent to the DAC via I2C, a standard 2-wire communication protocol.

$$Vout = (90DC_{scaled} - 4631593) >> 14 \tag{7}$$

where:

$Vout$ = 8bit word corresponding to desired output voltage
DC_{scaled} = scaled duty cycle

To avoid redundancy and wasted cycles, Equation 7 will only be performed if the scaled duty cycle is greater or less than the previous value. This allows the processor to quickly resume sampling for changes in duty cycle. Figure 7 gives a high-level view of the MCU program flow.

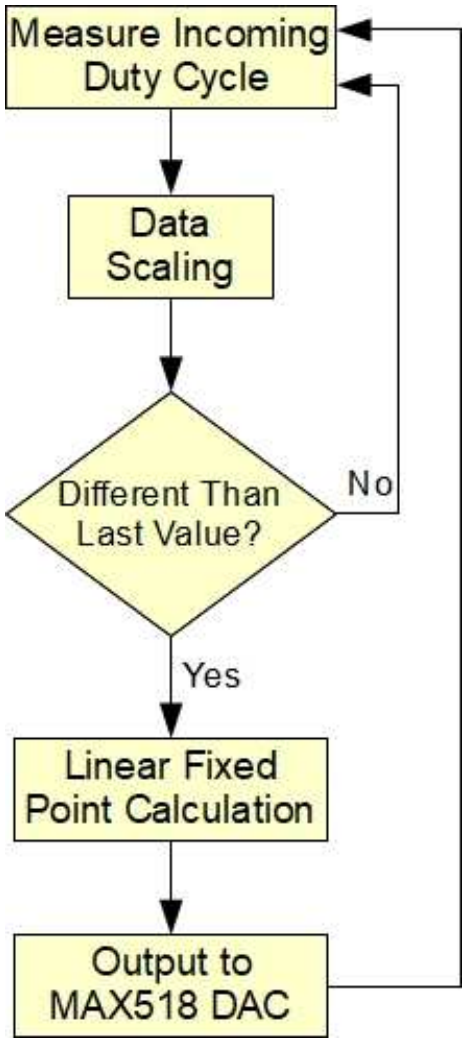

Figure 7: High level microprocessor program flow.

Digital to Analog Converter

Information from the MAX 518 datasheet (Maxim Integrated Products, 2002) states it is an 8-bit device, meaning the output can range from near 0V to the supply voltage, in this case, 5VDC. 8-bit resolution allows for $2^8 - 1 = 255$ voltage levels at $\frac{5v}{255bit} = 0.019608v/bit$. The device accepts a data rate of up to 400kbps, provides buffered outputs, low full-scale error of $\pm$20mV from 0V to supply voltage to ensure an accurate reproduction of the desired voltage level. The device has a 6μs settling time when changing output voltage levels to provide fast response time. Communication between the DAC and the MCU is facilitated by the I2C protocol. The MAX518 datasheet

(Maxim Integrated Products, 2002) states that the device considers a logic high to be $0.7VDD$, or since the Mokai $VDD = 5VDC$, 3.5V. This would imply the 3.3V used by the MCU would be insufficient to trigger the gates, however bench testing found the DAC responded to logic high voltages as low as 3.0V. Due to time constraints the SDA and SCL lines were provided pullup resistance to 3.3V with the provisions for level translation if required in the future.

Low Pass Filter

A simple, passive, first order resistor and capacitor (RC) based low pass filter was implemented at the output of the circuit. The aim of the interfacing hardware is to force the autopilot to mimic human input in order to fall within the original design constraints of the kayak. The joystick steering control is responsive, but slow, taking between two and three seconds for the thruster to sweep its full range of motion, with similar response from the throttle. For these reasons it was decided the filter corner frequency[d] would be 3Hz to ensure remove any input outside the original, expected control parameters, including switching artefacts from the DAC.

Equation 8 shows the process of verifying the corner frequency (f_c). Since we are limited to standard valued components when choosing circuit elements, the true f_c may differ slightly from calculations. The chosen components are as follows: Capacitor value, $C = 100 \times 10^{-6}F$, and resistor value $R = 500\Omega$, inputting these into Equation 8 gives an f_c of 3.1813 Hz.

$$f_c = \frac{1}{2\pi RC} \tag{8}$$

where:

$f_c =$ Corner frequency
$R =$ Resistor value
$C =$ Capacitor value

[d] Corner Frequency denotes the point in a filter's response where the output of the filter is half the power of the original input signal (Horowitz, W. Hill, and Robinson, 1989b).

Implementation

To facilitate both operator and autonomous control, a switch operated 12VDC, Dual Pole Dual Throw (DPDT) relay was used to control which input the kayak electronics would receive, switching between manual joystick control and autonomous control. The relay, circuit, and supporting hardware were placed in a 3D-printed case within reach of the operator when seated in the craft. Cabling was terminated with 12 position Deutsch connectors of appropriate style to mate with existing kayak circuitry, allowing the autonomous functionality to be an in-line, 'black box' style component requiring no actual modification of the kayak electronics.

Transducer Elevator

Placement of the transducer required careful thought. Traditionally the SONAR transducer is mounted on the transom or mount of an outboard motor in such a way that the transducer is submerged during regular operation (Navico Holding AS, 2021). The Lowrance manual states that the transducer should never be mounted on the underside of the craft as this will expose it to damage during operation and transportation. Given the topology of the Mokai this presented some challenges. The Mokai is jet propelled which produces substantial turbulence at the rear of the craft, further, the thruster physically moves left to right for steering, all of which may interfere with the transducer. The modular nose of the craft was ruled out as even at low speeds the nose tends to lose contact with the surface, a behaviour that increases proportionally with speed. The ideal location is one that would be submerged at operating speeds, yet allow the transducer to be protected in the shallow water and in transport.

In order to get the best results, a novel solution was conceived. A device that allows the transducer to reside within the hull of the kayak, only to be deployed when appropriate and safe to do so. The field ready version of the device encapsulates the SONAR transducer in a 3D-printed housing, and makes use of two stepper motors to evenly raise and lower the transducer. Using the same microprocessor as the Pixhawk to

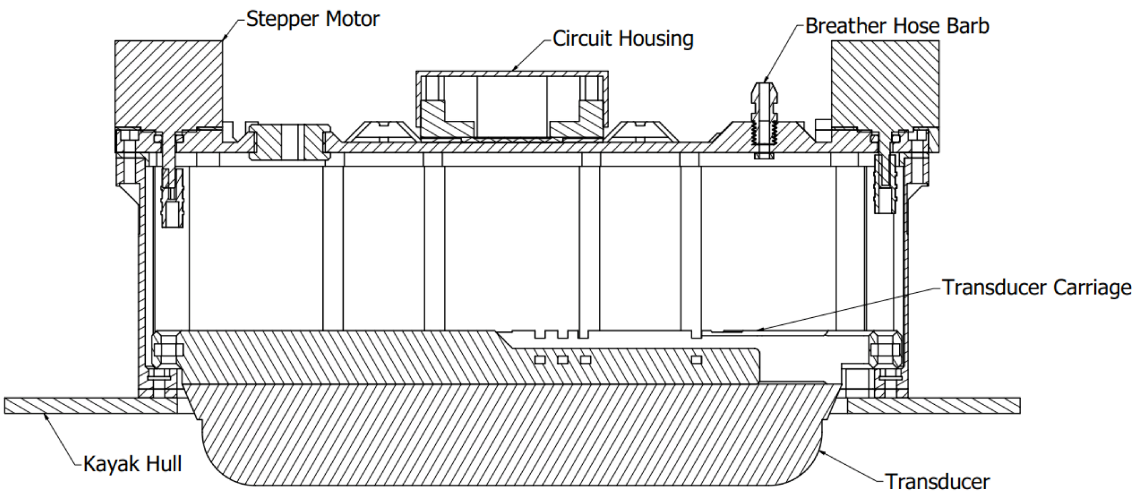

Figure 8: Cross section of the transducer elevator.

Mokai interface circuitry, a computer controlled circuit was created that receives commands from the Pixhawk, enabling the transducer to be deployed or retracted without operator input at certain locations in a mission. An in-craft operator may manually raise and lower the transducer using push-buttons, and while not in use for this current study, input from bump sensors would cause the transducer to recess in the event the kayak strikes a floating object. The transducer itself moves on a 3D-printed carriage supported by printed linear bearings guided by brass rods. Magnetic sensors are used to ensure that the carriage has reached the proper position, signalling the motors to stop. As a fail-safe, there is a software time-out that reverses the motor to the last position if these sensors are not activated to avoid jamming. A full cut-away view is provided in Figure 8.

Consumer grade fish finders are available in a through-hull format though these only provide depth sensing ability in relation to SONAR mapping. The Lowrance HDS Live series fish finders with the ’3-in-1’ transducer were successful in similar field operations and so was deemed to be the best choice for the current study. The added benefit of the ’3-in-1’ is that side-scan data can be collected in tandem with depth information. While side-scan imagery is outside the scope of this project in terms of tailings bathymetry, the imagery may still provide useful data to mining proponents, with potential science data should this project be adapted for use in future autonomous imagery surveys. Figures 9 and 10 show the transducer in its recessed and deployed states.

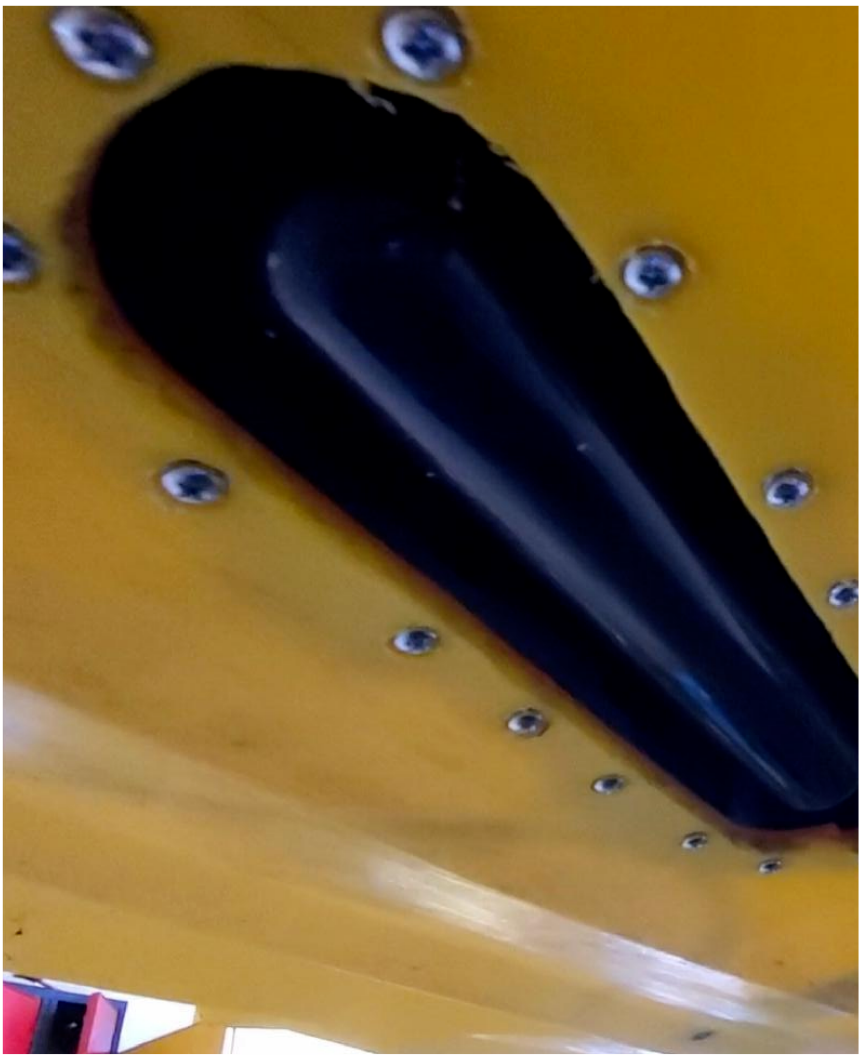

Figure 9: Transducer in the recessed state.

Figure 10: Transducer in the deployed state.

The transducer housing using a 3D-printed gasket to prevent water intrusion to the hull. Unfortunately local field testing showed this gaskets persistently leaked in a single location as a result of manufacturing limitations. Leaks were arrested with the application of marine sealant.

Water Management

Bilge pumps have been in use for hundreds of years as crucial components of a sea-fearing vessels (Oertling, 1996). Because the transducer elevator required modifying the hull to enable the sensor to be recessed within the body of the kayak, there was requirement for some form of hull water reduction in the event the transducer elevator housing leaked or was damaged during a mission. Further reason for in-craft water mitigation is simply to reduce water that enters the hull through wave or weather action, and spray from the thruster. Because the intended operating area for the ASV is an acidic tailings medium, a pump that had internal chemical resistance was required. Alongside environmental resistance, the pump would require an automatic start and stop, and a minimum run time to ensure a some minimum amount of water had been evacuated from the craft.

A small, permanent magnet DC motor peristaltic pump was selected for its low

current draw (250mA) and ease of control, the pump can move approximately 1L of fluid per minute. Peristaltic pumps mimic biological action by compressing a flexible tube to facilitate the movement of fluids, they function like a closed valve when not in use, and their internal workings do not contact the medium being pumped (Latham, 1966). Silicone tube was selected for its chemical resistance (Engineering ToolBox, 2014) and mechanical flexibility.

A float switch was created using a single pole single throw switch with packing Styrofoam on a lever arm. The arm is biased in such a way that a minimal amount of water at the lowest point of the craft will trigger the pump circuit. The pump circuit relies on a 555-timer configured as a 'one-shot' with a 5 second run time. When the switch closes the pump will run for minimum of 5 seconds, or as long as the switch is closed. This ensures that there will be no oscillatory behaviour where the pump is rapidly triggered by a threshold water level. The output of the pump is connected to a 3D-printed effluent port on the left side of the craft.

Hull Lighting

Since the engine power is less than 7500W there are few regulations to follow (Government of Canada, 2021), however some small craft are still required to have lighting. Appropriate lighting is pragmatic to make the ASV more visible to observers. Since the craft will be field tested in public waters, highly visible nautical lighting is a requirement to ensure warning visibility to potential pleasure craft operators.

Given the ASV's power and size, navigational lights required are green, red, and white. The white light requires a 360° field of view, red and green lights are required on the left, and right side respectively (Drive a Boat Canada, 2021; Government of Canada, 2021; Government of Canada, 2021). These are available in a variety of styles, so those that best balanced visibility and current consumption were selected.

STUDY LOCATION AND SURVEY METHODOLOGY

Given that this study occurred during 2021, the COVID-19 pandemic had greatly limited all but essential access to facilities, one result of this circumstance was the inability to perform the study in a real-world tailings facility, necessitating a substitute survey area. Field data was collected at West Oliver Lake (16UCU0662449302), a freshwater lake located near Thunder Bay Ontario. The lake has a soft, muddy bottom to mimic the bottom type presented by an effluent impound. The lake has gentle sloping sub-surface features and some submerged objects that, while not the focus of this study, can be used to opportunistically and qualitatively evaluate the imaging ability of the SONAR. Surveys will take place near shore with transects parallel to that shoreline in near north-south direction. The surveys extend approximately 100 to 180 metres into the lake and are executed at speeds of 2.5ms^{-1}, 3.0ms^{-1}, 4.0ms^{-1}, and 5.0ms^{-1}. Surveys were prepared with Mission Planner installed on a windows laptop. The laptop, or base station, was equipped with appropriate telemetry radio to communicate with the Pixhawk for active monitoring during surveys.

It is important to note that due to egregious pandemic related delays, field data collection was limited to the 17th and 24th of November 2021. Due to these delays, the mission length on the second day was altered to ensure the maximum number of surveys were performed, this accounts for the difference in transect patterns in Figure 11 and 12. After day one, the ASV's steering parameters were adjusted to allow the craft to more accurately follow the planned route, the results of which are shown in the results section.

On the first day, the survey extended approximately 180m into the lake, transect spacing was a fixed 10m and began 20m off the shore. The area of the survey was 23546m^2 as measured in Mission Planner, and divided into 16 transects as shown by Figure 11. Seven surveys were performed, their number and speed are detailed in Table 3.

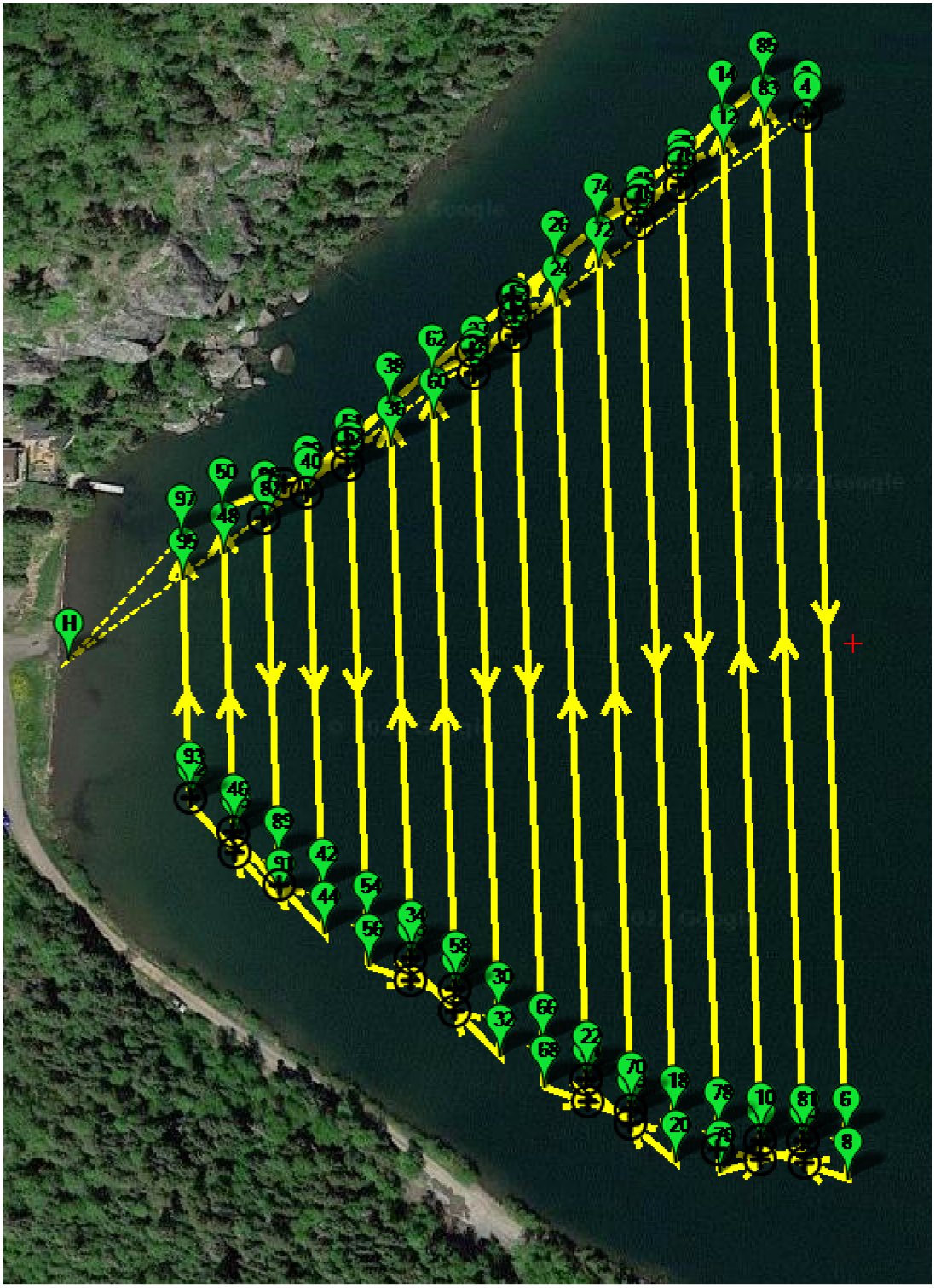

Figure 11: West Oliver day one waypoint mission plan with 16 transects.

Mission	Survey Speed(ms^{-1})
1	2.5
2	2.5
3	2.5
4	3.0
5	3.0
6	4.0
7	5.0

Table 3: Day One survey details.

The second day required shorter missions to maximize the available time, resulting in a reduced mission area. The survey again begins 20m off shore though only extends 100m into the lake with a total area of 6833m^2 divided into 7 transects, again with fixed 10m spacing as seen in Figure 12. Nine surveys were performed at the same selection of speeds as day one. These are detailed in Table 4.

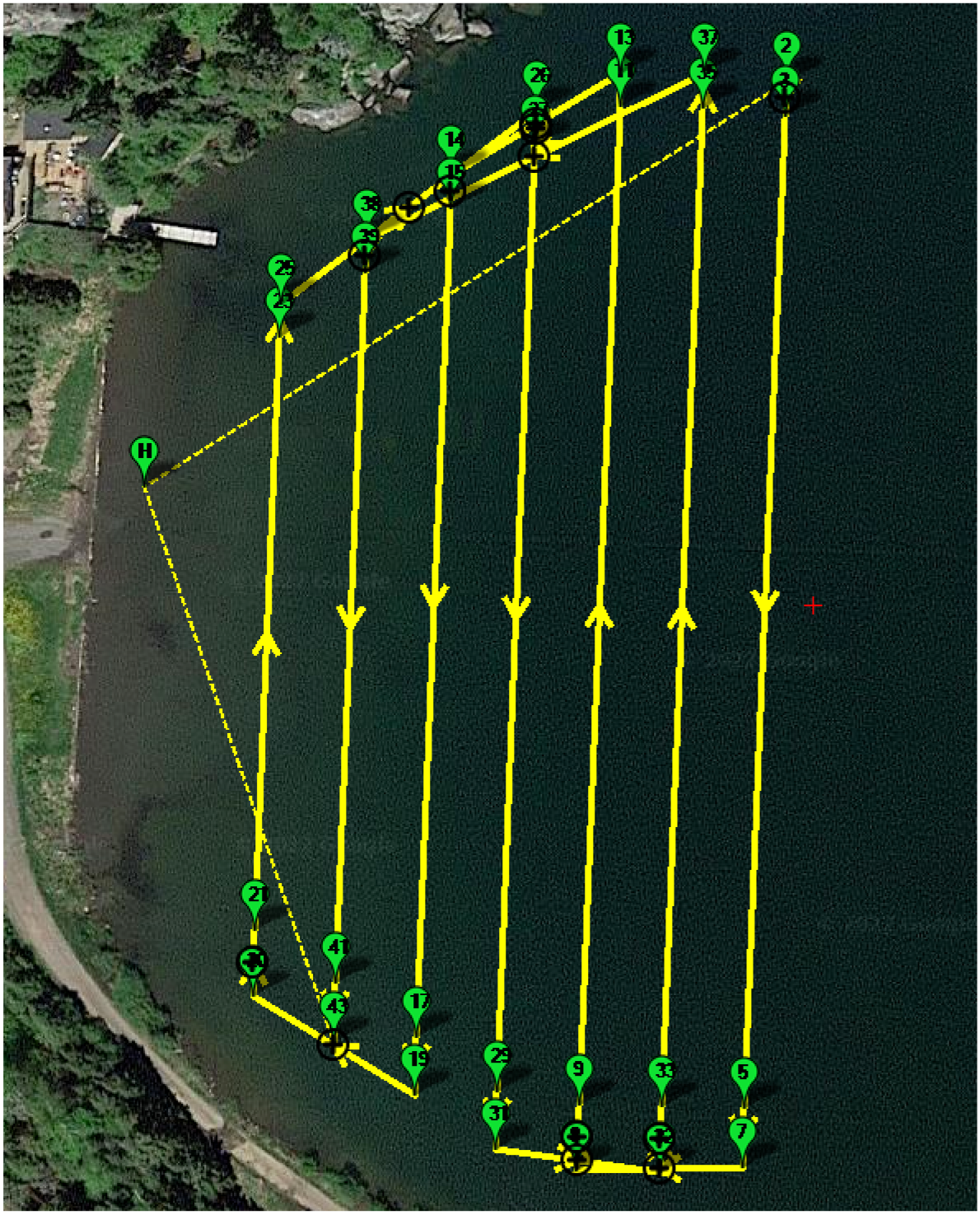

Figure 12: West Oliver day two waypoint mission plan with seven transects.

Mission	Survey Speed(ms^{-1})
1	2.5
2	2.5
3	3.0
4	3.0
5	4.0
6	4.0
7	4.0
8	5.0
9	5.0

Table 4: Day Two survey details.

BATHYMETRY

Because the Lowrance manual states a maximum speed for survey efficacy but no minimum speed (Navico Holding AS, 2018a), the assumption made in this study is that data quality is inversely proportional to speed, therefore 2.5ms^{-1} will be considered the speed that delivers the most accurate information. The 2.5ms^{-1} surveys will be used to check consistency of other speeds and make comparisons to historic data. Bathymetric data will be sampled by the fish finder continuously from the time the craft launches to the time it returns to shore. The data will be imported to Reef Master where it will then be exported in a generic **.csv* format for use in ArcGIS pro, once in ArcGIS, all but the individual transects will be removed.

The process of preparing the data starts with the interpolation of survey data points previously imported as a **.csv* file, interpolation is performed using Empirical Bayesian Kriging with the following settings: subset size of 100, overlap factor of 2, 100 simulations with between 25 and 50 neighbours and a radius of 25 metres, creating a raster with a 1m resolution. Since interpolation error increases with distance from the source data

points, sampling as close as possible to the source is desired. Discrete points are created in ArcGIS along the center of each transect at approximately $\frac{1}{10}^{th}$ the total length of the transect. Depth data is then captured at these discrete points, creating a new dataset for each survey. This allows for comparisons across multiple speeds and surveys from fixed reference locations. The new datasets created are then exported to Excel where they are averaged by speed to reduce the influence from errors introduced by variation in the GNSS fix, unknown temperature fluctuations at depth, instrumentation error, and changes in transducer angle. Data from both field days must be combined since there are too few surveys to make statistically meaningful comparisons from either field day alone, though this will likely increase the error as the survey paths are slightly different. To facilitate the combination of data, only those discrete points that are common to day one and two are used, resulting in 18 points. Appendix III contains the discrete point data from from each day independently. Table 5 shows the total number of surveys used to construct the 18 points.

Number of surveys	Survey Speed(ms^{-1})
5	2.5
4	3.0
4	4.0
3	5.0

Table 5: Number of surveys per speed.

Conditions during both survey days were fair, with negligible wind, current, or wave action, and therefore, environmental conditions are not likely responsible for variability in results.

The SONAR frequency used was 200kHz as this was the highest frequency available for depth sounding. A high frequency was used since the soft bottom would be less permissive to higher frequency, and therefore there would be potentially fewer incidence of misreporting depth. To accommodate for instances of misreported depth, the data

would be manually corrected in Reef Master for instances where the numerical depth value is reported as above or below the true sonograph represented in the software.

Historic data was collected from the website Geodisy *(https://geo.frdr-dfdr.ca)* (Ontario Data Catalogue, 2018). Positioning was acquired via GNSS, with measurements provided by 'GIS derived means'. The survey date was 29 August 2003, has positional accuracy within 5m, and draws a new depth contour every 3m (Ontario Data Catalogue, 2018). The contour data was converted to point data in ArcGIS and interpolated using the same Bayesian Kriging interpolation settings from previous interpolation, this is done to allow the historic data to be sampled by the same discrete points. Also contained in the historic data was the point sample locations, though these only contain positional data. All field transects are shown together with the historic sample points and topography lines in the results section, Figure 23.

STATISTICAL ANALYSIS

Combining points common to both field days allowed for a minimum of three surveys per speed to be evaluated. The resultant data consists of 18 points per survey speed. The depth values at these points were exported from ArcGIS and imported to Excel where single data sets for each survey speed of 2.5ms^{-1}, 3.0ms^{-1}, 4.0ms^{-1}, and 5.0ms^{-1} were created by averaging the respective survey points. The statistical methods of comparison are Student's T-test and Root Mean Square Error (RMSE).

Equation 9 is for the confidence interval of 95%, Equation 10 shows the calculation for standard error, and Equation 11 is for standard deviation.

$$c_{i\pm} = \bar{x} \pm t_{0.05,n-1} S_{\bar{x}} \tag{9}$$

where:

$c_{i\pm}$ = ± Confidence interval value
$\bar{x}$ = The mean sample depth
$t_{0.05,n-1}$ = Value for 5% of a t-distribution with n-1 degrees of freedom
$S_{\bar{x}}$ = Standard error

$$S_{\bar{x}} = \frac{s}{\sqrt{n}} \tag{10}$$

where:

$S_{\bar{x}} =$ Standard error
$s \ =$ The mean depth
$n \ =$ Population size

$$\sigma = \sqrt{\frac{\sum i = 1^{n} (x_i - \mu)^2}{n - 1}} \tag{11}$$

where:

$\sigma \ =$ Standard deviation
$x_i =$ The i^{th} depth value
$\mu \ =$ Mean depth
$n \ =$ Number of depth samples

The t-test requires two samples, each with an assumed Gaussian distribution and equal variances. Samples are paired since each sample represents the depth at a specific location sampled at two different speeds; all datasets are of the same size and unit. Equation 12 is used for calculating the t statistic for each of the speed datasets. After finding t values, P values can be found using a t-test distribution table or a software package for more exact results, for this study, Microsoft Excel was used to calculate all statistical values.

$$t = \frac{\sum d}{\sqrt{\frac{n(\sum d^2) - (\sum d^2)}{n-1}}} \tag{12}$$

where:

$t \ \ =$ Student's t-test
$\sum d =$ Sum of differences between samples
$n \ \ =$ Sample size

The degrees of freedom for the t test is $n - 1$, where n is the number of samples.

RMSE is used to obtain a representation of how much one dataset differs from another. RMSE is the square root of the average of squared errors, in this context errors are considered values that differ from the 2.5ms^{-1} (reference) survey results, where lower values present a closer match between reference and test data, and zero shows

no difference at all. The effect of each error has a proportional impact on the resultant RMSE, meaning outliers will have a greater effect on the result than data that closely matches. RMSE provides the difference in the same units as the source data. The formula for RMSE is provided in Equation 13.

$$RMSE = \sqrt{\frac{\sum_{i=1}^{n}(x_i - \hat{x}_i)^2}{n}} \tag{13}$$

where:

$RMSE$ = Root Mean Square Error
i = Datum index
x_i = The i^{th} true datum
$\hat{x}_i$ = The i^{th} test datum
n = The total number of samples

There are no statistical methods used to evaluate the performance of the electronics, however, the results of appropriate circuit tests for systems relevant to autonomous operation are presented in the results section.

RESULTS

ELECTRONICS

System elements such as lighting, pump activity, and action of the transducer elevator play important roles in the operation of the craft, but do not affect the ability of the craft to navigate and collect data; these systems performed their intended functions as expected. Overall current usage was difficult to gauge as all systems would have to be operating at maximum current capacity to have a true measurement. Current measurement were made between the battery and the complete kayak circuit, these measurements fluctuated between 4A and 4.5A with the engine running, all systems active, and the thruster sweeping from left to right. Battery voltage was sustained between 12.5 and 13VDC during testing and field activities.

Interface Circuit

We have previously discussed the interfacing methods used to facilitate communication between the Pixhawk and the Mokai. In this section we present the results of circuit tests used to ensure the appropriate signals are being sent. All measurements excluding those taken from the filter are captured in-situ, this was required as the interfacing hardware can not perform the necessary frequency sweep to show proper filter response. Also to note, only the response of a single filter is presented here, this is because both filters are identical and would have the approximately identical response excluding effects from component variation or temperature and environmental effects.

Tuning adjustments were made to steering and throttle parameters in the Pixhawk configuration to ensure maximum range of motion from the thruster and throttle control systems. This manifests as a change in minimum and maximum percent duty cycle for both parameters to values other than 5.5% and 9.5%.

The frequency response of the filters is most easily demonstrated by a Bode plot. To

create the plot, the input and output voltage (peak to peak) of the filter were recorded as the input frequency was incremented logarithmically from 0.1Hz to 10kHz. These measurements were used in Equation 14 to calculate the filter gain as frequency increased, with the results plotted in Figure 13. The x-axis shows frequency on a logarithmic scale, the y-axis shows the gain of the filter at each frequency increment. A gain of 1 denotes no change between input and output, a decrease in gain corresponds to a decrease in output amplitude. In Figure 13, we see a gain of slightly less than 1 at maximum, this is because the filter has no amplifying elements so the output will always be less than the input even in the pass band.

$$A = 20log(\frac{Vout_{pp}}{Vin_{pp}}) \tag{14}$$

where:

A = Gain in dB
$Vout_{pp}$ = Output voltage (peak to peak)
Vin_{pp} = Input voltage (peak to peak)

We have previously calculated the ideal value of the corner frequency to be 3.1831 Hz using standard components, however, actual results will differ primarily based on component tolerances, slight differences will also occur based on component temperature, and unaccounted for inductance and capacitance from the circuit topology. Excel was used to find the exact frequency where the output amplitude would experience a -3dB gain, this was calculated from measurements to be 3.002821Hz.

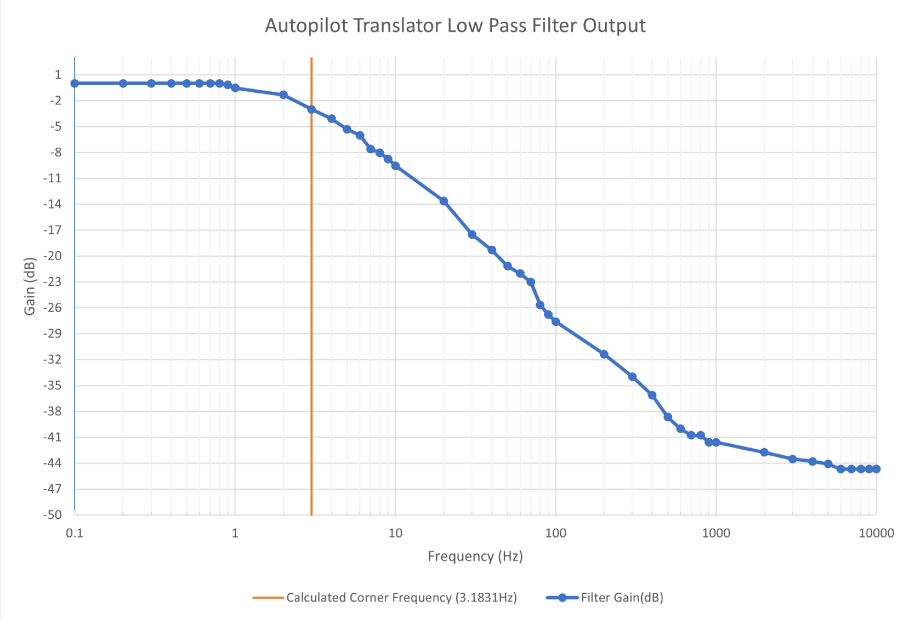

Figure 13: Low pass filter Bode plot with 3Hz corner frequency.

The result will be signals with frequencies greater than the corner frequency will begin to attenuate at a rate of -20dB per decade. Figures 14a and 14b illustrate how the filter effects signals passing through the circuit. Figure 14a shows a 0.5Hz signal in blue (channel 2) passing into the circuit, and a nearly identical signal in orange (channel 1) passing out. As the frequency of channel 2 increases the signal measured by channel 1 begins to attenuate and undergo a phase shift, this is clearly shown in Figure 14b where now the amplitude of the output (orange) is approximately 7.6% the of input.

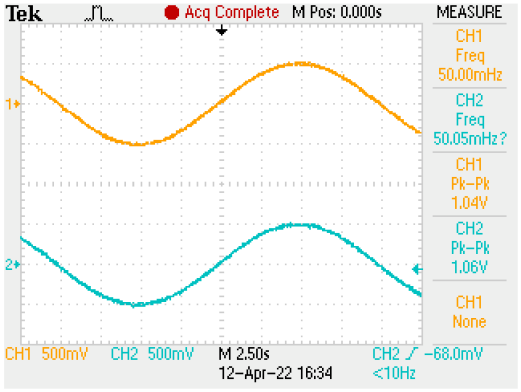

(a) Ch 1 output, Ch 2 input; 0.5Hz signal.

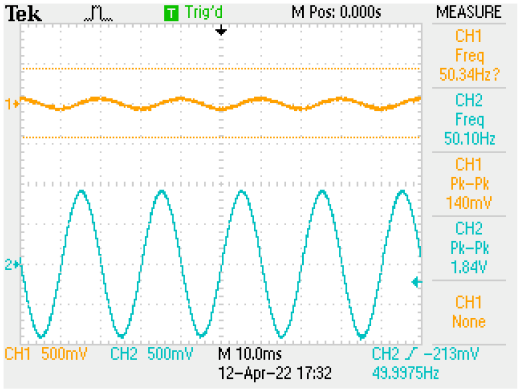

(b) Ch 1 output, Ch 2 input; 50Hz signal.

Figure 14: Filter response in and out of the passband.

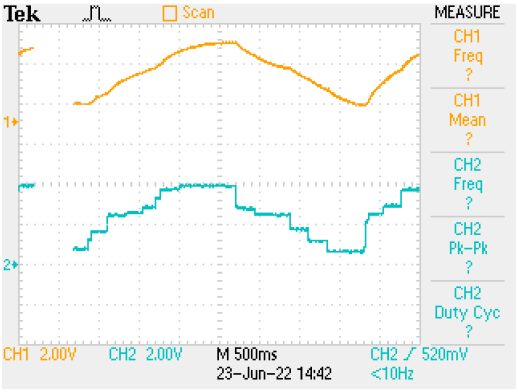

(a) Steering control pathway.

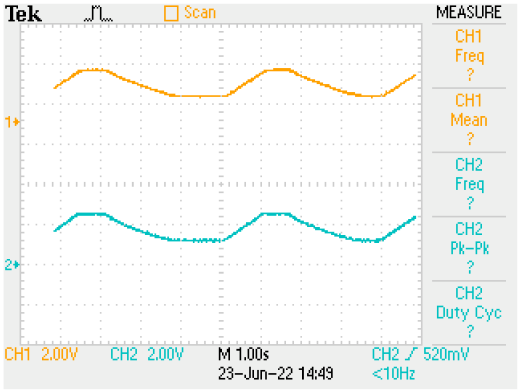

(b) Throttle control pathway.

Figure 15: Channel I DAC output. Channel 2 filter output.

With the filter in use showing anticipated results, we now look to the interface circuit for in-situ measurements of its filter behaviour and ability to translate the pulse train provided by the Pixhawk to the varying DC anticipated by the kayak. Figures 15a and 15b show the filter input signal provided by the DAC, and output of the filter for both steering and throttle filters. The pattern observed is caused by manually sweeping the steering and thruster between their extremes via manual control of the Pixhawk. The pseudo-sinusoidal pattern was intended to force abrupt changes in the DAC output to show how the high frequency components had been attenuated. It is important to note that in Figure 15b which shows the throttle pathway, we see a much smoother transition than in Figure 15a because the Pixhawk configuration option, *MOT_SLEWRATE* was set to 200. This forces the throttle to take a minimum of two seconds to sweep between minimum and maximum values to avoid sudden acceleration.

Figures 16a and 16b show the input and output of the interface circuit at both extremes for the steering pathway. We can see the duty cycles of 5.8% and 8.8% which reflect the desired tuned values. Similarly in Figures 16c and 16d we have the throttle pathway input and output from the interface circuit, again showing the minimum and maximum values. The 1.28v output is higher than what would normally be sent to the kayak, this was done to limit the Mokai's max speed to 5.0ms^{-1}.

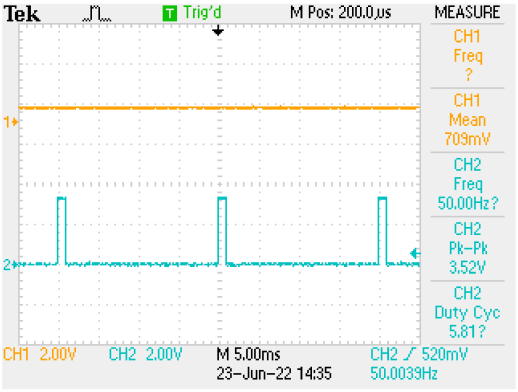

(a) Steering input at 5.8% Duty cycle, 0.7VDC output.

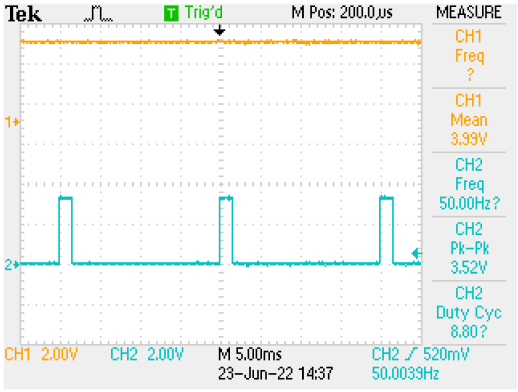

(b) Steering input at 8.8% Duty cycle, 4VDC output.

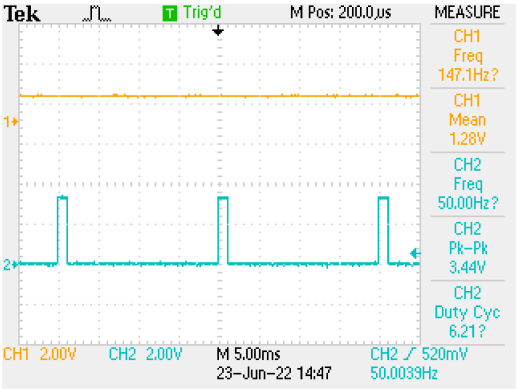

(c) Throttle input at 6.2% Duty cycle, 1.3 VDC output.

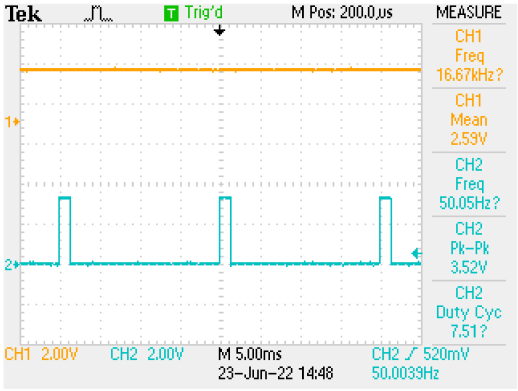

(d) Throttle input at 7.5% Duty cycle, 2.6VDC output.

Figure 16: Oscilloscope capture of steering and throttle control pathways.

Repeatability of Survey Transects

Repeatable surveys rely on the ability of the kayak to consistently follow the pre-planned route at multiple speeds. Points in Figure 17 are the locations where data was recorded. Mission speeds ranging from 2.5ms^{-1} to 5.0ms^{-1} from all surveys are overlaid to show the consistency of the transects.

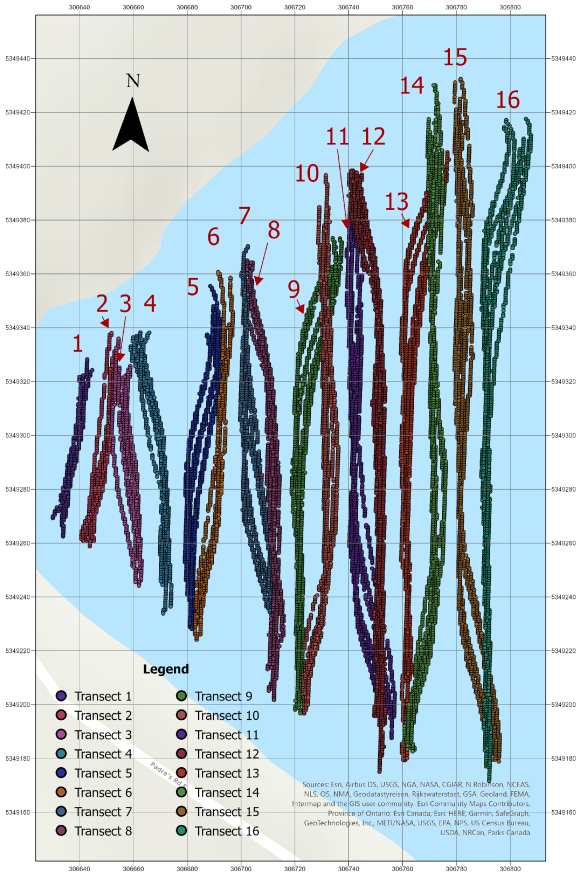

Figure 17: 2.5, 3.0, 4.0, and 5.0ms^{-1} transects from 17 November 2021.

Figure 18 shows all 9 day two surveys overlapped, steering parameters had been adjusted which accounts for improved adherence to the planned route.

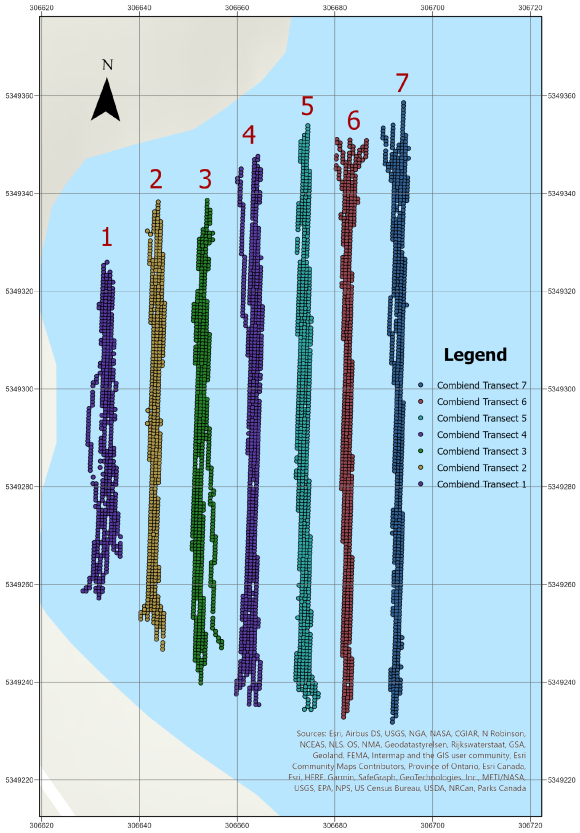

Figure 18: 2.5, 3.0, 4.0, and 5.0ms^{-1} transects from 24 November 2021.

Tables 6 and 7 show the transect information for both field days, the difference between well and poorly tuned steering parameters is highly evident.

Transect	Minimum X(m)	Maximum X(m)	Max. Width(m)	Minimum Y(m)	Maximum Y(m)	Transect Length(m)	X StdDev.(m)	X Mean(m)	Average Width(m)
1	306630.1137	306644.7005	14.5868	5349262.4851	5349328.2719	65.7868	2.9129	306638.4565	5.3833
2	306640.5655	306654.4713	13.9058	5349258.8104	5349337.9786	79.1682	3.2160	306648.7527	6.0738
3	306651.4006	306663.0556	11.6550	5349244.1714	5349335.8874	91.7160	3.1982	306657.7031	5.4147
4	306659.0170	306674.1309	15.1139	5349233.8512	5349338.2820	104.4308	3.9079	306670.7299	7.8827
5	306679.1069	306694.1112	15.0043	5349228.1534	5349360.6663	132.5129	4.6447	306686.0092	8.6006
6	306682.8829	306696.9901	14.1072	5349224.0844	5349360.6663	136.5819	3.3571	306692.7363	4.9892
7	306699.6445	306715.7902	16.1457	5349223.6840	5349370.3049	146.6209	4.5462	306705.6824	9.1662
8	306702.2150	306715.9260	13.7110	5349201.7472	5349364.9705	163.2233	2.8804	306710.9178	5.1746
9	306718.8030	306737.3769	18.5739	5349196.6935	5349373.2386	176.5451	4.6551	306724.0070	10.0779
10	306722.9784	306736.1341	13.1557	5349196.6935	5349396.6900	199.9965	2.5219	306730.9595	3.7412
11	306739.2022	306757.1328	17.9306	5349175.0460	5349398.3730	223.3266	4.6035	306745.6457	9.8653
12	306739.9717	306753.6235	13.6518	5349175.0460	5349398.3730	223.3266	3.2737	306749.8025	8.4929
13	306759.3383	306777.2529	17.9146	5349179.3960	5349405.1710	225.7751	4.1832	306763.9576	10.7985
14	306760.5346	306776.1262	15.5916	5349182.6390	5349430.0470	247.4074	3.3714	306770.4264	6.0982
15	306779.2867	306796.1174	16.8307	5349171.6610	5349432.3730	260.7123	4.4330	306784.6492	9.8848
16	306789.3211	306807.6876	18.3665	5349171.6610	5349417.5310	245.8699	3.6345	306792.9449	12.5878

Table 6: Day one geographic transect statistics, coordinates in UTM.

Transect	Minimum X(m)	Maximum X(m)	Max. Width(m)	Minimum Y(m)	Maximum Y(m)	Transect Length(m)	X StdDev.(m)	X Mean(m)	Average Width(m)
1	306628.4138	306636.1556	7.7418	5349257.2188	5349325.9226	68.7038	1.2578	306633.1955	2.6296
2	306640.2711	306645.1429	4.8718	5349246.7623	5349338.2512	91.4889	0.7806	306643.3103	1.6410
3	306650.8013	306656.8553	6.0540	5349239.8217	5349338.5773	98.7556	0.8933	306652.7874	2.4178
4	306659.8370	306665.2067	5.3697	5349235.4120	5349347.5718	112.1598	0.9565	306663.1761	1.9748
5	306671.9887	306676.5797	4.5910	5349234.3818	5349353.8992	119.5174	0.6948	306673.6953	1.4900
6	306680.2250	306686.4479	6.2229	5349232.8211	5349351.0276	118.2065	0.6714	306682.5862	1.6998
7	306689.8145	306695.0969	5.2824	5349231.8137	5349358.5750	126.7613	0.6757	306692.8990	1.2571

Table 7: Day two geographic transect data, coordinates in UTM.

COTS SONAR Data Sample Rate

Tables 8 and 9 show calculated SONAR sample rates. Figures 19 and 20 graphically represent the trend of increased sample frequency with increasing vehicle speed. Data recording rate is important as it informs the resolution of the sampled data.

Survey Number	Survey Speed(ms^{-1})	Mean Time Between Samples(s)	StdDev.(s)	Minimum(s)	Maximum(s)	Mean Sample Frequency(Hz)
1	2.5	0.2079	1.1088	0.0440	19.2850	4.8097
2	2.5	0.2420	0.9613	0.0430	19.0010	4.1319
3	2.5	0.3387	0.6443	0.0280	48.5100	2.9524
4	3.0	0.1660	0.8843	0.0100	32.1040	6.0238
5	3.0	0.2077	0.8990	0.0160	18.9910	4.8141
6	4.0	0.1655	1.0128	0.0330	17.6020	6.0420
7	5.0	0.2640	1.0111	0.0440	21.8570	3.7877

Table 8: Day one mean time between samples, and mean sample frequency.

Survey Number	Survey Speed(ms^{-1})	Mean Time Between Samples(s)	StdDev.(s)	Minimum(s)	Maximum(s)	Mean Sample Frequency(Hz)
1	2.5	0.2496	1.3141	0.0380	29.7810	4.0069
2	2.5	0.2494	0.9313	0.0450	17.7150	4.0096
3	3.0	0.2053	1.0147	0.0420	14.8980	4.8711
4	3.0	0.2396	1.3518	0.0420	12.7670	4.1731
5	4.0	0.1666	0.6790	0.0410	24.4130	6.0034
6	4.0	0.2092	0.8950	0.0400	26.6800	4.7798
7	4.0	0.1794	0.5578	0.0410	42.6670	5.5744
8	5.0	0.1497	1.0299	0.0440	12.7140	6.6781
9	5.0	0.1422	0.8287	0.0410	30.2690	7.0324

Table 9: Day two mean time between samples, and mean sample frequency.

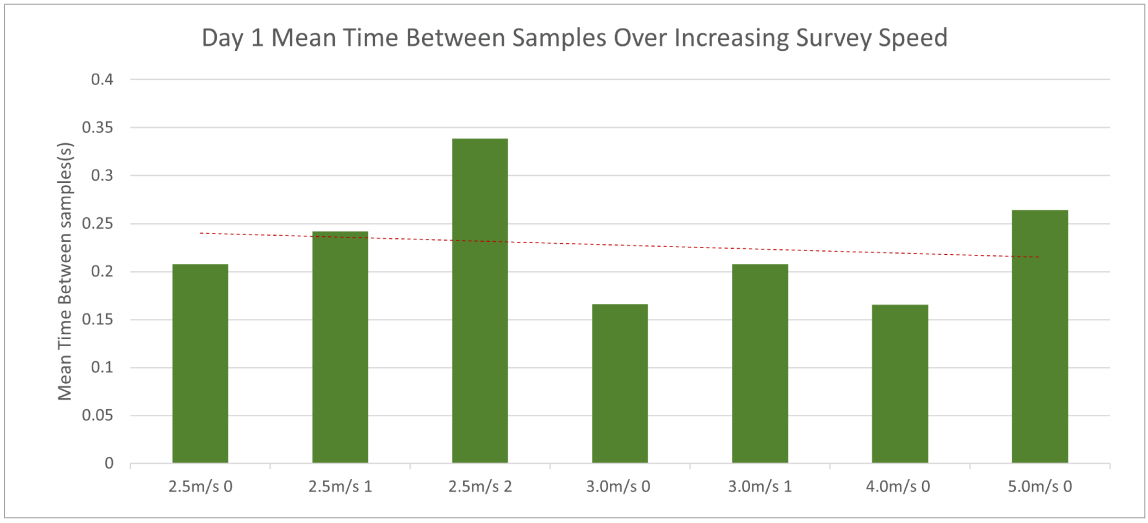

Figure 19: Day one sonar mean sample rate and standard deviation.

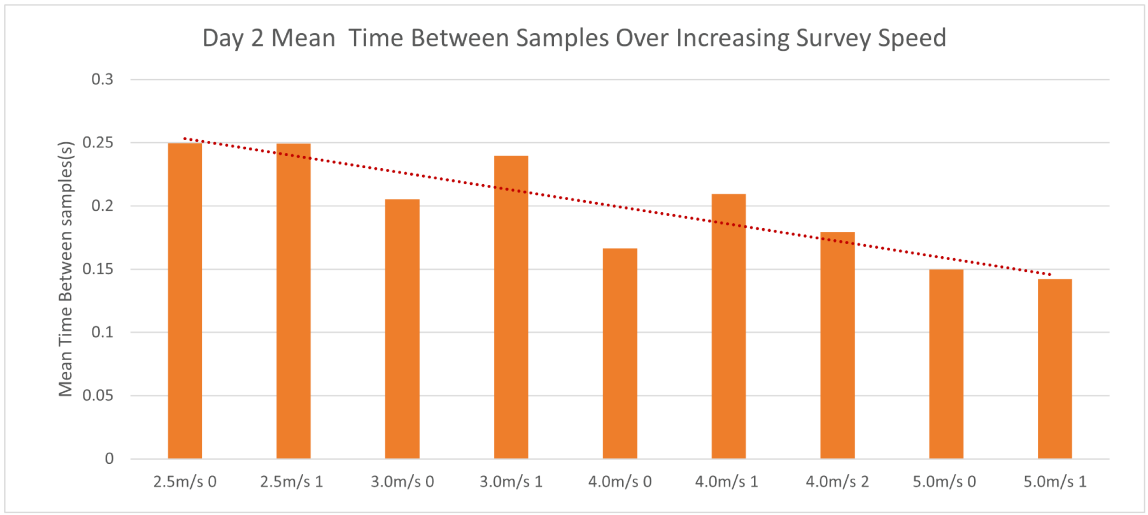

Figure 20: Day two sonar mean sample rate and standard deviation.

BATHYMETRY

In order to provide a minimum of three surveys at each speed, overlapping discrete points between field days one and two were used as discussed in Methods. Figure 21 shows the overlapping sample locations from both days. Figures 29 and 32 of Appendix III show the data points for day one and two respectively. Location data is provided by the saved SONAR log file created by the Lowrance fish finder, and can be considered accurate within 3m due to WAAS corrections.

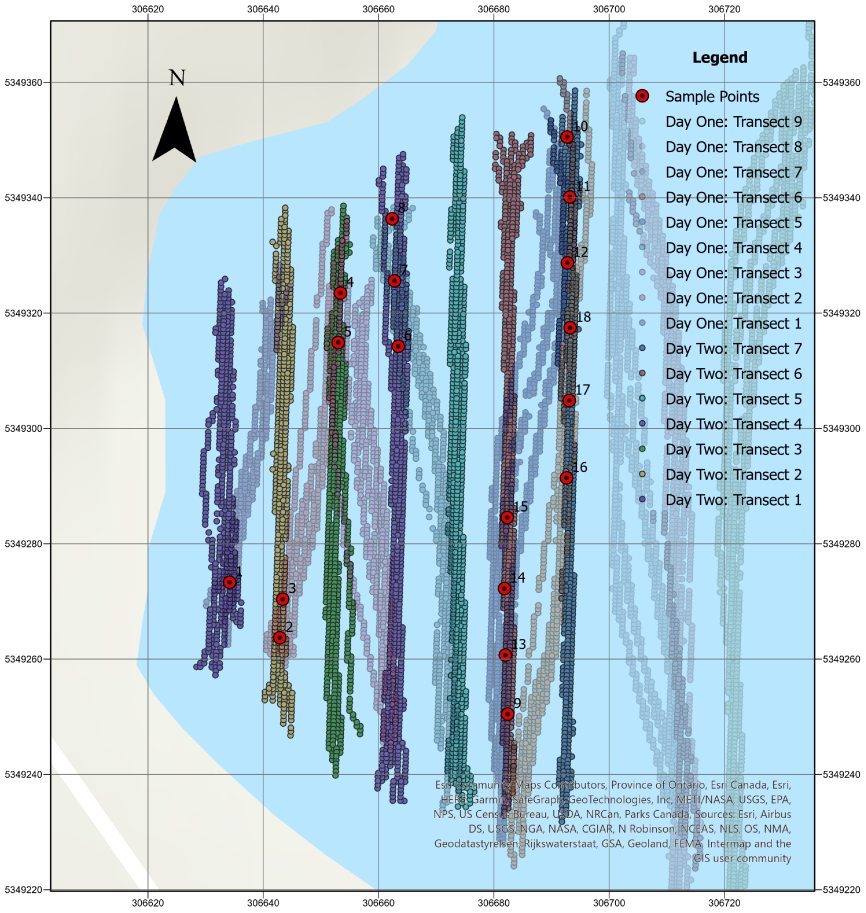

Figure 21: Combined survey sample points.

The following in Table 10 shows the sample number, the location for that sample in UTM coordinates, and the resulting averaged depth value for survey each speed and the historic data.

Sample Index	X Coordinate	Y Coordinate	2.5ms^{-1} Avg(m)	3.0ms^{-1} Avg(m)	4.0ms^{-1} Avg(m)	5.0ms^{-1} Avg(m)	Historic
1	306634.2	5349273.3	1.30194968	1.274931	1.342205375	1.378153	1.563748598
2	306642.9	5349263.7	2.346424198	2.13401	2.149841249	2.206258	2.567587137
3	306643.4	5349270.4	2.232788944	2.075406	2.095550358	2.080509	2.548142672
4	306653.4	5349323.5	2.405889893	2.4726	2.529096425	2.480642	2.894501925
5	306653	5349314.9	2.397480536	2.428145	2.53504324	2.436117	2.777612209
6	306663.4	5349314.2	5.10731926	4.620025	4.818288565	4.510707	4.063886642
7	306662.8	5349325.6	4.123791456	3.631323	3.961545587	3.853024	3.781098843
8	306662.3	5349336.4	3.669445515	3.495482	3.753793001	3.782088	3.50204277
9	306682.4	5349250.5	8.925782776	8.986962	9.00952816	8.947379	8.359323502
10	306692.7	5349350.5	8.916640091	8.94615	9.066776991	9.04614	8.118077278
11	306693.2	5349340.1	9.228710175	9.272859	9.355171919	9.250108	8.282571793
12	306692.8	5349328.7	9.328883743	9.416729	9.621622324	9.618934	8.021866798
13	306682	5349260.7	8.788443756	8.761067	8.829154015	8.894841	7.776986599
14	306681.8	5349272.2	8.535199928	8.62555	8.623222113	8.778879	7.273348808
15	306682.3	5349284.6	8.317502785	8.488136	8.517157316	8.632059	7.114650249
16	306692.6	5349291.4	9.400149918	9.366234	9.46851635	9.453844	8.569976807
17	306693.1	5349304.8	9.317472839	9.328719	9.520075798	9.418512	8.035682678
18	306693.2	5349317.5	9.266101074	9.354598	9.539625883	9.518031	7.906733513

Table 10: Combined day one and two resultant averaged survey data.

Figure 22 visualises the data presented in Table 10, historic data shown in red.

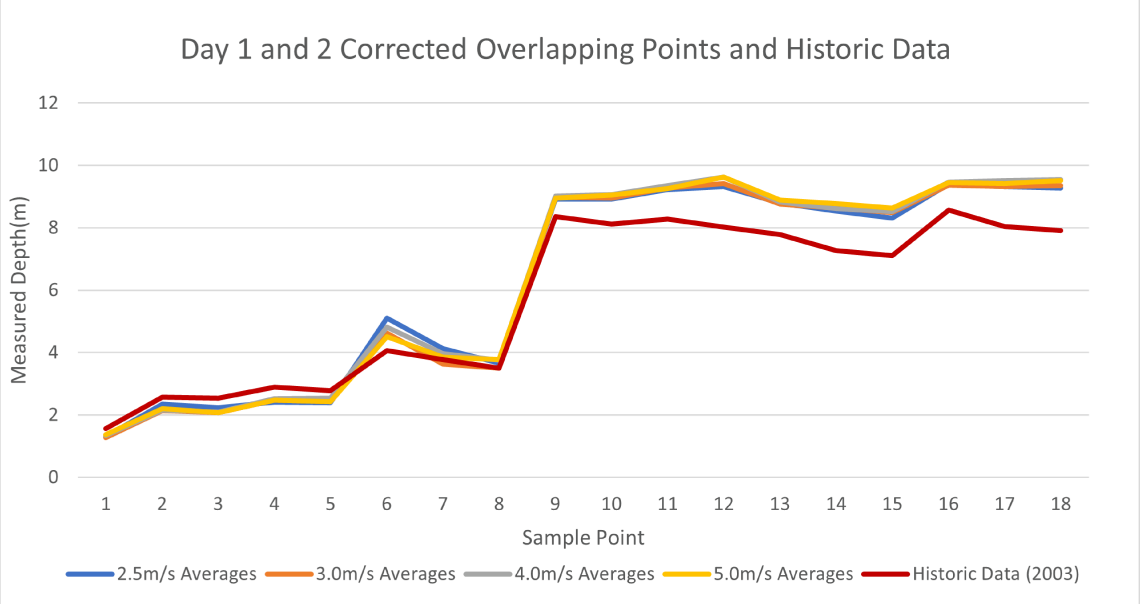

Figure 22: Survey averages and historic (2003) data.

Figure 23 shows the historic sample locations as red circles and depth contour lines. Depth starts at 0m and with a contour interval of 3m and 5m positional accuracy.

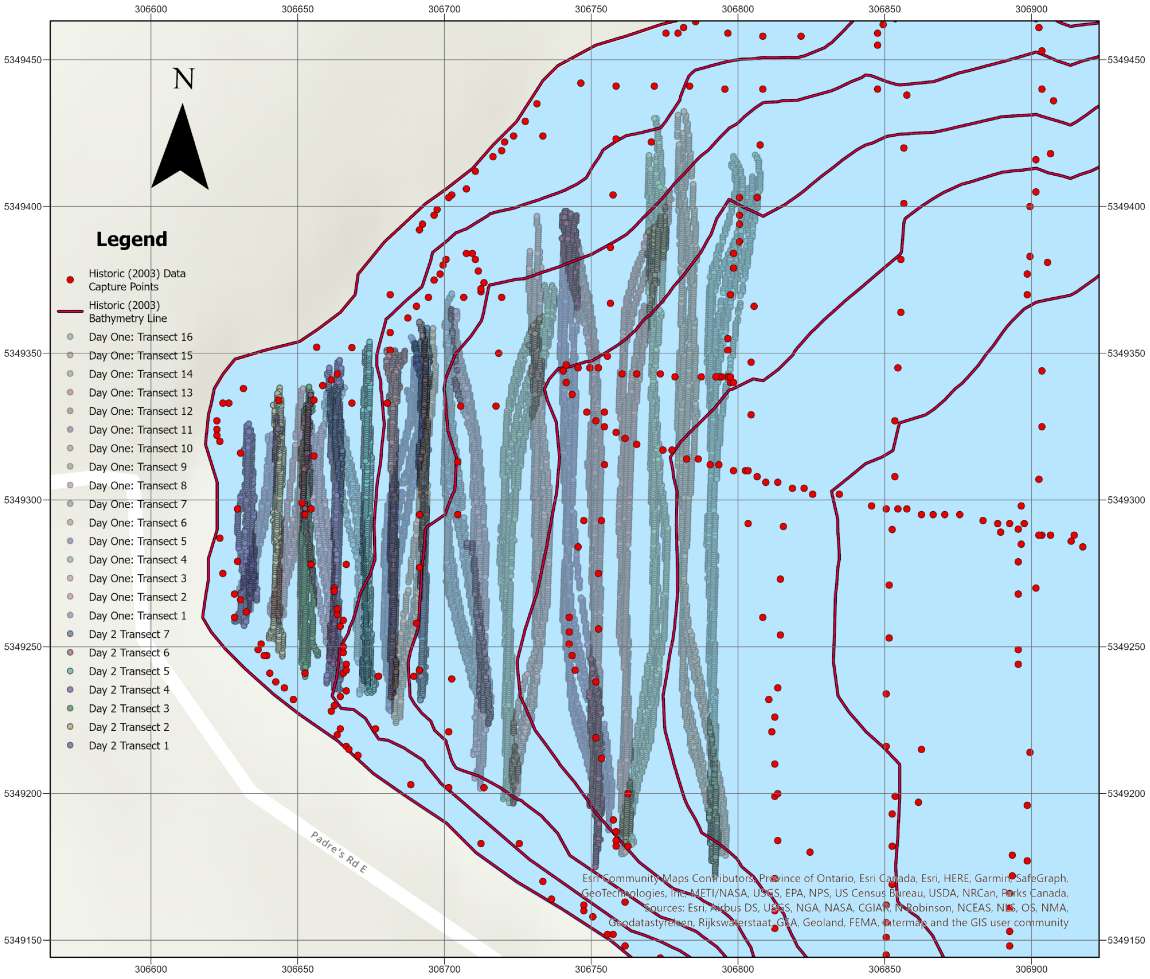

Figure 23: UTM 16N representation study and historic sample points.

Because we are considering the 2.5ms^{-1} surveys to be the most accurate, these are used to make a comparison between the historic sample locations and those acquired during the field study. Table 11 shows the number of points per survey, Table 12 shows basic statistics concerning the values in Table 11. Field surveys acquired between 786 and 965 points whereas historic data within the survey areas consists of 44 sample locations.

Field Survey(2.5ms^{-1})	Number of Samples
Day 1, survey 1	794
Day 1, survey 2	786
Day 1, survey 3	817
Day 2, survey 1	857
Day 2, survey 2	965

Table 11: Number of samples per 2.5ms^{-1} survey.

Mean samples	Minimum	Maximum	StdDev.
844	786	965	65.42599

Table 12: Field survey sample number statistics.

These tables are illustrated by Figures 24 and 25. Figure 24 Shows the historic depth sampling locations that fall within the survey area and Figure 25 shows how these samples compare to the sample locations from the second 2.5ms^{-1} survey of field day two. Figure 26 shows a comparison between contour lines generated using the average of all five 2.5ms^{-1} field surveys, and the historic contour lines. Field contour lines follow the same parameters as the historic data; a new contour drawn for every 3m increase in depth, starting with 0m at the shore line, though positional accuracy is 3 instead of 5m.

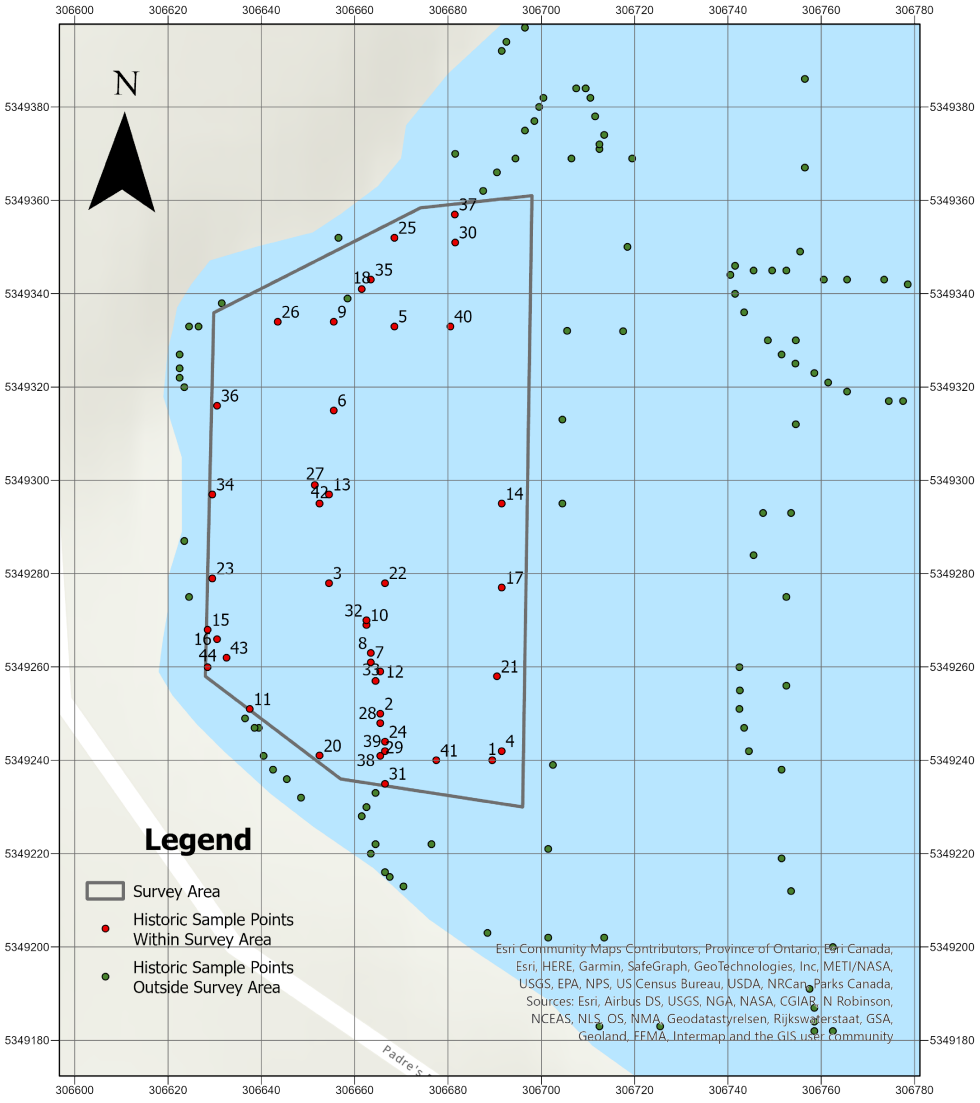

Figure 24: Historic depth sampling locations in the survey area.

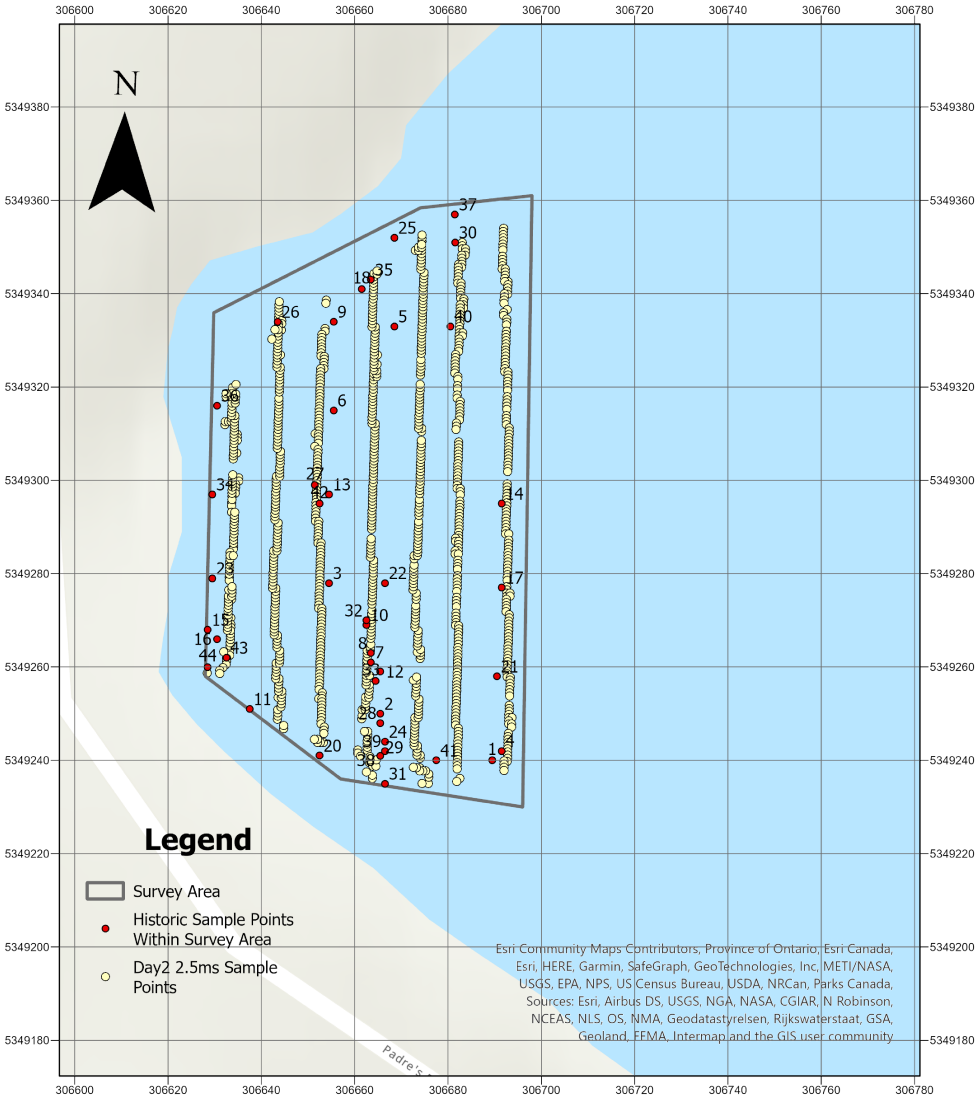

Figure 25: Historic and day two 2.5ms^{-1} field sample locations.

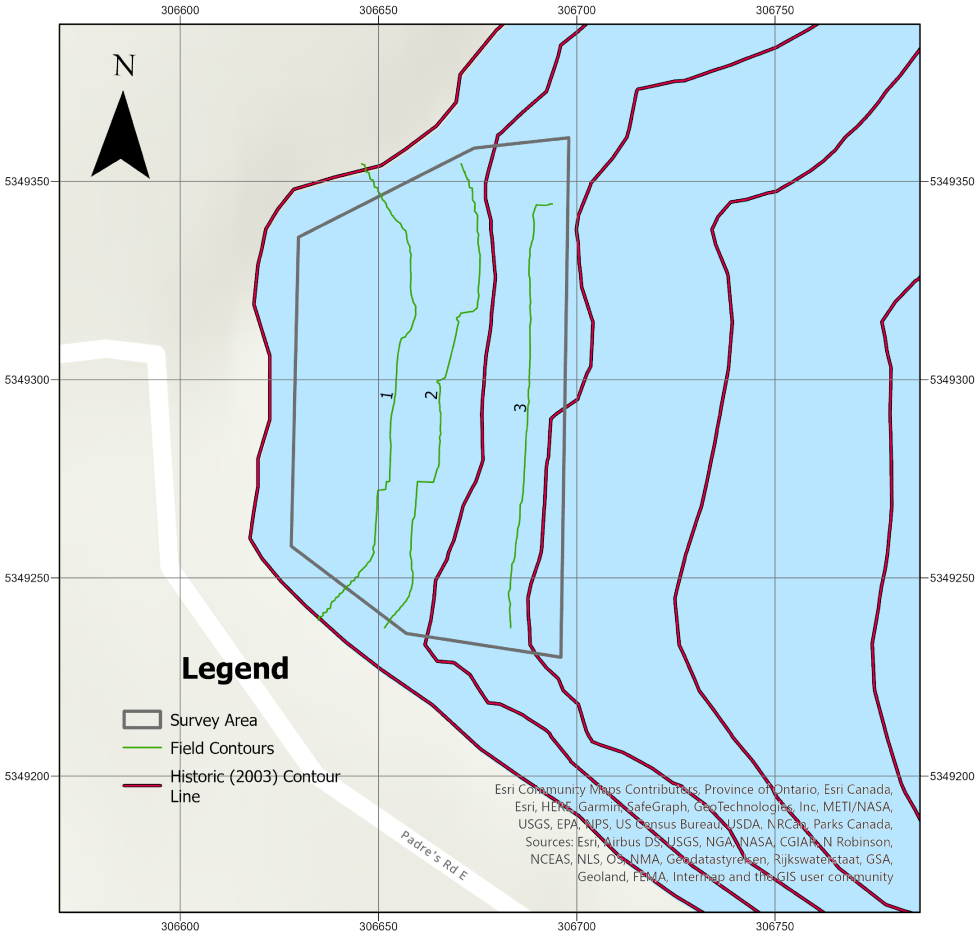

Figure 26: Historic and field contour lines, 3m per contour line.

Tables 13 to 16 show a summary of statistics, Table 17 shows the RMSE results.

Stat	2.5ms^{-1} Averages(m)	3.0ms^{-1} Averages(m)
Mean(m)	6.311665365	6.25994027
Variance(m)	10.28756477	10.87100367
Minimum Depth(m)	1.3019	1.2749
Maximum Depth(m)	9.4001	9.4167
Std. Deviation(m)	3.1171	3.2042
Degrees of Freedom	17	17
t Stat	1.168592928	
P(T<=t) two-tail	0.258694482	
t Critical two-tail	2.109815578	
95% Confidence interval	4.7616 to 7.8617	4.6667 to 7.8533

Table 13: 2.5ms^{-1} and 3.0ms^{-1} summary statistics.

Stat	2.5ms^{-1} Averages(m)	4.0ms^{-1} Averages(m)
Mean(m)	6.311665365	6.374234148
Variance(m)	10.28756477	10.8765027
Minimum Depth(m)	1.3019	1.3422
Maximum Depth(m)	9.4001	9.6216
Std. Deviation(m)	3.1171	3.2050
Degrees of Freedom	17	17
t Stat	-1.6486068	
P(T<=t) two-tail	0.117583862	
t Critical two-tail	2.109815578	
95% Confidence interval	4.7616 to 7.8617	4.7804 to 7.9680

Table 14: 2.5ms^{-1} and 4.0ms^{-1} summary statistics.

Stat	2.5ms^{-1} Averages(m)	5.0ms^{-1} Averages(m)
Mean(m)	6.311665365	6.349234688
Variance(m)	10.28756477	10.9648521
Minimum Depth(m)	1.3019	1.3782
Maximum Depth(m)	9.4001	9.6189
Std. Deviation(m)	3.1171	3.2180
Degrees of Freedom	17	17
t Stat	-0.72561913	
P(T<=t) two-tail	0.47794344	
t Critical two-tail	2.109815578	
95% Confidence interval	4.7616 to 7.8617	4.7489 to 7.9495

Table 15: 2.5ms^{-1} and 5.0ms^{-1} summary statistics.

Stat	2.5ms^{-1} Averages(m)	Historic (2003)
Mean(m)	6.311665365	5.730991046
Variance(m)	10.28756477	6.868880417
Minimum Depth(m)	1.3019	1.5637
Maximum Depth(m)	9.4001	8.5700
Std. Deviation(m)	3.1171	2.5470
Degrees of Freedom	17	17
t Stat	3.692022754	
P(T<=t) two-tail	0.001808897	
t Critical two-tail	2.109815578	
95% Confidence interval	4.7616 to 7.8617	4.4644 to 6.9980

Table 16: 2.5ms^{-1} and historic data summary statistics.

Root Mean Square Error for missions and historic data with respect to 2.5ms^{-1} survey data.

Survey Speed(ms^{-1})	Root Mean Square Error(m)
2.5	0.0000
3	0.1897
4	0.1685
5	0.2168
Historic	0.8705

Table 17: Root mean square error of all surveys with respect to 2.5ms^{-1}.

SIDE-SCAN IMAGERY

While not the focus of this study, side-scan data was collected opportunistically during surveys. Near the shore of West Oliver Lake was a submerged structure. This structure was present on the first transect and was therefore captured at various speeds. Figures 27a to 28b show how the side-scan imagery tends to change with increases in speed. The black bands present in 28a and 28b are caused by the transducer leaving the water while the craft is hitting its own wake or travelling so quickly the vehicle is at such an incline the transducer leaves the water briefly.

(a) Side-scan capture at 2.5ms^{-1}.

(b) Side-scan capture at 3.0ms^{-1}.

Figure 27: Side-scan imagery captured at speeds of 2.5ms^{-1} and 3.0ms^{-1}.

(a) Side-scan capture at 4.0ms^{-1}.

(b) Side-scan capture at 5.0ms^{-1}.

Figure 28: Side-scan imagery captured at speeds of 4.0ms^{-1}, and 5.0ms^{-1}.

DISCUSSION

The research objectives addressed here involved developing an understanding of the Mokai control electronics, the integration of the existing control circuitry with a COTS autopilot to facilitate autonomous navigation through the use of purpose built circuits, and determine the craft's ability to successfully perform consistent bathymetric surveys at various speeds without a human operator on-board. The overarching goal was to compare the data collected by an ASV created from COTS hardware with the data collected by a conventional crewed survey. This project does not seek to replace human operators, as crewed surveys are able to adapt to changing conditions and make context specific decisions. Similarly, this project does not propose a replacement for modern aerial drones since they are well suited for a multitude of remote sensing applications beyond the scope of this project. This study seeks to improve the ability of survey crews to perform bathymetry by providing a more efficient and systematic approach to surveying, and one that has potential to generate data that is significantly more dense with higher resolution all while improving operator safety.

Current use of human piloted surface surveys on the large gold tailings ponds present in NWO present a significant safety concern for the survey operators in the form of long-term health effects. Exposure to various toxic elements and compounds such as Arsenic or Cyanide in various forms pose a significant danger to human health. Operators require specialized training and Personal Protective Equipment (PPE), survey contractors would require insurance for those workers and the conventional craft they pilot. Ignoring the risks provided by the tailings environment, the multiple operators require salaries and per-diem if applicable. Transportation and maintenance costs of the larger crafts must be considered when contracted to conduct a survey. The ASV developed in this study has the potential to lower the costs of conducting surveys both to mine operators and survey contractors by providing a more cost-effective platform. The cost of the ASV in parts is similar to the cost of a single, low demand bathymetric survey. Obviously a contracted survey would supply the data analysis as part of the survey price,

however, this serves to illustrate the inexpensive nature of the ASV especially when compared to current similar solutions. Because the systems were developed to be in-line, 'drop-in' components, conversion kits could potentially be available to survey proponents which would allow for a low hassle conversion of a stock Mokai.

While the ASV in this study was deployed and tested individually, the software in its current state allows for 'swarm' operation, meaning multiple ASVs can work in tandem to cover a larger area in the same amount of time. Two ASVs would technically be able to reduce the time required on the water significantly through the division of responsibility.

The ASV is made entirely from COTS components excluding the interfacing circuitry developed for this study, because that circuitry only relates to guidance and not data collection, if the motor, fish finder, lighting etc. Suffers a deficiency of some sort it can be easily replaced without the need of specialized components that may be unavailable to proponents. Similarly, alternate components could be used, such as different remote sensing instruments. The Mokai uses a generic Kohler engine, meaning replacement engines can be purchased from multiple sources with a large body of open source information regarding their maintenance found online. For example, during the course of this study, an insufficiently tight motor belt snapped and a replacement was offered by three separate sources.

Considerations must be taken when using this ASV technology. The depth of the tailings can not be too shallow. While the ASV can traverse waters as shallow as 15cm, this is within the near-field range of many SONAR sources; the Lowrance fish finder used in this study can't report depths less than 40cm. An extremely shallow pond would likely be better suited to conventional survey methods such as space or aerial GIS means. Operators would need to be aware of sunken or floating features, such as fallen logs. The Mokai is robust in construction but survey speed would need to be carefully selected if there is a danger of collisions or if the topology of the pond is subject to change. Up to date aerial information would be an asset, this could be accomplished with low-cost drone photography before the survey was scheduled to take place.

Consideration must be given to the hardware in use. Collecting technical information

about the Lowrance HDS-7 Live was a time consuming process due to insufficient technical information available by the supplier. The ability to export SONAR data relies on Reef Master which has limited functionality. Since the **.sl3* files produced by the Lowrance are closed source, there are limited options in deciphering the log files. The reliance on closed source hardware and software reduces the ability of this technology to be used in a true autonomous format, however, this study represents a valid proof of concept, not a final product. It is possible modifications to the platform can overcome these issues.

Because the bulk of the danger is taken on by the ASV, there is less training for dangerous environments required by the operator. Transects and sailing paths would likely be planned by others than those conducting the survey, reducing the burden on field staff. Further, the labour of deploying a Mokai ASV is significantly reduced compared to a conventional watercraft. A single person with a quarter-ton truck is able to deploy, monitor, and retrieve the ASV. The ASV fits comfortably on a snow mobile or similarly sized trailer, and multiple vehicles can be transported at one time.

Field day one, 17 November 2021 saw transects that differed significantly from the planned route. The reason for this was poorly tuned steering parameters in the Pixhawk configuration. After noticing the divergence from the planned waypoints, surveys were allowed to continue in order to maximize the available time since stopping to diagnose and remedy what at the time was an unknown issue would have resulted in a considerable amount of lost field time. The responsible steering parameters were identified between survey days, before beginning data collection on the second field day, 24 November 2021, the craft was made to navigate in various box formations while the P-I-D control parameters were adjusted live over the air from shore. The result of this tuning is visible in the concise transects on the second day, and data in Appendix III, Figure 32. Steering parameters could likely be refined further, or tuned for specific types of missions to achieve the best transect adherence for specific circumstances.

Sample rate and number of samples are important for any sensing device since these determine the data resolution. The sample rate helps inform the maximum speed

at which a survey can be performed. If the rate is too slow, its possible that important bottom features would pass by the vessel in between samples and be omitted or only partially recorded resulting in false measurements; in the context of impound bathymetry this may have severe consequences. The data sample rate provided by the Lowrance fish finder was found to increase with speed as shown in Table 9. Day two saw an average sample rate of over 7Hz during the 5.0ms^{-1} missions, with a maximum sample rate of 24.39Hz, or 0.041 seconds between entries. At 5.0ms^{-1} this would represent a maximum resolution of $0.041s \cdot 5ms^{-1} = 0.205m$ were the kayak travelling at 5.0ms^{-1} in a straight line. Maximum time between recordings was found to be greater than 30 seconds, however this was during periods where the kayak was stationary or near stationary, a situation where rapid data sampling would result in redundant entries. The number of samples are of particular note when making comparisons to historic data. It was found that only 44 points were recorded in the survey area, compared to a maximum of 965 collected during the second 2.5ms^{-1} survey on field day two, as seen in Table 12.

When comparing the data collected at survey speeds of 3.0ms^{-1}, 4.0ms^{-1}, 5.0ms^{-1} against the 2.5ms^{-1} data, we see no significant difference between survey speeds (P>0.05). When investigating the difference between surveys provided by the RMSE calculation, we see the highest error when comparing 2.5ms^{-1} to 5.0ms^{-1} though this amount is only 0.2168m. An interesting comparison can be made between day one RMSE in Appendix III, Table 20 and day two RMSE in Appendix III, Table 22. In the day one data we see maximal RMSE comparing 2.5ms^{-1} and 5.0ms^{-1} of 0.5869m. After tuning the steering parameters for day two, the RMSE between 2.5ms^{-1} and 5.0ms^{-1} is 0.1084m, or slightly over 10cm. This indicates that subsequent data collection with the updated parameters may provide more accurate survey data at all available speeds, but more testing is required to know with certainty. The high error seen between day one surveys is likely caused the craft sampling slightly different locations during repeat surveys due to the poorly tuned steering parameters allowing the craft to wander on the transect.

There is a significant difference between the 2.5ms^{-1} study data and the historic

data (P=0.0018), this is reflected by a RMSE of 0.8705m. The reason for this discrepancy cannot be ascertained directly. There is insufficient information presented about how the 2003 data was collected, though we can create a hypothesis based on the number of historic samples and their locations compared to those captured during this study. Figure 24 shows the spread of the 44 historic sample locations, compared to a typical day two field survey shown in Figure 25. It is clear the field data contains significantly more samples across a larger area which captured more data. The discrepancy between the field and historic data is exacerbated by the approximate 50m spacing employed in the historic survey, such a wide spacing would omit much of the subsurface features in the relatively shallow water of the survey area and would rely extensively on interpolation. Referencing Figure 2 we can see that in the study area where depths are between 1 and 10m, the radius of the SONAR footprint, assuming the 2003 SONAR had a 20° field of view, is at most 1.76m, emphasising that wide transects will miss much of the available features in shallow water. It is likely that the difference between the historic and field data is that the 2003 survey collected less information about the sample area than what was captured by the ASV, omitting advances in SONAR and GNSS technology. The transect spacing was likely chosen at 50m to maximize the time the original survey crew spent on the water, using a closer transect spacing would have potentially made the survey intractable. Interestingly, this is an issue the ASV proposed by this study can directly address. This study has shown the lake could be surveyed at 5.0ms^{-1} with tight or wide transect spacing where appropriate without putting the burden of monitoring transects on human operators, and potentially reduce overall survey time by employing multiple ASVs.

The highest quality side-scan imagery was produced at low speed. Surveys of 4.0ms^{-1} and higher caused the craft to travel on-plane, occasionally hitting waves or wake which caused the transducer to leave the water and produce black bands on the side-scan image as seen in Figure 28. This could be potentially improved by changing the transducer placement further to the rear of the craft, however it does appear that overall image quality decreases with speed, likely due to the incline of the ASV altering the angle of the transducer and distorting the image.

Some error may be introduced by the lack of a Real Time Kinematic (RTK) GPS. The use of such positional correcting technology would allow the craft to navigate with centimetre accuracy, environment permitting. Use of RTK GPS would ensure the craft is sampling the area of interest, though the positional information of the saved data is provided by the fish finder rather than the navigational GPS. Therefore, positional accuracy of the data recording could potentially be improved by using an external, high quality GPS antenna. Since separate GPS units are used for navigation and data recording, it is possible there is some mismatch between the desired sample location and the location stored in data, however it could be seen from Figure 18 and Table 7 that GPS performance is at least consistent, with a minimum and maximum transect width of 1.2571 and 2.6296m respectively. By using WAAS corrections, the Lowrance data has a 95% chance of being accurate within 3m, but future survey requirements would dictate if this level of accuracy is acceptable.

A secondary source of error is introduced by interpolating the depth data. The data was interpolated since it would be impossible for the craft to sample the exact physical location multiple times, interpolating the data allowed for the study to make comparisons between depth data at fixed locations rather than attempting to compare the entire survey area, doing so would have relied more heavily on interpolation and introduce a larger potential error.

A third source of error is introduced by combining data from both survey days. It can be seen from Appendix III, Tables 20 and 22, and Figures 30 and 33 that there are differences between the consistency of data on day one and two, with day one containing more variance between surveys. This is likely due to poor transect adherence resulting in each survey sampling slightly different bottom features since the route was not well followed. Future surveys would likely see better accuracy using the current, appropriately tuned steering parameters.

Some difficulties encountered during the construction of the ASV related to water fastness of the transducer elevator. Every intention was made to rely on 3D printed gaskets as they were able to be crafted with the exact dimensions. These worked well in

sealing small parts, however the gasket which occupies the interface between the hull and the elevator consistently leaked to varying degrees as a direct result of issues in the printing process. Marine sealant was applied to both sides of the gasket which eliminated leaks. A secondary challenge was the lack of a Standard Operating Procedure (SOP) in preparing the craft for a mission. On one occasion the craft had just completed a crewed yet autonomous mission in Lake Tamblyn. Having reached the shore in manual mode, the operator was set to perform the same mission a second time with no one in the craft. It was noticed after the craft had drifted out of reach that the on-board hardware switch which selects between autonomous and manual operation was still set to manual. This resulted in a swimmer being dispatched and then closely followed by the development of the pre-launch checklist in Appendix II, Table 19. Such a procedure was required as there would be significantly less recovery options in the field.

This project has great potential to be a disruptive force in the field of hydrographic surveys. With the Mokai's flexibility in terms of instrument payloads, the possibilities for many practical applications are limited only by creativity. Future considerations would be the use of a through-hull depth sounding SONAR if only depth information was required. Installation and operation would be incredibly simple and only require the use of a different style transducer. If imaging was still desired, changing the placement of the transducer to somewhere more to the rear of the craft would keep the sensor in submerged if they the kayak reaches a greater plane angle. It would be possible using pre-existing functionality in the Pixhawk to devise a system that allows the transducer to make orientation corrects to compensate for movement of the craft. It would also be possible to use the technology and knowledge gained from this project to produce a small-scale electric version of the ASV that could fulfil less intense demands. Due to the Mokai's ample hull space and robustness, one could convert the ASV to a full electric drive, fitted with solar panels for energy harvesting to meet specific requirements. The Pixhawk has a provision for obstacle avoidance using ultrasonic sensors, these would be an excellent addition to future versions of the ASV. The kayak would require hydrophones rather than conventional ultrasonic sensors, however this would allow the

craft to autonomously alter its course to avoid objects before a collision.

The ideal version of this ASV is one that self-deploys, conducts the survey without interaction, and delivers to proponents a full report of the tailings impound, roadblocks to this start with the choice of fish finder. Many consumer fish finders use a closed format SONAR log file, much like Lowrance's **.sl3* format which require deciphering by third party software such as Reef Master. Reef Master lacks the ability to operate at the command line level which prevents extracting depth information from the log files without human labour. If this was not the case, most of the data analysis could be automated via scripting languages such as Python by performing the required interpolation and volume calculations immediately after a survey completes. A package containing collected imagery, contour maps, or other valuable data could be made available within an hour of a survey. A secondary roadblock to full automation is that Mission Planner requires several manual steps before the craft will activate and perform a waypoint mission, it may be possible to address these using the existing hardware or other base station software, but such investigation was outside the scope of this study.

While this study shows promising results in the field of autonomous bathymetry, only the minimum amount of data was able to be collected to show a statistical trend. Because there is a significant difference between established historical data and the study data, it would be wise to perform numerous surveys ($n>3$) at the speeds used in this study, but in a water body with a well textured bottom and pre-existing depth data that consists of multiple, agreeing, independent sources.

CONCLUSION

The use of an ASV created from COTS components for use in autonomous bathymetry has the potential to dramatically improve the safety of human workers and increase survey efficiency. With properly tuned steering parameters, the craft was able to perform surveys with consistent transects at speeds of 2.5ms^{-1}, 3.0ms^{-1}, 4.0ms^{-1}, and 5.0ms^{-1} with no statistically significant difference. There was significant difference between study and historic (2003) data, though this is likely due to excessively wide transect spacing and low resolution when compared to the narrow transects and high sample rate provided by the ASV. Data required manual verification to ensure the reported depth matched the sonograph in Reef Master, however this was a simple process that could be performed after momentary instruction. The fuel capacity of approximately 15L and range of over 90km coupled with the small size and ease of transportation make the ASV an attractive option for large scale survey operations. While the ASV was intended to operate in the extensive gold tailings impounds found in NWO, such a craft would be a great addition to any large-scale survey operation. The vehicle cost may be attractive to budget concious organizations and academics intent on using the autonomous Mokai as a multi-purpose instrument platform.

This study is a proof of concept for using COTS components to create an easy to modify ASV as a substitute for conventional watercraft in hazardous environments that would otherwise pose significant short or long-term risk to human operators. The results are promising but ultimately more data is required to determine if this current suite of hardware is an adequate stand-in for conventional surveys. Future research would be directed to testing the craft in adverse conditions and automating more of the survey process.

APPENDIX I - MOKAI DEUTSCH CONNECTOR PINOUT

Pinout of the Mokai 12pin Deutsch connector.

Pin	Wire Colour	Function	Signal
1	White	Kill Switch	Open in Acc or Start, else Gnd
2	Orange	Key power in	12VDC
3	Brown	Accessory Power	12VDC
4	White	Starter	Floating, short to Pin 2 on key turn
5	Green	Key Switch Ground	Gnd
6	White	Joystick Ground	Gnd
7	No Wire	Not Connected	Not Connected
8	Yellow	Joystick Forward/Back	0.515VDC to 4.563VDC
9	Blue	Joystick Left/Right	0.511VDC to 4.562VDC
10	Red	Joystick Power	5VDC
11	Black	Accessory 2 Power (Toggle)	12VDC
12	Purple	Accessory 1 Power (Toggle)	12VDC

Table 18: Mokai control box wiring harness pinout.

APPENDIX II - PRE-LAUNCH CHECK-LIST

Check	Rationale
Set the Key to the 'On' position.	Provides power to all systems.
Connect the base station to the kayak autopilot via telemetry radio.	Facilitates communication link.
Ensure the in-vehicle control switch is in the manual position.	Prevents the kayak from performing any unintended action while human operators are nearby.
Verify the thruster and throttle move under joystick control to both extremes.	Provides visual proof the vessel is under human control and systems are functioning correctly.
Set the control to manual in mission planner, set the in-vehicle control switch to automatic, and use the controller to move thruster to extremes.	verifies remote control is functioning correctly.
Reset the in-vehicle control switch to manual and start the kayak.	Ensures the kayak is in a safe state while it is active,
Ensure the kayak is facing a safe direction and set the in-vehicle control switch to automatic, moving the thruster left and right using the controller.	Ensures the kayak is operating under remote control now that it is active.

Continued on next page.

Table 19 continued.

Check	Rationale
Arm the autopilot via hardware switch on the craft's GPS, watching for successful arm status on Mission Planner.	Perform final steps before allowing the kayak to operate automatically.
Carefully test the throttle via remote control, verifying the engine reacts.	Ensures the system is armed and functioning properly.
All hands clear of the vessel, manually navigate the kayak close to the mission start point.	Allows for final verification all systems are functioning and the craft is navigating well.
Set the vehicle mode to 'auto' using Mission Planner	Begins the autonomous waypoint mission.

Table 19: Pre-Launch check-list.

APPENDIX III - BATHYMETRIC DATA

DAY ONE

Day one sample point locations along transects.

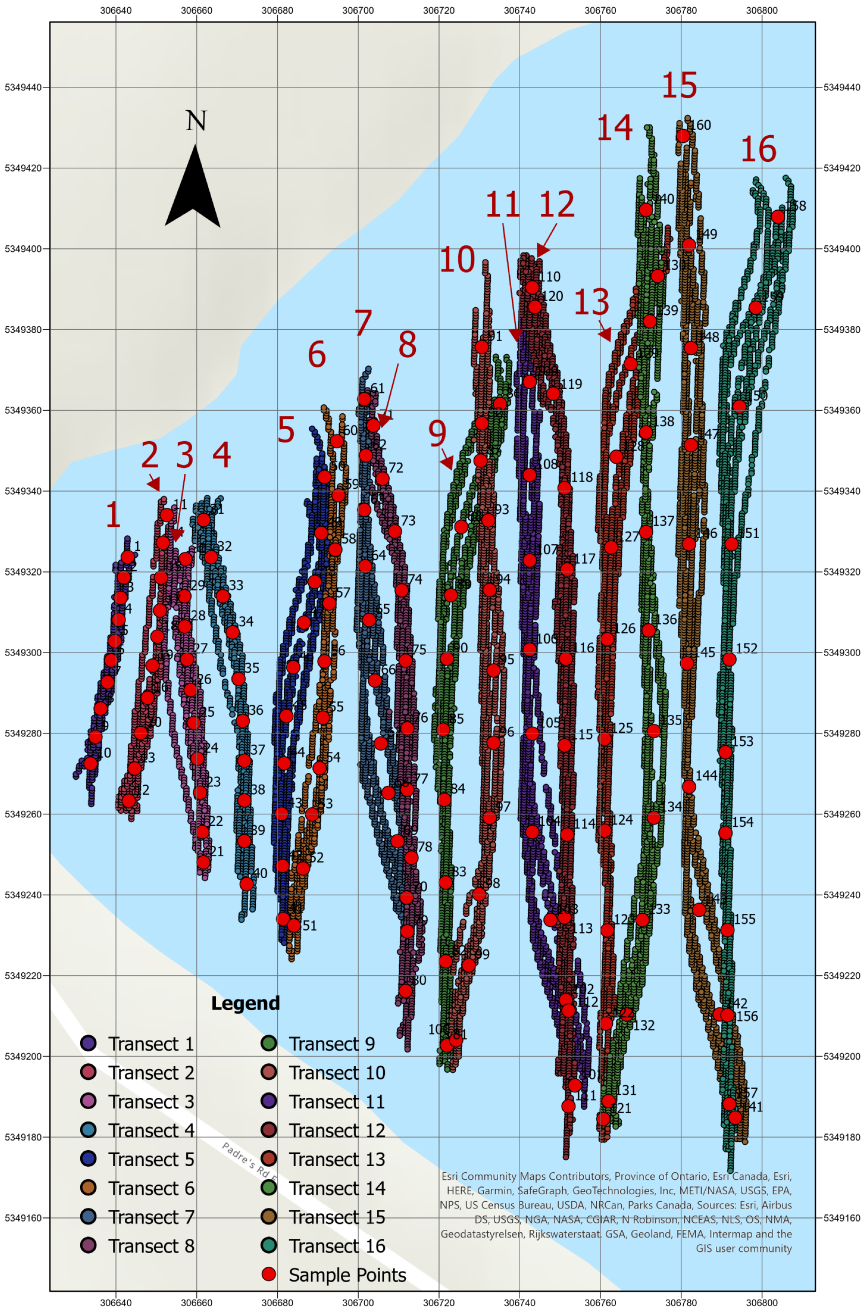

Figure 29: Day one sample points.

Plots of depth data by discrete point.

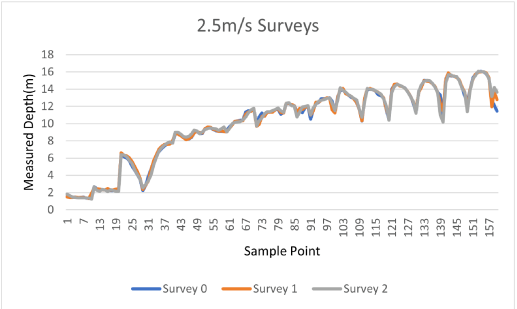

(a) 2.5ms^{-1} surveys.

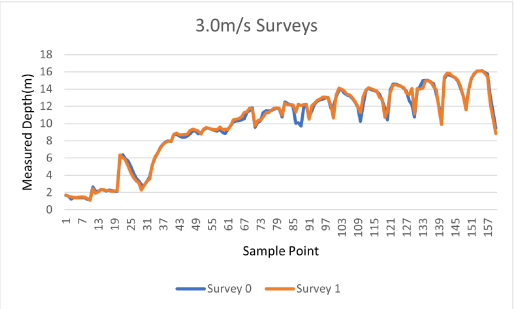

(b) 3.0ms^{-1} surveys.

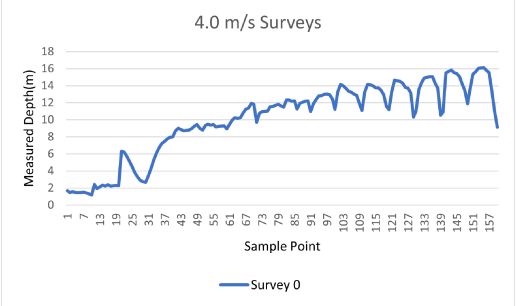

(c) 4.0ms^{-1} surveys.

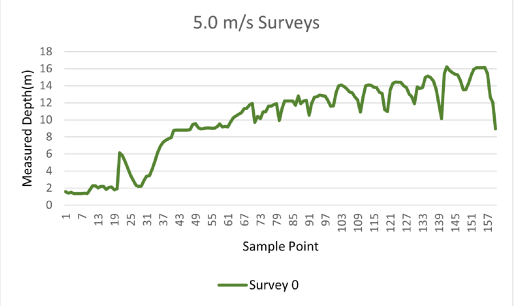

(d) 5.0ms^{-1} surveys.

Figure 30: Day one depth measurements at 2.5, 3.0, 4.0, and 5.0ms^{-1}.

Averages of all day one surveys overlaid.

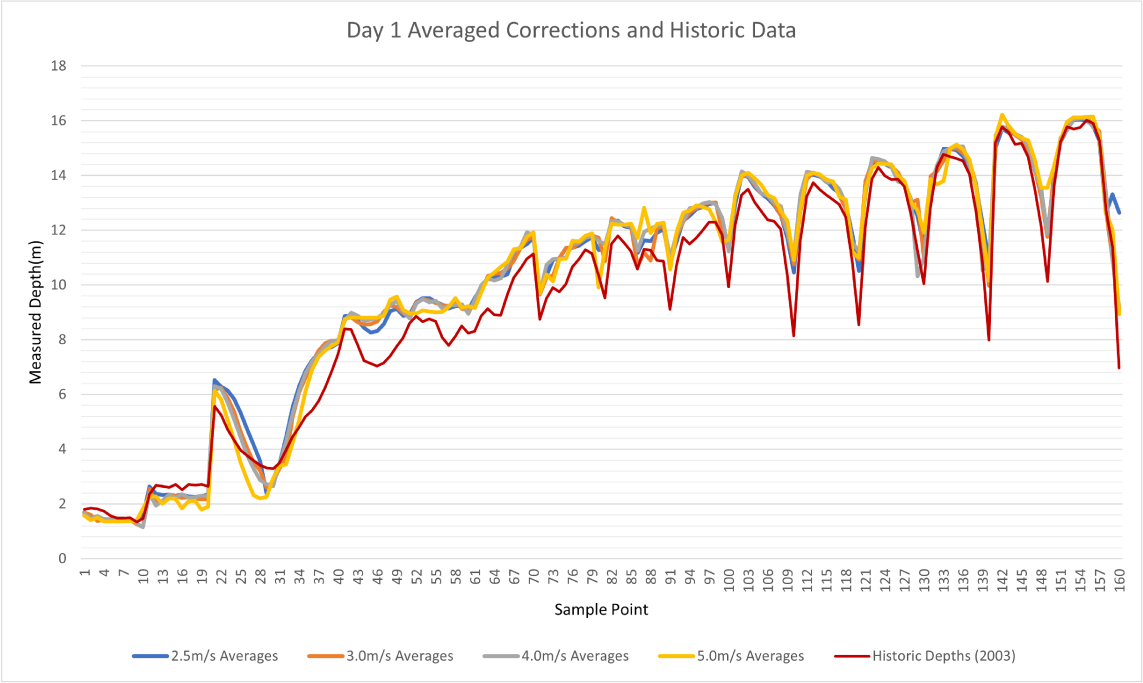

Figure 31: Historic data compared to field day one corrected data.

Day one RMSE

Survey Speed(ms^{-1})	Root Mean Square Error(m)
2.5	0.0000
3	0.4090
4	0.3934
5	0.5869
historic	0.6080

Table 20: Root mean square error of day one surveys with respect to 2.5ms^{-1}.

Averaged depth information by point.

Sample Index	X Coordinate	Y Coordinate	2.5 ms^{-1} Avg.(m)	3.0 ms^{-1} Avg.(m)	4.0 ms^{-1} Avg.(m)	5.0 ms^{-1} Avg.(m)
1	306642.8863	5349323.67	1.700528	1.684956	1.667299	1.567587
2	306641.968	5349318.685	1.538605	1.597275	1.466123	1.401526
3	306641.1809	5349313.568	1.453253	1.377446	1.558829	1.496276
4	306640.6561	5349308.189	1.449777	1.421828	1.45	1.36
5	306639.7377	5349302.81	1.40188	1.418827	1.45098	1.360241
6	306638.8194	5349298.088	1.408299	1.426098	1.474918	1.368818
7	306637.9011	5349292.709	1.426922	1.442282	1.478134	1.37
8	306636.2638	5349286.149	1.384179	1.425856	1.424393	1.379404
9	306634.9151	5349279.149	1.35208	1.268324	1.296254	1.372741
10	306633.7029	5349272.505	1.506943	1.158104	1.1529	1.820135
11	306652.5946	5349334.034	2.636181	2.54993	2.398638	2.267529
12	306643.1487	5349263.322	2.371406	2.043885	1.938516	2.275073
13	306644.5918	5349271.324	2.322645	2.091073	2.11988	2.006976
14	306651.6762	5349327.212	2.34368	2.338322	2.349555	2.208606
15	306651.1515	5349318.554	2.301729	2.305816	2.229742	2.191368
16	306647.8717	5349288.773	2.343857	2.213759	2.35448	1.8443
17	306650.8891	5349310.42	2.268722	2.244707	2.226224	2.087409
18	306650.2331	5349303.991	2.262194	2.191689	2.247039	2.113229
19	306649.0524	5349296.776	2.291165	2.169568	2.297401	1.79153
20	306646.1662	5349280.114	2.344835	2.177988	2.269349	1.896031
21	306661.6468	5349248.103	6.52716	6.181913	6.302977	6.140015
22	306661.3844	5349255.581	6.291738	6.242368	6.220737	5.823675
23	306660.8596	5349265.29	6.147882	5.885705	5.709686	5.090625
24	306660.2037	5349273.686	5.842392	5.379785	5.09938	4.337583
25	306659.2853	5349282.607	5.3407	4.657373	4.445059	3.519216
26	306658.4982	5349290.741	4.731137	4.047617	3.790372	2.883189
27	306657.5798	5349298.35	4.162002	3.523809	3.289067	2.31203
28	306657.0551	5349306.484	3.572192	3.221759	2.87252	2.207407
29	306656.9239	5349313.962	2.382357	2.593968	2.724193	2.252654
30	306657.1863	5349323.145	2.894081	2.819985	2.648349	2.927239
31	306661.737	5349332.862	3.487334	3.304417	3.475712	3.388908
32	306663.5819	5349323.637	4.447652	3.704801	4.2816	3.447299

Continued on next page.

Table 21 continued.

Sample Index	X Coordinate	Y Coordinate	2.5 ms^{-1} Avg. (m)	3.0 ms^{-1} Avg. (m)	4.0 ms^{-1} Avg. (m)	5.0 ms^{-1} Avg. (m)
33	306666.4517	5349314.003	5.526305	5.172372	5.300214	4.235804
34	306668.9115	5349304.983	6.303004	6.073509	6.136703	5.064681
35	306670.3465	5349293.504	6.881429	6.627566	6.798277	6.135522
36	306671.3714	5349283.05	7.248904	7.176405	7.217208	6.918049
37	306671.7814	5349273.21	7.519007	7.598267	7.478956	7.380137
38	306671.7814	5349263.371	7.653899	7.869502	7.777976	7.600925
39	306671.7814	5349253.327	7.728975	7.969981	7.952734	7.775684
40	306672.3963	5349242.667	7.881946	7.927971	7.98	7.904911
41	306681.4158	5349234.058	8.857818	8.764575	8.699583	8.75545
42	306681.2108	5349247.177	8.896826	8.816849	8.99	8.814951
43	306681.0058	5349260.091	8.70786	8.637427	8.874471	8.81
44	306681.6208	5349272.595	8.42794	8.558286	8.7	8.81
45	306682.2358	5349284.28	8.261765	8.563337	8.74	8.81
46	306683.8756	5349296.374	8.322414	8.668633	8.795197	8.81
47	306686.5405	5349307.443	8.57371	9.012455	8.966357	8.879286
48	306689.2053	5349317.488	9.040496	9.249382	9.265357	9.46
49	306690.8452	5349329.582	9.125519	9.196495	9.428056	9.572462
50	306691.6651	5349343.521	8.875014	8.961782	9.018401	9.087596
51	306684.0806	5349232.418	8.936361	8.856414	8.777234	8.954826
52	306686.3355	5349246.562	9.383241	9.355292	9.318228	8.962301
53	306688.5903	5349259.886	9.526101	9.485	9.492898	9.066712
54	306690.4352	5349271.365	9.520243	9.438415	9.368806	9.036778
55	306691.2552	5349283.87	9.384252	9.339303	9.429386	9.002142
56	306691.6651	5349297.809	9.281306	9.266484	9.144406	9.015122
57	306692.8951	5349312.158	9.147141	9.219864	9.236458	9.201145
58	306694.33	5349325.482	9.226544	9.452751	9.27221	9.527421
59	306695.1499	5349339.011	9.249642	9.122938	9.297369	9.166434
60	306694.74	5349352.335	9.100051	9.104943	8.942101	9.232181
61	306701.5045	5349362.79	9.539798	9.33111	9.475654	9.161798
62	306701.9145	5349348.851	9.912882	9.796081	9.989352	9.745484
63	306701.5045	5349335.321	10.23343	10.32946	10.23473	10.2713
64	306701.7095	5349321.382	10.27397	10.40021	10.16539	10.46122
65	306702.7345	5349308.058	10.30427	10.44976	10.24574	10.66155
66	306704.1694	5349293.094	10.38685	10.60061	10.75	10.84749
67	306705.6043	5349277.515	11.07206	10.89739	11.22	11.31
68	306707.4492	5349265.216	11.35204	11.33411	11.38264	11.3358
69	306709.704	5349253.326	11.49421	11.64751	11.92144	11.76
70	306711.9589	5349239.387	11.73209	11.76272	11.81061	11.92539
71	306703.7594	5349356.23	9.746409	9.656233	9.684242	9.707603
72	306706.0143	5349343.111	10.348	10.28138	10.73873	10.38693
73	306709.0891	5349329.992	10.91411	10.34956	10.94828	10.14
74	306710.729	5349315.438	10.97965	11.00635	10.96	10.95405
75	306711.7539	5349298.014	11.35141	11.35666	11.00426	10.96
76	306712.1639	5349281.205	11.36234	11.35509	11.52	11.62
77	306712.1639	5349266.036	11.43257	11.53769	11.55057	11.59734
78	306713.1889	5349249.227	11.6084	11.71981	11.71834	11.80492
79	306712.1639	5349230.983	11.74444	11.80153	11.79597	11.88668
80	306711.7539	5349216.224	11.28589	11.73265	11.62068	9.918204
81	306721.9777	5349202.72	11.28398	10.8834	11.47596	11.351
82	306721.6574	5349223.539	12.32441	12.44471	12.34	12.242
83	306721.6574	5349243.077	12.35026	12.26388	12.32485	12.21
84	306721.3371	5349263.576	12.13295	12.19383	12.19	12.21
85	306721.0168	5349280.872	12.09762	12.10555	12.21	12.23758

Continued on next page.

Table 21 continued.

Sample Index	X Coordinate	Y Coordinate	2.5 ms^{-1} Avg. (m)	3.0 ms^{-1} Avg. (m)	4.0 ms^{-1} Avg. (m)	5.0 ms^{-1} Avg. (m)
86	306735.1097	5349361.585	11.16752	10.69383	11.25361	11.71782
87	306730.3053	5349347.493	11.63713	11.18265	11.93768	12.82465
88	306725.5009	5349331.158	11.61088	10.88827	12.07115	11.9
89	306722.9385	5349314.182	11.90942	12.09344	12.16	12.23988
90	306721.9777	5349298.488	12.04	12.12841	12.22	12.28
91	306730.6256	5349375.678	10.84298	10.65051	10.9679	10.56559
92	306730.6256	5349356.781	11.59657	11.79266	11.9	11.94003
93	306732.227	5349332.759	12.34405	12.29851	12.3526	12.64502
94	306732.5473	5349315.463	12.5247	12.65172	12.81	12.72112
95	306733.5082	5349295.605	12.77265	12.79018	12.84243	12.90265
96	306733.5082	5349277.669	12.84951	12.95864	12.97	12.84976
97	306732.5473	5349259.092	12.96737	13.01143	13.02933	12.76
98	306729.985	5349240.194	12.98918	13.01379	12.94272	12.29713
99	306727.4226	5349222.578	12.19314	11.94	12.44985	11.59
100	306724.2197	5349204.001	11.34869	11.32465	11.2275	11.64088
101	306753.6866	5349192.791	12.96434	13.23743	13.2829	13.24354
102	306751.4446	5349213.93	14.02074	13.98942	14.15012	14.01
103	306747.6011	5349233.789	13.94195	13.97881	14.00488	14.09705
104	306743.117	5349255.569	13.57719	13.64893	13.71	13.9
105	306743.117	5349279.911	13.34312	13.34711	13.34098	13.65834
106	306742.4764	5349300.73	13.15952	13.25945	13.25	13.29
107	306742.4764	5349322.83	12.90384	12.9421	13.00001	13.17936
108	306742.4764	5349343.969	12.54883	12.53973	12.88	12.69
109	306742.4764	5349367.03	11.72284	11.90821	11.90007	12.34598
110	306743.117	5349390.412	10.45887	10.75699	11.06773	10.91046
111	306752.0852	5349187.666	12.84404	12.66763	13.28	12.7779
112	306752.0852	5349211.368	13.99735	13.87793	14.13329	14.01
113	306751.1243	5349234.429	14.02333	14.10404	14.0962	14.09346
114	306751.7649	5349254.928	13.96	13.97406	13.99	14.04619
115	306751.1243	5349277.028	13.82232	13.86496	13.75	13.84492
116	306751.4446	5349298.488	13.53682	13.75	13.74	13.79
117	306751.7649	5349320.588	13.3478	13.25101	13.49449	13.23
118	306751.1243	5349340.766	12.93124	12.77787	12.95854	13.11459
119	306748.2417	5349364.148	11.83023	11.24581	11.5644	11.20737
120	306743.7576	5349385.607	10.5087	10.92429	11.20458	10.98676
121	306760.7331	5349184.464	13.80049	13.76133	13.29425	13.54239
122	306761.3737	5349208.165	14.42448	14.51533	14.64195	14.26141
123	306761.694	5349231.226	14.57553	14.54	14.59327	14.44333
124	306761.0534	5349255.889	14.41334	14.43994	14.51421	14.41677
125	306761.0534	5349278.63	14.29129	14.33386	14.31	14.41
126	306761.694	5349303.292	14.09841	14.10887	13.77	14.00293
127	306762.6548	5349326.033	13.66509	13.63546	13.72	13.80337
128	306763.936	5349348.453	13.10806	13.0072	13.15	13.03505
129	306767.4592	5349371.515	12.51076	13.11293	10.32325	12.72573
130	306774.1854	5349393.294	11.3738	10.95331	11.00998	11.91162
131	306762.0143	5349188.948	13.72593	13.96698	13.51573	13.86749
132	306766.4984	5349210.407	14.30597	14.16227	14.37047	13.67
133	306770.3419	5349233.789	14.97817	14.5406	14.88	13.79833
134	306773.2245	5349259.092	14.97359	14.98331	14.99	14.99077
135	306773.2245	5349280.551	14.91528	14.98679	15.06804	15.13
136	306771.9433	5349305.534	14.69138	14.81068	15.06	14.95
137	306771.3027	5349329.876	14.289	14.47792	14.32398	14.57
138	306771.3027	5349354.539	13.58383	13.69912	13.71994	13.54305

Continued on next page.

Table 21 continued.

Sample Index	X Coordinate	Y Coordinate	2.5 ms^{-1} Avg. (m)	3.0 ms^{-1} Avg. (m)	4.0 ms^{-1} Avg. (m)	5.0 ms^{-1} Avg. (m)
139	306772.2636	5349382.084	12.23224	11.83073	10.52685	11.91736
140	306771.3027	5349409.629	10.8701	9.974415	10.89277	10.14371
141	306793.4029	5349184.784	15.03231	15.28212	15.48718	15.42
142	306789.4594	5349210.387	15.71184	15.7905	15.66331	16.22479
143	306784.4347	5349236.291	15.57185	15.69315	15.8233	15.8
144	306781.9325	5349266.819	15.50843	15.48751	15.52315	15.53
145	306781.432	5349297.347	15.39941	15.3189	15.40997	15.37
146	306781.9325	5349326.874	15.04033	14.96427	15.07	15.28127
147	306782.4329	5349351.396	14.1954	14.23457	14.24476	14.58
148	306782.433	5349375.418	13.48864	13.19466	13.46873	13.55
149	306781.9325	5349400.941	11.84082	11.75709	11.8734	13.55
150	306794.4439	5349360.905	13.90729	14.03744	13.62	14.31635
151	306792.442	5349326.874	15.22011	15.21471	15.36701	15.29
152	306791.9416	5349298.348	15.65679	15.77649	15.63529	15.95021
153	306790.9407	5349275.327	16.02156	16.10277	16.06	16.13
154	306790.9407	5349255.308	16.03482	16.10716	16.08	16.13
155	306791.4412	5349231.286	16.0187	16.11942	16.1	16.13261
156	306791.4412	5349210.267	15.83161	15.86916	15.77937	16.14605
157	306791.9416	5349188.247	15.26101	15.60696	15.54767	15.42
158	306803.9526	5349407.948	12.61619	12.725	13.38305	12.65
159	306798.4475	5349385.427	13.30703	10.941	10.96233	12.02886
160	306780.4311	5349427.966	12.63879	9.156994	9.124322	8.937858

Table 21: Day one depth per sample location by averaged speeds.

DAY TWO

Day two sample point locations along transects.

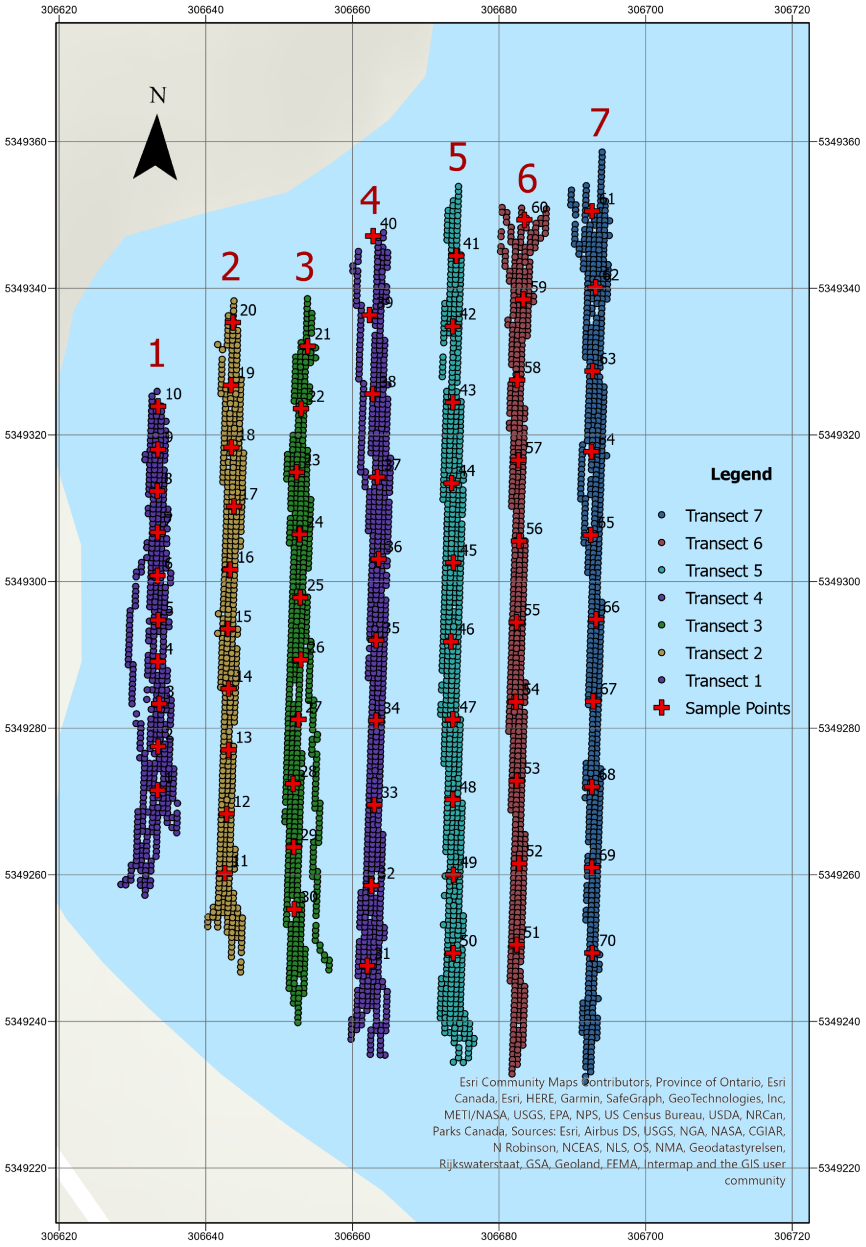

Figure 32: Day two sample points.

Plots of day two depth data by discrete point.

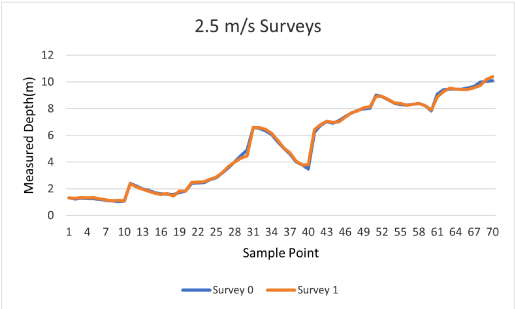

(a) 2.5ms^{-1} surveys.

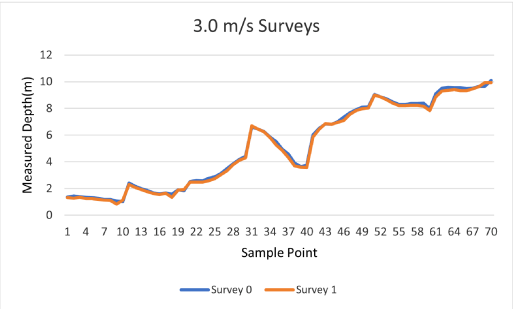

(b) 3.0ms^{-1} surveys.

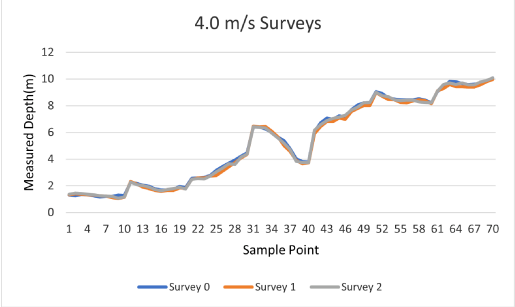

(c) 4.0ms^{-1} surveys.

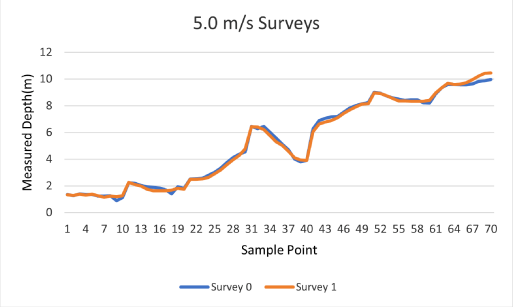

(d) 5.0ms^{-1} surveys.

Figure 33: Day two depth measurements at 2.5, 3.0, 4.0, and 5.0ms^{-1}.

Averages of all surveys overlaid.

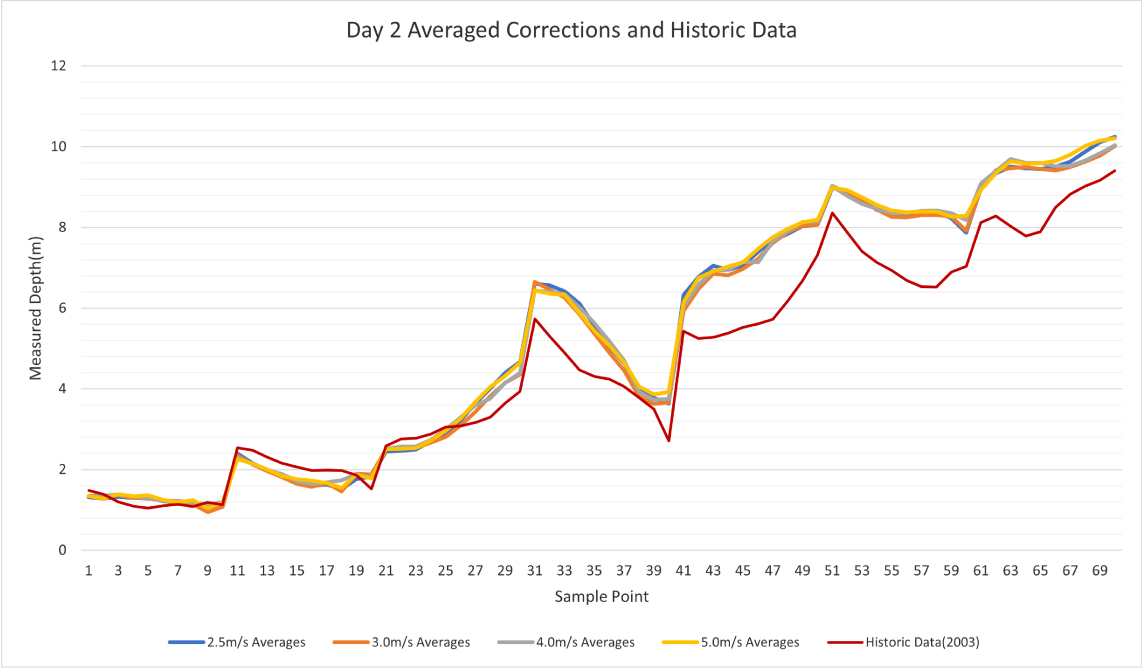

Figure 34: Historic data compared to field day two corrected data.

Day two RMSE

Survey Speed(ms^{-1})	Root Mean Square Error(m)
2.5	0.0000
3	0.1326
4	0.1285
5	0.1084
Historic	0.9943

Table 22: Root mean square error of day two surveys with respect to 2.5ms^{-1}.

Averaged depth information by point.

Sample Index	X Coordinate	Y Coordinate	2.5 ms^{-1} Avg.(m)	3.0 ms^{-1} Avg.(m)	4.0 ms^{-1} Avg.(m)	5.0 ms^{-1} Avg.(m)
1	306633.4404	5349271.536	1.31694	1.347788	1.336878	1.339236
2	306633.4961	5349277.501	1.280221	1.360174	1.357288	1.275923
3	306633.647	5349283.326	1.323182	1.366703	1.378158	1.386872
4	306633.4661	5349289.101	1.293613	1.301066	1.338041	1.330535
5	306633.5101	5349294.74	1.310379	1.278831	1.298182	1.360899
6	306633.4205	5349300.798	1.221706	1.235168	1.227398	1.250462
7	306633.4273	5349306.7	1.160332	1.160247	1.229004	1.192182
8	306633.374	5349312.356	1.112106	1.145813	1.185102	1.238414
9	306633.4808	5349318.007	1.086598	0.944681	1.138025	1.040371
10	306633.4998	5349323.901	1.096736	1.078659	1.194304	1.184238
11	306642.5992	5349260.215	2.402414	2.352406	2.292001	2.253766
12	306642.856	5349268.306	2.163224	2.134411	2.140303	2.148564
13	306643.1129	5349277.039	1.986517	1.963534	1.989534	2.001381
14	306643.1129	5349285.387	1.843602	1.811924	1.888732	1.840829
15	306643.0332	5349293.552	1.680077	1.647756	1.715099	1.761335
16	306643.3362	5349301.631	1.598154	1.575543	1.640296	1.726765
17	306643.8559	5349310.252	1.626328	1.663207	1.690052	1.663006
18	306643.4877	5349318.301	1.515331	1.457342	1.734941	1.539001
19	306643.4351	5349326.77	1.766834	1.892828	1.889128	1.880129
20	306643.7065	5349335.332	1.833703	1.87694	1.804525	1.784222
21	306653.9075	5349332.1	2.447798	2.50035	2.516446	2.507572
22	306652.9985	5349323.582	2.470439	2.548479	2.568205	2.512528
23	306652.4007	5349314.904	2.492495	2.534861	2.574404	2.532531
24	306652.8117	5349306.438	2.704792	2.668283	2.736702	2.713688
25	306652.8939	5349297.808	2.862336	2.805484	2.984624	2.96363
26	306652.9761	5349289.342	3.216864	3.094278	3.296415	3.261255
27	306652.6473	5349281.205	3.6376	3.423175	3.58873	3.673947
28	306651.9076	5349272.41	4.00354	3.818465	3.762132	4.048924
29	306651.9898	5349263.78	4.394297	4.150754	4.144979	4.323702
30	306652.072	5349255.314	4.677488	4.35873	4.392909	4.654081
31	306662.0174	5349247.588	6.59912	6.655565	6.431526	6.442898
32	306662.5927	5349258.52	6.561943	6.460293	6.399241	6.352906

Continued on next page.

Table 23 continued.

Sample Index	X Coordinate	Y Coordinate	2.5 ms^{-1} Avg. (m)	3.0 ms^{-1} Avg. (m)	4.0 ms^{-1} Avg. (m)	5.0 ms^{-1} Avg. (m)
33	306663.0037	5349269.534	6.409424	6.257005	6.345421	6.328297
34	306663.2503	5349281.041	6.106994	5.838822	6.015505	5.873355
35	306663.2503	5349291.972	5.564269	5.378494	5.637918	5.440411
36	306663.5791	5349303.068	5.047516	4.899925	5.190848	5.072848
37	306663.4147	5349314.247	4.637392	4.456908	4.705097	4.652606
38	306662.7571	5349325.589	4.047181	3.805531	3.920784	4.050565
39	306662.3462	5349336.357	3.781722	3.622477	3.733313	3.867621
40	306662.8393	5349347.124	3.640133	3.661295	3.748972	3.917342
41	306674.182	5349344.412	6.330068	5.940865	6.050766	6.152624
42	306673.6888	5349334.795	6.779035	6.476021	6.58868	6.757408
43	306673.6888	5349324.439	7.04678	6.854948	6.925499	6.910072
44	306673.5245	5349313.425	6.943064	6.81195	6.94938	7.03472
45	306673.771	5349302.575	7.058528	6.977893	7.147572	7.139697
46	306673.4423	5349291.808	7.394696	7.220127	7.137445	7.464314
47	306673.6888	5349281.205	7.680951	7.613822	7.645139	7.75415
48	306673.6888	5349270.273	7.841681	7.879636	7.90931	7.959577
49	306673.771	5349259.999	8.033475	8.042757	8.13942	8.127211
50	306673.771	5349249.314	8.068877	8.065834	8.154023	8.188363
51	306682.4013	5349250.465	8.969106	9.024373	9.01608	8.985509
52	306682.7301	5349261.561	8.910509	8.858854	8.786147	8.926577
53	306682.4013	5349272.821	8.681324	8.678647	8.579679	8.743093
54	306682.3192	5349283.589	8.427645	8.435122	8.456263	8.557245
55	306682.4013	5349294.438	8.338422	8.256208	8.352407	8.418069
56	306682.7301	5349305.534	8.263624	8.25	8.354031	8.370311
57	306682.6479	5349316.548	8.325805	8.310319	8.408641	8.391104
58	306682.4835	5349327.48	8.388671	8.305	8.416987	8.392834
59	306683.3055	5349338.494	8.225646	8.276776	8.349529	8.268464
60	306683.4699	5349349.343	7.865449	7.91247	8.183372	8.29011
61	306692.697	5349350.531	8.979853	8.983653	9.094564	8.935241
62	306693.1687	5349340.138	9.342046	9.414097	9.401477	9.349862
63	306692.7577	5349328.713	9.504335	9.464252	9.699152	9.640347
64	306692.5933	5349317.699	9.465021	9.493526	9.600901	9.580029
65	306692.5111	5349306.356	9.45	9.447321	9.5986	9.587732
66	306693.2509	5349294.849	9.502309	9.409589	9.516463	9.647602
67	306692.8399	5349283.671	9.623573	9.496272	9.52004	9.801019
68	306692.6755	5349271.999	9.873226	9.628777	9.655549	10.01351
69	306692.6755	5349260.985	10.11157	9.783915	9.837535	10.1489
70	306692.7248	5349249.337	10.245	10.01505	10.03283	10.21094

Table 23: Day two depth per sample location by averaged speeds.

COMBINED DAYS

The following in Figure 35 show the non-averaged data per point by survey speed.

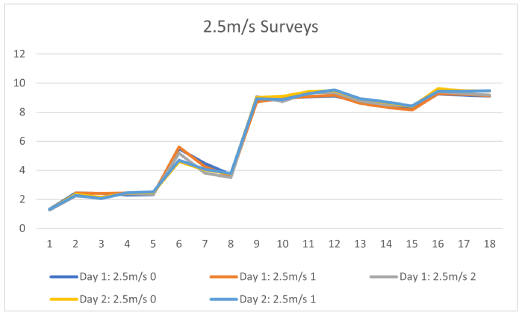

(a) 2.5ms^{-1} surveys.

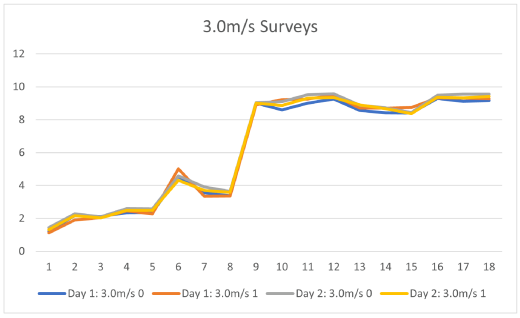

(b) 3.0ms^{-1} surveys.

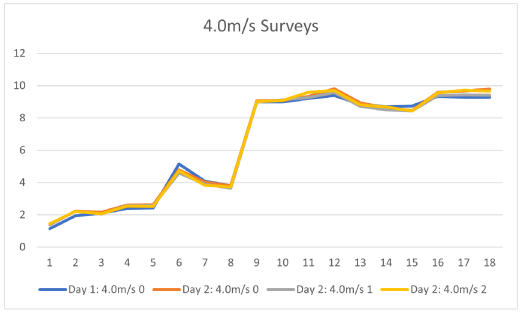

(c) 4.0ms^{-1} surveys.

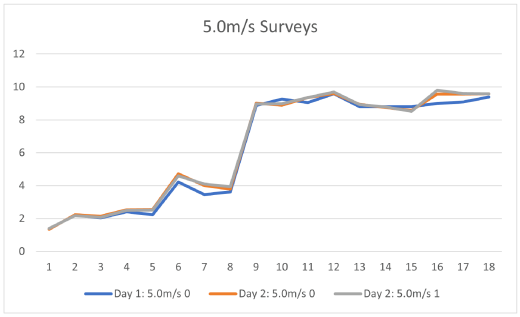

(d) 5.0ms^{-1} surveys.

Figure 35: day two depth measurements at 2.5, 3.0, 4.0, and 5.0ms^{-1}.

LITERATURE CITED

A.Schulman (1981). “Chemical resis-
tance of high and low density polyethylene”. In: URL: https://cipax.com/storage/D14CC380DD097BFF446DDBF078916FEAE74724963C50734BA7983182C36B490C/0289184f4438400b80d9ea28f2338399/pdf/media/62c4de02a21e484cb074213b23e58a40/Chemical%20resistance.pdf.

Abdalla, Osman A.E. et al. (2010). “Cyanide from gold mining and its effect on groundwater in arid areas, Yanqul mine of Oman”. In: Environmental Earth Sciences 60.4, pp. 885–892. ISSN: 18666280. DOI: 10.1007/s12665-009-0225-z.

Allen, Erik W. (2008). “Process water treatment in Canada’s oil sands industry: I. Target pollutants and treatment objectives”. In: Journal of Environmental Engineering and Science 7.2, pp. 123–138. ISSN: 14962551. DOI: 10.1139/S07-038.

ArduPilot Dev Team (2021). The Cube Overview. URL: https://ardupilot.org/copter/docs/common-thecube-overview.html (visited on 02/22/2022).

Bakatula, E. N. et al. (2012). “Characterization of cyanide in a natural stream impacted by gold mining activities in the Witwatersrand Basin, South Africa”. In: Toxicological and Environmental Chemistry 94.1, pp. 7–19. ISSN: 02772248. DOI: 10.1080/02772248.2011.638637.

Banks, K. W. et al. (2007). “Geomorphology of the Southeast Florida continental reef tract (Miami-Dade, Broward, and Palm Beach Counties, USA)”. In: Coral Reefs 26.3, pp. 617–633. ISSN: 07224028. DOI: 10.1007/s00338-007-0231-0.

Barcroft, Joseph (1931). “The Toxicity of Atmospheres containing Hydrocyanic Acid Gas”. In: Journal of Hygiene 31.1, pp. 1–34. ISSN: 00221724. DOI: 10.1017/S0022172400010664.

Basov, Vladimir (2021). Top 10 largest gold mines in Canada in 2020 - report. URL: https://www.kitco.com/news/2021-03-12/Top-10-largest-gold-mines-in-Canada-in-2020-report.html.

Bhargava, D. S. and Dejene W. Mariam (1991). “Light penetration depth, turbidity and reflectance related relationship and models”. In: ISPRS Journal of Photogrammetry and Remote Sensing 46.4, pp. 217–230. ISSN: 09242716. DOI: 10.1016/0924-2716(91)90055-Z.

Birkebak, Matthew et al. (2018). “The effect of surface waves on airborne lidar bathymetry (ALB) measurement uncertainties”. In: Remote Sensing 10.3, pp. 1–18. ISSN: 20724292. DOI: 10.3390/rs10030453.

Bouwmeester, E. C. and A. W. Heemink (1993). “Optimal line spacing in hydrographic survey”. In: International Hydrographic Review 70.1, pp. 37–48. ISSN: 0020-6946.

Bowen, Zachary H. and Robert G. Waltermire (2002). “Evaluation of light detection and ranging (LIDAR) for measuring river corridor topography”. In: Journal of the American Water Resources Association 38.1, pp. 33–41. ISSN: 1093474X. DOI: 10.1111/j.1752-1688.2002.tb01532.x.

Braskem (2005). “Polyethylene Chemical Resistance”. In: pp. 1–8.

Burkhardt, Rike, Peter Rosenbluth, and Julee Boan (2012). “Mining in Ontario: A Deeper Look”. In: pp. 1–40.

Cashion, J. D. and L. J. Brown (1998). “Gold mineralogy and extraction”. In: Hyperfine Interactions 111.1-4, pp. 271–280. ISSN: 03043843. DOI: 10.1023/A:1012674205425.

CDF Corporation (2004). Polyethylene Chemical Resistance Chart. Tech. rep. 1, pp. 1–6. URL: http://www.cdf1.com/technical%20bulletins/Polyethylene_Chemical_Resistance_Chart.pdf.

Central, GPS (2021). What is WAAS? URL: https://www.gpscentral.ca/what-is-waas/ (visited on 06/28/2022).

Charles Kerfoot, W. et al. (2012). “Light detection and ranging (LiDAR) and multispectral studies of disturbed Lake Superior coastal environments”. In: Limnology and Oceanography 57.3, pp. 749–771. ISSN: 00243590. DOI: 10.4319/lo.2012.57.3.0749.

Che Awang, Nur Aklima (2011). “Hydrographic Survey Using Real Time Kinematic”. In: Geoinformation Sceince Journal 11.1, pp. 1–14.

Clark, D R (1991). “Where a drink of water may mean death: gold isn’t the only legacy from mines”. In: Calif. Fish Game 77, pp. 17–18.

contributors, Wikipedia (2022a). Lixiviant: Wikipedia The Free Encyclopedia. URL: https://en.wikipedia.org/w/index.php?title=Lixiviant&oldid=1064151666.

— (2022b). Port scanner: Wikipedia The Free Encyclopedia. URL: https://en.wikipedia.org/w/index.php?title=Port_scanner&oldid=1077182531.

Danson, E (2006). “Understanding lidar bathymetry for shallow waters and coastal mapping”. In: FIG XXIII International Congress.

Dashora, Ajay, Bharat Lohani, and Kalyanmoy Deb (2014). Lidar Flight Planning. URL: https://www.gim-international.com/content/article/lidar-flight-planning (visited on 04/21/2021).

Datta, Manoj (2003). “Geotechnical study for hydraulic barrier systems at tailings pond”. In: Practice Periodical of Hazardous, Toxic, and Radioactive Waste Management 7.3, pp. 163–169. ISSN: 1090025X. DOI: 10.1061/(ASCE)1090-025X(2003)7:3(163).

Davies-Colly, R. J. and D. G. Smith (2001). “Turbidity, Suspended Sediment, and Water Clarity: A Review”. In: JOURNAL OF THE AMERICAN WATER RESOURCES ASSOCIATION 37.5, pp. 1085–1101.

Drive a Boat Canada (2021). When Should You Use Navigation Lights on a Boat? URL: https://driveaboatcanada.ca/boat-navigation-lights/ (visited on 02/22/2022).

Dubé, M. G. et al. (2005). “Effects of metal mining effluent on Atlantic salmon (Salmo salar) and slimy sculpin (Cottus cognatus): Using artificial streams to assess existing effects and predict future consequences”. In: Science of the Total Environment 343.1-3, pp. 135–154. ISSN: 00489697. DOI: 10.1016/j.scitotenv.2004.09.037.

Dunbabin, Matthew, Alistair Grinham, and James Udy (2009). “An Autonomous Surface Vehicle for water quality monitoring”. In: ACRA 2009.

Engineering ToolBox (2014). Engineering Toolbox - Silicone Resistance. URL: https://www.engineeringtoolbox.com/silicone-chemical-resistance-d_1879.html (visited on 02/22/2022).

Fawcett, Skya E. et al. (2015). “Arsenic and antimony geochemistry of mine wastes, associated waters and sediments at the Giant Mine, Yellowknife, Northwest Territories, Canada”. In: Applied Geochemistry 62, pp. 3–17. ISSN: 18729134. DOI: 10.1016/j.apgeochem.2014.12.012. URL: http://dx.doi.org/10.1016/j.apgeochem.2014.12.012.

Ferreira, H. et al. (2007). “SWORDFISH: An autonomous surface vehicle for network centric operations”. In: OCEANS 2007 - Europe, pp. 1–6. DOI: 10.1109/oceanse.2007.4302467.

Furnans, Jordan and Barney Austin (2008). “Hydrographic survey methods for determining reservoir volume”. In: Environmental Modelling and Software 23.2, pp. 139–146. ISSN: 13648152. DOI: 10.1016/j.envsoft.2007.05.011.

Garmin Ltd. (2017). What is WAAS? URL: https://www8.garmin.com/aboutGPS/waas.html (visited on 06/28/2022).

Glotov, Vladimir E. et al. (2018). “Causes and environmental impact of the gold-tailings dam failure at Karamken, the Russian Far East”. In: Engineering Geology 245, pp. 236–247. ISSN: 00137952. DOI: 10.1016/j.enggeo.2018.08.012. URL: https://doi.org/10.1016/j.enggeo.2018.08.012.

Government of Canada (2020a). Acquiring hydrography data. URL: https://www.dfo-mpo.gc.ca/science/hydrography-hydrographie/data-acquisition-eng.html.

— (2020b). Deadlines and most recent changes: National Pollutant Release Inventory. URL: https://www.canada.ca/en/environment-climate-change/services/national-pollutant-release-inventory/report/deadlines-changes.html.

— (2020c). Guide for Reporting to the National Pollutant Release Inventory, 2020 and 2021.

— (2021). Licensing of Pleasure Craft - SOR/2010-91. URL: https://laws-lois.justice.gc.ca/eng/regulations/sor-2010-91/page-2.html%7B%5C#%7Dh-769536 (visited on 02/22/2022).

Government of Ontario (2022). Ontario’s Ring of Fire. URL: https://www.ontario.ca/page/ontarios-ring-fire (visited on 05/22/2022).

Halmai, Ákos et al. (2020). “Applicability of a recreational-grade interferometric sonar for the bathymetric survey and monitoring of the Drava River”. In:

ISPRS International Journal of Geo-Information 9.3. ISSN: 22209964. DOI: 10.3390/ijgi9030149.

Hayley (2021). A Beginner's Guide to LIDAR Surveying. URL: https://coptrz.com/a-beginners-guide-to-lidar-surveying/ (visited on 04/21/2021).

Henny, Charles J., Robert J. Hallock, and Elwood F. Hill (1994). "Cyanide and migratory birds at gold mines in Nevada, USA". In: Ecotoxicology 3.1, pp. 45–58. ISSN: 09639292. DOI: 10.1007/BF00121387.

Hodges, Richard P (2010a). "Transmission Loss". In: Underwater Acoustics - Analysis, Design and Performance of SONAR. Wiley. Chap. 5.

— (2010b). "Transmission Loss: Interaction with Boundaries". In: Underwater Acoustics - Analysis, Design and Performance of SONAR. Chap. 6.

— (2010c). Underwater Acoustics, Analysis, Design, and Performance of SONAR. 1, pp. 4, 1–15, 23. ISBN: 9788578110796. arXiv: arXiv:1011.1669v3.

Horowitz, Paul, Winfield Hill, and Ian Robinson (1989a). The art of electronics - Chapter 1. Vol. 2. Cambridge university press Cambridge. Chap. 1:Foundati.

— (1989b). The art of Electronics - Chapter 6. Vol. 2. Cambridge university press Cambridge. Chap. 6: Filters.

Hulburt, E.O. (1935). "The Ionosphere , Skip Distances of Radio Waves, and the Propagarion of Microwaves". In: 22.12.

Kimball, Peter et al. (2015). "The WHOI Jetyak: An autonomous surface vehicle for oceanographic research in shallow or dangerous waters". In:

2014 IEEE/OES Autonomous Underwater Vehicles, AUV 2014. DOI: 10.1109/AUV.2014.7054430.

Klemens, Kevin William (2017). “Development and Evaluation of a USV Based Mapping System for Remote Sensing of Eelgrass Extent in Southern California”. In: May. DOI: 10.13140/RG.2.2.29336.19201.

Latham, thomas walker (1966). Fluid Motions in a Peristaltic Pump.

LeBlond, Jane B. and Lawrence K. Duffy (2001). “Toxicity assessment of total dissolved solids in effluent of Alaskan mines using 22-h chronic Microtox®and Selenastrum capricornatum assays”. In: Science of the Total Environment 271.1-3, pp. 49–59. ISSN: 00489697. DOI: 10.1016/S0048-9697(00)00830-5.

Lee, Kit Hong, Swee King Phang, and Yen Myan Felicia Wong (2020). “Small scale autonomous watercraft for aquatic mapping”. In: AIP Conference Proceedings 2233.May. ISSN: 15517616. DOI: 10.1063/5.0001371.

MacKinnon, M D (1989). “Development of the tailings pond at Syncrude’s oil sands plant: 1978–1987”. In: AOSTRA J. Res 5.2, pp. 109–133.

MacKinnon, M. D. and Hans Boerger (1986). “Description of Two Treatment Methods For Detoxifying Oil Sands Tailings Pond Water”. In: Water Policy Research Canada 21.4, pp. 496–512.

Madeo, Dario et al. (2020). “A Low-Cost Unmanned Surface Vehicle for Pervasive Water Quality Monitoring”. In: IEEE Transactions on Instrumentation and Measurement 69.4, pp. 1433–1444. ISSN: 0018-9456. DOI: 10.1109/tim.2019.2963515.

Mara, Septimius et al. (2007). “Criteria for identifying the major risks associated with tailings ponds in Romania”. In: Mine Water and the environment 26.4, pp. 256–263.

Markovic, Z., N. Vusovic, and D. Milanovic (2010). “Old copper flotation tailings waste reprocessing”. In: XXV International Mineral Processing Congress 2010, IMPC 2010 5.September, pp. 3825–3829.

Mason, D. C., C. Gurney, and M. Kennett (2000). “Beach topography mapping - a comparison of techniques”. In: Journal of Coastal Conservation 6.1, pp. 113–124. ISSN: 14000350. DOI: 10.1007/BF02730475.

Maxim Integrated Products (2002). MAXIM 517/519 DAC Datasheet. Tech. rep., pp. 1–16.

McManamon, Paul (2019a). “History of LiDAR”. In: LiDAR technologies and systems. SPIE. ISBN: 9781510625396.

— (2019b). “Introduction To LiDAR”. In: LiDAR technologies and systems. Vol. 1. 1. SPIE. ISBN: 9781510625396.

Medina, Diego and Corby G. Anderson (2020). “A review of the cyanidation treatment of copper-gold ores and concentrates”. In: Metals 10.7, pp. 1–11. ISSN: 20754701. DOI: 10.3390/met10070897.

Mikula, R J, K L Kasperski, and R D Burns (1996). “Consolidated tailings release water chemistry”. In: 9 pages.

Minister of the Environment and Climate Change (2019). Approval of the Rainy River Gold Mine Environmental Assessment.

Mokai Manufacturing (2020). Mokai Owners Manual. New York. URL: www.mokai.com.

Moore, Johnnie and Samuel Luoma (1990). “Hazardous Wastes from Large-scale Metal Extraction : The Clark Fork Waste Complex , MT”. In: Scholar Works, University of Montana.

Müezzinogˇlu, Aysen (2003). “A review of environmental considerations on gold mining and production”. In: Critical Reviews in Environmental Science and Technology 1.33, pp. 45–71.

Muscatello, Jorgelina R. et al. (2006). “Larval deformities associated with selenium accumulation in northern pike (Esox lucius) exposed to metal mining effluent”. In: Environmental Science and Technology 40.20, pp. 6506–6512. ISSN: 0013936X. DOI: 10.1021/es060661h.

Navico Holding AS (2018a). “Active ImagingTM transducers: Active Imaging 3-IN-1, Active Imaging SideScan Installation manual”. In: Advanced Optical Technologies 3.2, pp. 139–140. ISSN: 21928584. DOI: 10.1515/aot-2014-0013.

— (2018b). HDS Live Operator Manual. Tech. rep. Navico. URL: https://www.lowrance.com/en-ca/downloads/#000-14415-001.

— (2021). HDS Live Installation Manual. Tech. rep. URL: https://www.lowrance.com/en-ca/downloads/#000-14415-001.

Navico Technical Support (2021). Tech Support Contact. URL: lowrance.canada@navico.com.

Ngole-Jeme, Veronica Mpode and Peter Fantke (2017). “Ecological and human health risks associated with abandoned gold mine tailings contaminated soil”. In: PLoS ONE 12.2, pp. 1–24. ISSN: 19326203. DOI: 10.1371/journal.pone.0172517.

Nicholson, David P. et al. (2018). “Rapid Mapping of Dissolved Methane and Carbon Dioxide in Coastal Ecosystems Using the ChemYak Autonomous Surface Vehicle”. In: Environmental Science and Technology 52.22, pp. 13314–13324. ISSN: 15205851. DOI: 10.1021/acs.est.8b04190.

Noreland, Daniel (2003). “Numerical Techniques for Acoustic Modelling and Design of Brass Wind Instruments”. In.

Ocean Alpha (2018). Autonomous Survey Boat. URL: https://www.oceanalpha.com/product-item/me40/.

Oertling, Thomas James (1996). Ships' Bilge Pumps: A History of Their Development, 1500-1900. 2. Texas A\&M University Press.

Oil Sands Magazine (2021). Tailings Ponds 101. URL: https://www.oilsandsmagazine.com/technical/mining/tailings-ponds (visited on 05/22/2022).

Ontario Data Catalogue (2018). Bathymetry points. URL: https://geo.frdr-dfdr.ca/catalog/geodisy:open_84c9057c-5505-4998-81c5-8cceada7fd10?locale=en (visited on 03/22/2022).

Ontario Mining Association (2021). Facts and Figures. URL: https://oma.on.ca/en/ontario-mining/facts_figures.aspx (visited on 05/22/2022).

Pailhas, Yan, Yvan Petillot, and Chris Capus (2010). "High-resolution sonars: What resolution do we need for target recognition?" In: Eurasip Journal on Advances in Signal Processing 2010. ISSN: 16876172. DOI: 10.1155/2010/205095.

PX4 (2021). PX4 User Guide. URL: https://docs.px4.io/master/en/ (visited on 02/11/2021).

Pyrchla, Krzysztof, Jerzy Pyrchla, and Tadeusz Kantak (2018). "Hydrographic Multisensory Unmanned Watercraft". In: Proceedings - 2018 Baltic Geodetic Congress, BGC-Geomatics 2018, pp. 231–235. DOI: 10.1109/BGC-Geomatics.2018.00050.

Reece, R (1997). "Cyanide toxicity to birds". In: ACMRR. Short course notes on management of cyanide mining. Perth: ACMRR.

Report, Application (2006). “Efficient Multiplication and Division Using MSP430”. In: September, pp. 1–15.

Rusby, JSM and J Revie (1975). “LONG-RANGE SONAR MAPPING OF THE CONTINENTAL SHELF”. In: URL: https://www.sciencedirect.com/science/article/abs/pii/0025322775900857.

Ryan, P and R Shanks (1996). “Tailings dams”. In: Aust. Bird Watch July, pp. 7–11.

Schumann, G. et al. (2008). “Comparison of remotely sensed water stages from LiDAR, topographic contours and SRTM”. In: ISPRS Journal of Photogrammetry and Remote Sensing 63.3, pp. 283–296. ISSN: 09242716. DOI: 10.1016/j.isprsjprs.2007.09.004.

Shahmoradi, Javad et al. (2020). “A comprehensive review of applications of drone technology in the mining industry”. In: Drones 4.3, pp. 1–25. ISSN: 2504446X. DOI: 10.3390/drones4030034.

Siemens (2020). Sound Fields: Free versus Diffuse Field, Near versus Far Field. URL: https://community.sw.siemens.com/s/article/sound-fields-free-versus-diffuse-field-near-versus-far-field (visited on 11/21/2022).

Souren, AWMG (2000). “Living with cyanide”. In: Geochem News 105, pp. 16–26.

Taylor, Jessilynn (2006). Health Effects. US Department of Health and Human Services, Public Health Service. Chap. 3.

Texas Instruments Incorporated (2021). MSP-EXP430G2ET Value line MSP430 LaunchPad™ development kit. URL: https://www.ti.com/tool/MSP-EXP430G2ET (visited on 02/22/2022).

Transport Canada (2020). Getting a drone pilot certificate. URL: https://tc.canada.ca/en/aviation/drone-safety/drone-pilot-licensing/getting-drone-pilot-certificate (visited on 05/22/2022).

Türkman, Ayşen (1998). “Cyanide behaviour in soil and groundwater and its control”. In: International Journal of Environmental Studies 54.2, pp. 107–122. ISSN: 00207233. DOI: 10.1080/00207239808711143.

Waite, Ashley (2002a). “Active Sonar”. In: SONAR for Practicing Engineers. Baflhs Lane, Chichester: John Wiley and Sons, LTD. Chap. 9. ISBN: 0 471 49750 9.

— (2002b). “Propagation of Sound in the Sea”. In: SONAR for Practicing Engineers. Baflhs Lane, Chichester: John Wiley and Sons, LTD. Chap. 3. ISBN: 0 471 49750 9.

— (2002c). SONAR for Practicing Engineers. 3rd ed. Baflhs Lane, Chichester: John Wiley and Sons, LTD. ISBN: 0 471 49750 9.

Wölfl, Anne Cathrin et al. (2019). “Seafloor mapping - The challenge of a truly global ocean bathymetry”. In: Frontiers in Marine Science 6.JUN, pp. 1–16. ISSN: 22967745. DOI: 10.3389/fmars.2019.00283.

Xie, Feng, David Dreisinger, and Fiona Doyle (2013). “A review on recovery of copper and cyanide from waste cyanide solutions”. In: Mineral Processing and Extractive Metallurgy Review 34.6, pp. 387–411. ISSN: 15477401. DOI: 10.1080/08827508.2012.695303.

Zagury, Gérald J, Kahina Oudjehani, and Louise Deschênes (2004). “Characterization and availability of cyanide in solid mine tailings from gold extraction plants”. In: Science of the Total Environment 320.2-3, pp. 211–224.